International Scientific-Technical and Production Journal

CONTENTS

FRICTION STIR WELDING OF COMPOSITE, GRANULATED AND QUASICRYSTALLINE ALUMINIUM ALLOYS

A.G. POKLYATSKY, A.Ya. ISHCHENKO and **V.E. FEDORCHUK**
E.O. Paton Electric Welding Institute, NASU, Kiev, Ukraine

Structural peculiarities and mechanical properties of welded joints on strengthened aluminium alloys are studied. It is shown that the use of friction stir welding does not lead to any substantial phase-structural changes in the weld metal and adjoining regions.

One of the important trends in current engineering is decrease in weight and dimensions of structures with retention of their functional capabilities. Particular emphasis is placed on these requirements in manufacture of aircraft and spacecraft engineering products, overland and water transport. During the last decades this problem has been addressed through a wider utilisation of new high-strength aluminium alloys with high indicators of specific strength, elasticity modulus, corrosion resistance and resistance to propagation of fatigue cracks in the process of operation. However, the possibilities for further improvement of properties of commercial aluminium alloys produced by the traditional methods of casting and subsequent rolling have practically been exhausted. Therefore, a substantial improvement of performance of parts can be achieved by manufacturing them from qualitatively new advanced materials based on aluminium alloys. Such materials include modern granulated aluminium alloys strengthened by dispersed intermetallics that contain oversaturated solid solution of transition metals, composite materials reinforced by dispersed nanosized particles, and alloys strengthened by meta-stable quasicrystalline particles produced at high solidification rates. However, realisation of potential

capabilities of such advanced materials in fabrication of efficient welded structures depends to a considerable degree upon the quality of their joining.

The purpose of this study was to evaluate the efficiency of application of friction stir welding (FSW) for production of sound joints on composite, granulated and quasicrystalline aluminium-base alloys.

Investigations were conducted by using some composite materials based on aluminium alloys with dispersed reinforcing ceramic particles of aluminium oxide Al_2O_3 or silicon carbide SiC (Table 1). These structural materials hold much promise owing to their high values of elasticity modulus, wear and corrosion resistance, and low values of specific weight and thermal expansion and friction coefficients [1, 2].

Structure of a composite material consists of matrix grains of an aluminium alloy, intermetallic inclusions and particles of a reinforcing phase, which are more or less uniformly distributed in the bulk of the matrix (Figure 1).

Fusion welding of composite materials causes complete melting of some of their volume in the zone of formation of a permanent joint under the effect of a high-temperature heat source, solidification of this volume resulting in formation of the weld. Reinforcing particles that remain non-melted are very non-uniformly distributed in the solidifying weld metal (Figure 2, *a*). Moreover, if in welding of composite materials reinforced with silicon carbide particles the temperature of metal heating exceeds 660 °C, their interaction with aluminium may result in formation of acicular inclusions of aluminium carbide Al_4C_3 (Figure 2, *b*). This leads to substantial deterioration of properties of the weld metal and, hence, of the welded joints.

Characteristics of composite materials are greatly affected by fractional composition and uniformity of distribution of reinforcing particles in the matrix, in addition to mechanical properties of a filling compound and matrix alloy, proportion of the volume contents of components, structure of composite castings and character of heat or thermomechanical treatment. Sizes of the particles determine both their in-

Table 1. Composition and tensile strength of 2 mm thick sheets of composite materials based on aluminium alloys

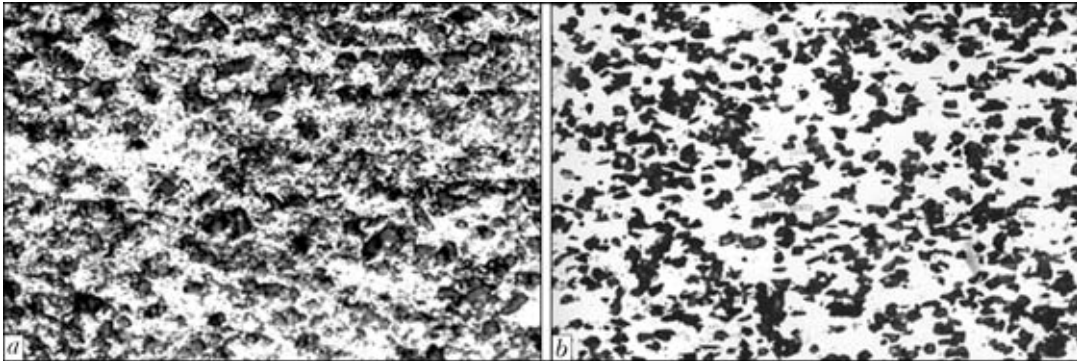| Matrix alloy	Content and composition of reinforcing particles	Sizes of reinforcing particles, μm	Distance between reinforcing particles, μm	Tensile strength σ_t, MPa
AMg5	27 % Al_2O_3	3−.15	3−20	340
AL25	25 % Al_2O_3	5−20	5−60	267
D16	20 % SiC	3−5	1−5	512
AL25	18 % SiC	5−15	3−50	278
AD0	7 % Al_2O_3	≤ 0.1	0.1−2.5	148
D16	20 % SiC	≤ 0.1	0.1−2.5	574

Figure 1. Microstructures of composite materials based on aluminium alloys D16 with 20 % SiC (a — ×600) and AMg5 with 27 % Al_2O_3 (b — ×400)

ternal structure and structure of interfaces with the matrix. Decrease in sizes of the reinforcing particles causes decrease in density of dislocations and level of internal stresses in the boundary layers. Elastic bending of the lattice at junctions of individual grains takes place in coarser particles, this inducing elastic stresses in these regions. In addition, increase in sizes of the particles leads to increase in density of their structural defects, quantity of twins and stacking faults [3, 4]. Therefore, composite materials with nanodispersed reinforcing particles of aluminium oxide Al_2O_3 or silicon carbide SiC are among the most promising structural materials for fabrication of efficient welded structures.

It is of critical importance that during welding of aluminium-base composites reinforced with the nanodispersed particles these particles be uniformly distributed over the entire volume of the weld metal and their accumulation be prevented. As shown by the investigations conducted, the solid-state FSW process can provide preservation of the initial nanodispersion of the reinforcing particles and degree of their distribution across the section of the weld at a level of the base material (Figure 3).

The efficiency of the solid-state FSW process was evaluated [5] also on granulated aluminium alloys 1419 (%: Al−2Mn−1Cr−0.6Ti−0.6Zr−0.6V), 1579 (%: Al−5.5Mg−0.3Mn−0.75Cr−0.8Zr−0.15Co) and 1995 (%: Al−3Mg−4.9Zn−0.28Mn−0.65Cr−0.21Ti) produced by the powder metallurgy methods. The level of doping of aluminium alloys with refractory transi-

tion metals, such as chromium, zirconium, titanium etc., can be substantially increased owing to a high rate of cooling of granules during solidification. The above metals form abnormally oversaturated solid solutions in solidification of the granules. Decomposition of such solid solutions taking place during further technological heating cycles results in formation of dispersed intermetallic compounds that provide strengthening of the alloys. Mechanical properties of the 2 mm thick sheets of these alloys are given in Table 2.

Results of experimental studies prove that in FSW of the investigated granulated alloys the minimal hardness of metal is fixed in the weld and zones of its transition to the base metal. Width of the weakening zone and value of the minimal metal hardness depend on the grade of an alloy. For instance, in welding of sheets of alloy 1419 with hardness HRB 86 (all measurements of hardness were made under load $P = 600$ N) the minimal hardness of the weld metal is at a level of HRB 75, while the width of the weakening zone is about 14 mm. In welding of sheets of alloy 1579 with hardness HRB 105, the minimal hardness of the weld metal is HRB 100, and the width of the weakening zone is 16 mm. Hardness of the weld metal produced in welding of sheets of alloy 1994 (HRB 112) is at a level of HRB 106, weakening taking place in a zone 20 mm wide.

Specimens of the FSW joints on these composite materials subjected to uniaxial tension fracture in the thermomechanically affected zone at the weld to base
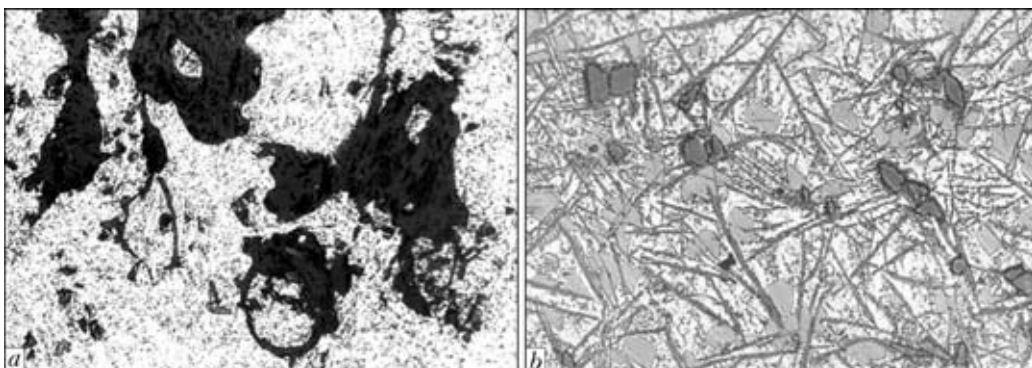

Figure 2. Microstructures of metal of the welds produced by fusion arc welding of composite materials based on aluminium alloy AL25 with 25 % Al_2O_3 (a — ×400) and 18 % SiC (b — ×600)
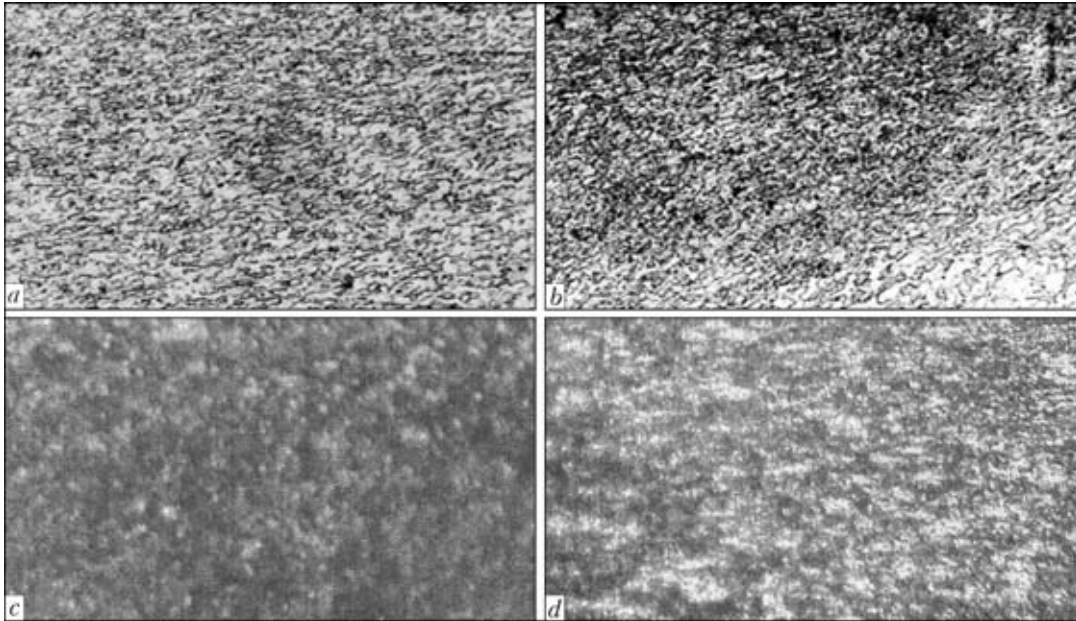
Figure 3. Microstructures of metal of the welds (*a*, *c*) and zones of their interfacing with the base material (*b*, *d*) in FSW of composite nanodispersed materials based on aluminium alloy AD0 with 7 % Al_2O_3 (*a*, *b* — ×400) and aluminium alloy D16 with 20 % SiC (*c*, *d* — ×200)

metal interface, which is characterised by formation of regions with certain structural differences. In this zone the weld nugget having a finely dispersed structure adjoins the base material, which was subjected to the thermal effect and changed the direction of its texture because of rotational and translational movement of the welding tool (Figure 4).

At the same time, no appreciable eutectic precipitations take place in interlayers between the grains. That is why strength of the friction stir welds on the granulated alloys is much higher than the welds made by TIG welding in argon atmosphere. For example, tensile strength of specimens of the solid-state welded joints on alloy 1419 is at a level of 255 MPa, this constituting 75 % of this characteristic of the base material (Table 3). Specimens of the FSW joints on alloy 1579 have tensile strength of about 354 MPa, and those of the FSW joints on alloy 1995 — 483 MPa, this making up 71 and 79 % of tensile strength of the base materials.

As shown by mechanical tests, in uniaxial tension the specimens with weld reinforcement produced by TIG welding in argon atmosphere using filler wire SvAMg63 fracture in the weld to base metal fusion zone. Tensile strength of such joints depends on the doping system of an alloy. For instance, the welded joints on alloy 1419 have tensile strength at a level

of 243 MPa, those on alloy 1579 — 385 MPa, and those on alloy 1995 — 430 MPa.

Fracture of the specimens without weld reinforcement occurs in the weld metal having a cast coarse-crystalline structure (Figure 4). Moreover, particles of oxide inclusions and intermetallics formed as a result complete melting of the granules containing oversaturated solid solution of transition metals precipitate along the grain boundaries both in the weld metal and in the zones of its fusion with the base material. Such welds have low tensile strength. Tensile strength of the TIG weld metal on alloy 1419 is no more than 215 MPa, this making up 63 % of this characteristic of the base material. Tensile strength of the weld metal on alloy 1579 is 287 MPa, and that on alloy 1995 — 291 MPa, this being only 57 and 48 % of tensile strength of the base metal.

Structural peculiarities of the welds and their mechanical properties were also investigated in FSW of 1 mm thick sheets of heat-resistant aluminium alloy Al94Fe2.5Cr2.5Ti1 reinforced with meta-stable quasicrystalline particles [6]. The presence of quasicrystals with a size of 100—200 nm and an intermetallic that had no time to acquire the crystalline structure

Table 2. Mechanical properties of granulated aluminium alloys

Alloy grade	Tensile strength σ_t, MPa	Yield stress $\sigma_{0.2}$, MPa	Elongation δ, %	Bending angle α, deg
1419	340	280	14.0	115
1579	500	420	8.0	61
1995	610	530	8.5	22

Table 3. Tensile strength of welded joints on granulated aluminium alloys produced by TIG welding in argon atmosphere using filler wire SvAMg63 and by FSW, MPa

Welding method	1419	1579	1995
TIG welding (with weld reinforcement)	246−233 / 243	391−379 / 385	436−420 / 430
TIG welding (without weld reinforcement)	220−208 / 215	290−283 / 287	297−287 / 291
FSW	257−253 / 255	357−350 / 354	490−478 / 483
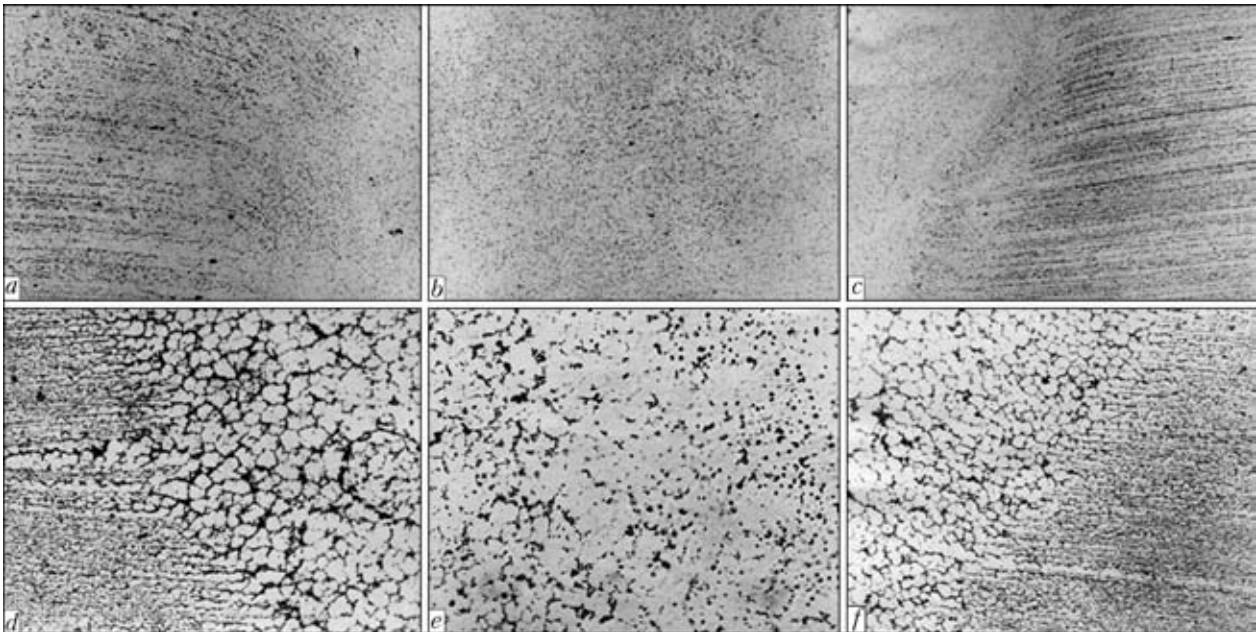
Figure 4. Microstructures (×400) of welded joints on 2 mm thick alloy 1579 produced by FSW (*a*, *c* — weld to base metal interfaces in the thermomechanically affected zone; *b* — weld nugget) and TIG welding in argon atmosphere using filler wire SvAMg63 (*d*, *f* — weld to base metal fusion zones; *e* — weld)

in this alloy provides tensile strength of a sheet equal to 585 MPa and elongation of 8.4 % at room temperature, and 345 MPa and 3.9 %, respectively, at a temperature of 300 °C. It is practically impossible to produce sound permanent joints on such a material by fusion welding. Firstly, when heated to a high temperature (above $0.8T_{melt}$), the meta-stable quasicrystalline particles take the form of crystalline intermetallics, as a result of which the material becomes brittle and loses its strength and ductile characteristics [7]. At the same time, as the material is melted, the reinforcing particles precipitate from the aluminium matrix and prevent formation of a common weld pool and a continuous dense weld (Figure 5).

The conducted experimental studies showed that FSW, which is implemented in the solid state and does not change the phase-structural state of initial semi-finished products, is a promising method for production of sound permanent joints on such materials. As revealed by metallographic examinations, the mean size of grains of the α-Al matrix in the weld metal is approximately 200–300 nm, and that of quasicrystals is 100–200 nm, like in the base metal (Figure 6).
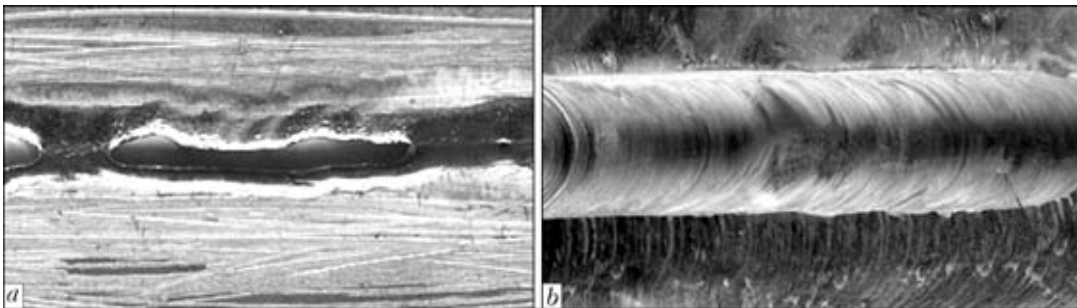
Figure 5. Appearance of the welds made by TIG welding in argon atmosphere (*a*) and FSW (*b*) on 1 mm thick aluminium alloy Al94Fe2.5Cr2.5Ti1
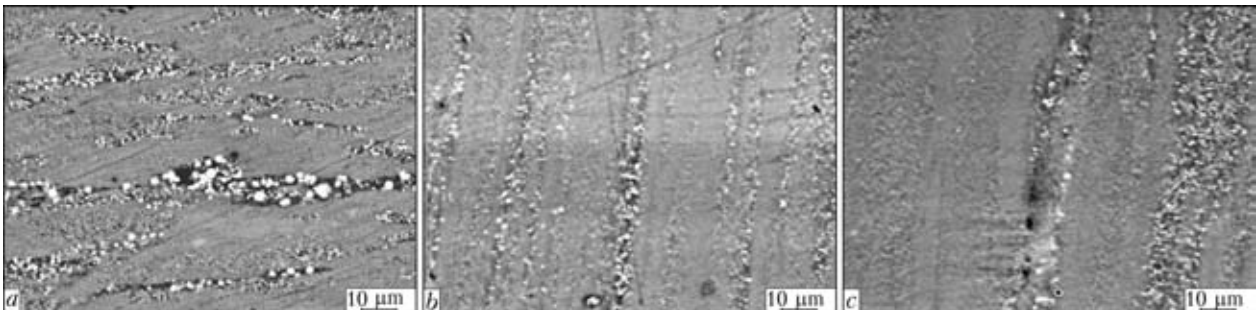
Figure 6. Microstructures of the base material in transverse (*a*) and longitudinal (*b*) directions and of the weld nugget (*c*) produced by FSW on 1 mm thick aluminium alloy Al94Fe2.5Cr2.5Ti1
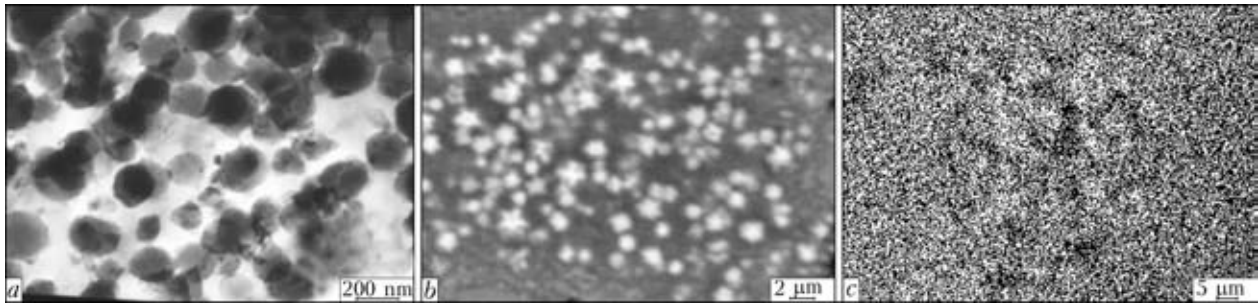
Figure 7. Images of quasicrystalline particles of intermetallic phase in light-field TEM picture (*a*), back-scattered electron SEM picture (*b*) and in characteristics X-ray radiation (*c*)
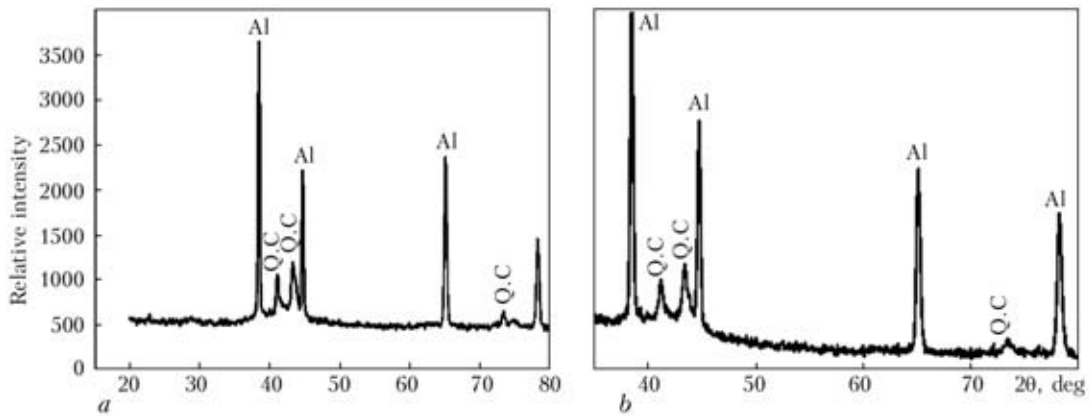
Figure 8. Fragments of diffraction X-ray spectrum of base (*a*) and weld (*b*) metals

Analysis of fine structure indicates that the reinforcing meta-stable quasicrystalline particles have a round shape, diffuse boundaries in the light-field image and characteristic herringbone contrast in the dark-field image both in the base material and in the welds produced by FSW (Figure 7). At the same time, the weld metal is composed of a uniform mixture of grains of the α-Al matrix and quasicrystalline particles.

The welding process does cause heating of metal to high temperatures. Hence, all of the reinforcing particles retain their quasicrystalline structure, which is confirmed by results of X-ray structure analysis (Figure 8).

The welding process results in reorientation of fibres in the thermomechanically affected zone at the weld to base metal interface, this reorientation being caused by the force effect exerted by the rotating welding tool moving along the joining line (Figure 9).

Mechanical tests with uniaxial tension of specimens of the FSW joints showed that their fracture at
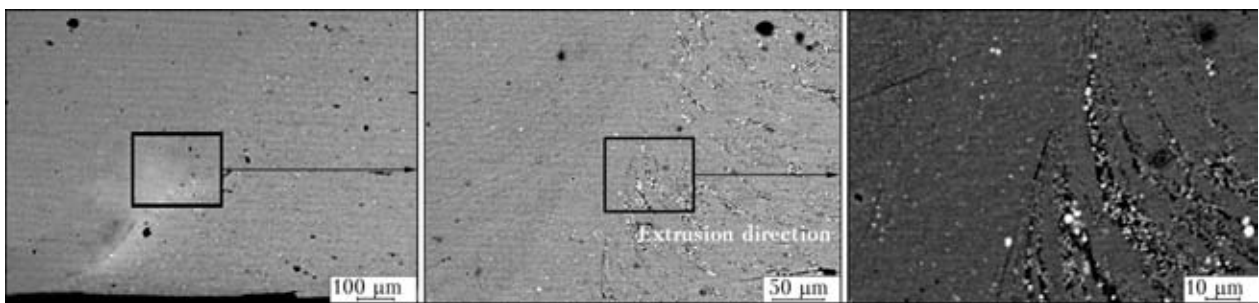
Figure 9. Microstructures of the weld to base material interface zone in FSW of 1 mm thick alloy Al94Fe2.5Cr2.5Ti1
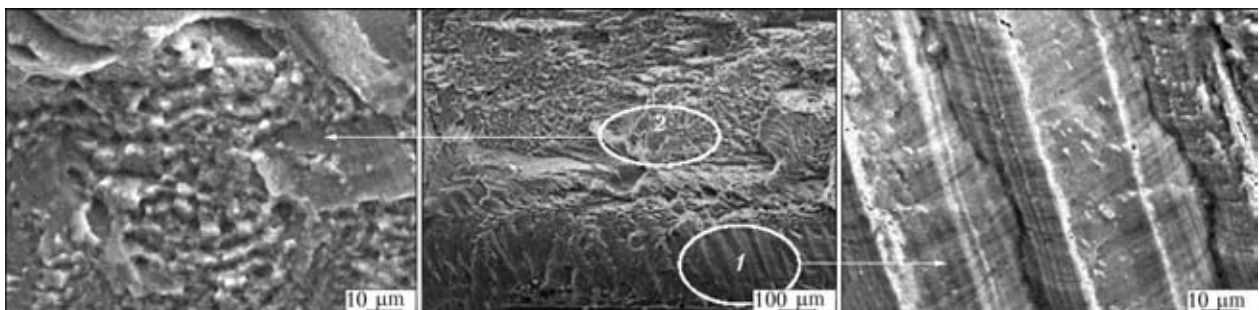
Figure 10. Microstructures of the specimen fracture surface and individual fracture regions

temperatures of 20 and 300 °C occurs in the zone of transition from the weld to base metal and propagates to the weld metal and thermomechanically affected zone (Figure 10). Recesses, which are indicative of a tough character of fracture of the specimens, can be easily seen on the fracture surfaces at high magnification.

Tensile strength of the joints is at a level of 370 MPa at a test temperature of 20 °C, and 197 MPa at 300 °C. The strength factor of the FSW joints is 0.63 at a test temperature of 20 °C and 0.57 at 300 °C. Elongation of the specimens remains at a level of 3.3 and 2.2 %, respectively, for the above test temperatures.

It should be noted in conclusion that due to formation of welds in the solid state, the FSW process allows the sound permanent joints to be produced on granulated, quasicrystalline and composite aluminium alloys without changing their phase-structural state. The granules containing oversaturated solid solution of refractory transition metals are uniformly distributed over the entire volume of the matrix in the weld metal, this providing tensile strength of such joints at a level of 70—80 % of that of the base material. No intermetallics are formed in the weld metal on aluminium alloy reinforced with the quasicrystalline particles, while the quasicrystals, the size of which remains within 100—200 nm, like in the base material, are uniformly distributed between grains of the α-Al matrix, thus providing welds with high strength and ductility values. No dissociation of the reinforcing particles is fixed in welding of composite materials, while their dispersion degree and uniformity of distribution in the weld metal remain at a level of the base material.

1. Falchenko, Yu.V., Muravejnik, A.N., Kharchenko, G.K. et al. (2010) Pressure welding of micro-dispersed composite material AMg5 + 27 % Al₂O₃ with application of rapidly solidified interlayer of eutectic alloy Al + 33 % Cu. *The Paton Welding J.*, **2**, 7—10.
2. Ryabov, V.R., Muravejnik, A.N., Budnik, V.P. et al. (2001) Investigation of weldability of dispersion-strengthened Al/SiC composite material. *Ibid.*, **11**, 13—16.
3. (2008) Inorganic materials science. In: *Materials and technologies:* Encyclop. Ed. by G.G. Gnesin, V.V. Skorokhod. Vol. 2, Book 1. Kiev: Naukova Dumka, 434—444.
4. Markashova, L.I., Ryabov, V.R., Statsenko, V.V. et al. (1995) Investigation of structure of aluminium-based composite material strengthened with silicon carbide particles. *Avtomatich. Svarka*, **8**, 35—38.
5. Dobatkin, V.I. (2001) *Selected works*. Moscow: VILS.
6. Kimura, H.M., Sasamori, K., Inoue, A. (2000) Al—Fe based bulk quasicrystalline alloys with high elevated temperature strength. *J. Mater. Res.*, **12**, 2737—2744.
7. Takeuchi, S., Edagawa, K., Tamura, R. (2001) Deformation mechanism of quasicrystals. *Mater. Sci. and Eng. A*, **319—321**, 93—96.

FORCE EFFECT ON WELDED SURFACES INITIATED BY RUNNING OF SHS REACTION IN NANOLAYERED INTERLAYER

E.A. VELIKOIVANENKO, A.I. USTINOV, G.K. KHARCHENKO, Yu.V. FALCHENKO, L.V. PETRUSHINETS and **G.F. ROZYNKA**
E.O. Paton Electric Welding Institute, NASU, Kiev, Ukraine

The case of welding samples of titanium aluminide through nanostructured Ti/Al interlayer was used to calculate stresses arising in the surface layers of welded intermetallide samples, initiated by intensive heat evolution at running of the reaction of self-propagating high-temperature synthesis in the interlayer.

Studies [1, 2] show that an application of nanolayered foils based on elements forming intermetallides as interlayers significantly improves the conditions necessary for formation of solid phase permanent joints, i.e. heating temperature, delay time and pressure, applied for the joint obtaining, are reduced. Analysis of a diffusion zone of titanium aluminide based welded joint determined that its size increases 4 times in comparison with the diffusion zone, obtained in welding of intermetallide without the interlayer under similar conditions.

It is well-known fact that a reaction of self-propagating high-temperature synthesis (SHS), accompanied by intensive heat evolution, can be initiated in the process of heating. SHS reaction in Ti/Al foils, for example, took place in a mode of gas-free burning or heat explosion [3, 4] depending on initial temperature, thickness of the layers and their amount. Burning rate achieves 150 cm/s at 1100—1300 °C temperature. An intensity of heat evolution at running of SHS reaction, for example, in Ni/Al foils, can make 4 W/m². Such a pulse heat effect on the surface layers of welded materials can provoke in them appearance of the elastic stresses, besides local temperature increase, which also have influence on mass transfer

processes similar to that appearing at impact effects on the welded surfaces [5, 6].

In this connection evaluation of a level of stresses which appear in the surface layers of samples being joined through the interlayer at initiation in it of SHS reaction was carried out in present study by example of γ-TiAl titanium aluminide.

The mathematical calculations were carried out for initial period of welding when temperature of the plates in the process of heating achieves the level of initiation temperature of SHS reaction under following conditions: size of welded samples of titanium aluminide is 10 × 10 × 5 mm; foil thickness being 20 μm; rate of preheating made 20 °C/min; pressure at preliminary contraction is 8 MPa; temperature of initiation of SHS reaction being 400 °C; foil «burning» front temperature made 1200 °C, running of SHS reaction simultaneously along the whole surface of nano-layered foil; time of running is $2 \cdot 10^{-5}$ s.

Two-dimensional problem was considered due to small size of the welded samples and their uniform heating on thickness. The foil was simulated as a gap δ_g between the plates.

Firstly, in the process of heating a temperature filed $T(x, y, t)$ in time was determined for analysis of stress-strain state in the studied plates of length L_x, height L_y and thickness δ (Figure 1):

$$\frac{\partial}{\partial x}\left(\lambda \frac{\partial T}{\partial x}\right) + \frac{\partial}{\partial y}\left(\lambda \frac{\partial T}{\partial y}\right) = c\gamma \frac{\partial T}{\partial t}, \quad (1)$$

where λ is the coefficient of heat conductance of the plate material; $c\gamma$ is the coefficient of volumetric heat capacity of the plate material; and t is the heating time.

Further, the problem on determination of stress and strain kinetics was solved. At that, the methods of sequential tracking in time with step Δt and finite-element method in space were used, i.e. given area was divided with step h_x and h_y and represented by population of rectangular element of $h_x \times h_y$ size.
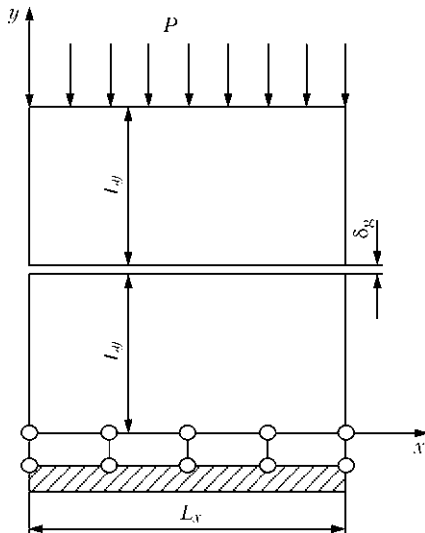
Figure 1. Design scheme of welded joint

The solution for each tracking step (in each point of time t) is found taking into account that was obtained for previous step $t - \Delta t$. The temperature in point of time t in the nods of mesh of finite-element space is determined through solving of a system of algebraic equations, obtained as a result of minimization of E_T functional in temperature in the nods of elements [7]:

$$E_T = -\frac{1}{2}\int_S \left[\lambda_x \left(\frac{\partial T}{\partial x}\right)^2 + \lambda_y \left(\frac{\partial T}{\partial y}\right)^2 + \frac{c\gamma}{\Delta t}\left(T - T_*\right)^2\right] \times$$
$$\times\, dxdy + \frac{1}{2}\int_\Gamma \beta_n (T - T_{env})^2 d\Gamma; \quad (2)$$
$$\partial E_T / \partial T_{mn} = 0, \quad m = 1, 2, \ldots,$$

$n = 1, 2 \ldots$ is the numeration of nods in x, y direction,

where $T_* = T(x, y, t - \Delta t)$ is the already known temperature in point of time $t - \Delta t$ starting form the initial one ($t = 0$); S is the considered area; Γ are the outside boundaries of part; β_n is the coefficient of heat exchange with environment of T_{env} temperature.

The derivatives $\partial T/\partial x$, $\partial T/\partial y$ are expressed through temperature in the nods for each rectangular element. Thus, the integral of area S is substituted by sum of finite element integrals of area ΔS. The same is done with integral Γ in surface.

Let us consider an algorithm for solving of mechanical problem at loading stage corresponding to point of time t, assuming that the solution is completely known relative to stress tensors σ_{ij}, strain ε_{ij} and movements U_i in scope of described above two-dimensional stress state at $t_* = t - \Delta t$.

For this, expression (2) is integrated in time in the ranges from $t - \Delta t$ to t:

$$\Delta\varepsilon_{ij} = \left\{\frac{\sigma_{ij} - \delta_{ij}\sigma}{2G} + \delta_{ij}[K\sigma + \alpha_T(T - T_0)]\right\}_t -$$
$$- \left\{\frac{\sigma_{ij} - \delta_{ij}\sigma}{2G} + \delta_{ij}[K\sigma + \alpha_T(T - T_0)]\right\}_{t - \Delta t} + \quad (3)$$
$$+ \Delta\lambda\overline{(\sigma_{ij} - \delta_{ij}\sigma)},$$

where $\delta_{ij}\sigma$ is the spherical tensor (here σ is the average pressure in a point; δ_{ij} is the unit function); G is the shear modulus; K is the modulus of volume compression equal $(1-2\nu)/E$; ν is the Poisson's ratio; E is the Young's modulus; α_T is the coefficient of thermal linear expansion (CTLE); T_0 is the initial temperature; $\overline{\sigma_{ij} - \delta_{ij}\sigma}$ is the average value of $\sigma_{ij} - \delta_{ij}\sigma$ at interval from $t - \Delta T$ to t, calculated based on average value of specific integral.

If Δt value is small then $\overline{\sigma_{ij} - \delta_{ij}\sigma}$ value can be substituted by desired value in the point of time t. Than, the following will be obtained for two-dimensional stressed state instead of (3):

$$\Delta\varepsilon_{xx} = B_1\sigma_{xx} + B_2\sigma_{yy} - b_{xx};$$
$$\Delta\varepsilon_{yy} = B_1\sigma_{yy} + B_2\sigma_{xx} - b_{yy}; \qquad (4)$$
$$\Delta\varepsilon_{xy} = \psi\sigma_{xy} - b_{xy},$$

where σ_{xx}, σ_{yy} are the normal stresses; σ_{xy} are the tangential stresses;

$$B_1 = \frac{2\psi + K}{3}; \quad B_2 = \frac{K - \psi}{3}; \quad \psi = \frac{1}{2G} + \Delta\lambda;$$
$$b_{ij} = \left(\frac{\sigma_{ij}}{2G}\right)_{t-\Delta t} + \delta_{ij}\left[\sigma\left(K - \frac{1}{2G}\right)\right]_{t-\Delta t};$$
$$\delta_{ij}\Delta\varphi, \ i, j = x, y; \ \Delta\varphi = [\alpha_T T - T_0)]_t - [\alpha_T(T - T_0)]_{t-\Delta t},$$

where φ is the function of temperature elongation.

It can be seen, hence, that b_{ij} is determined by a solution in the point of time $t - \Delta t$ and known value of $\Delta\varphi$. Function ψ of a state of material in element volume in the point of time t contains nonlinearity, connected with yield condition.

It is assumed that value $\psi(x, y, t)$ is known. Solving (4) relative to stresses, the following is obtained:

$$\sigma_{xx} = A_1\Delta\varepsilon_{xx} + A_2\Delta\varepsilon_{yy} + Y_{xx};$$
$$\sigma_{yy} = A_1\Delta\varepsilon_{yy} + A_2\Delta\varepsilon_{xx} + Y_{yy}; \qquad (5)$$
$$\sigma_{xy} = \frac{1}{\psi}\Delta\varepsilon_{xy} + Y_{xy}; \quad \sigma_{zz} = \sigma_{xz} = \sigma_{yz} = 0,$$

where $A_1 = \dfrac{2\psi + K}{\psi(\psi + 2K)}$; $A_2 = \dfrac{\psi - K}{\psi(\psi + 2K)}$; $Y_{xx} = A_1 b_{xx} +$ $+ A_2 b_{yy}$; $Y_{yy} = A_1 b_{yy} + A_2 b_{xx}$; $Y_{xy} = b_{xy}/\psi$.

The relationship between deformation increment $\Delta\varepsilon_{ij}$ and components of vector of movement increment ΔU_i can be presented in a form of

$$\Delta\varepsilon_{xx} = \frac{\partial\Delta U_x}{\partial x}; \quad \Delta\varepsilon_{yy} = \frac{\partial\Delta U_y}{\partial y};$$
$$\Delta\varepsilon_{xy} = \frac{1}{2}\left(\frac{\partial\Delta U_y}{\partial x} + \frac{\partial\Delta U_x}{\partial y}\right). \qquad (6)$$

Equation of consistency of strains looks like

$$\frac{\partial^2\Delta\varepsilon_{xx}}{\partial y^2} + \frac{\partial^2\Delta\varepsilon_{yy}}{\partial x^2} = 2\frac{\partial^2\Delta\varepsilon_{xy}}{\partial x\partial y}. \qquad (7)$$

Equilibrium equation can be represented as

$$\frac{\partial\sigma_{xx}}{\partial x} + \frac{\partial\sigma_{xy}}{\partial y} = 0; \quad \frac{\partial\sigma_{xy}}{\partial x} + \frac{\partial\sigma_{yy}}{\partial y} = 0. \qquad (8)$$

The conditions on plate boundary in a point with normal n, i.e. in part of boundary where the forces Γ_P are applied, can be found using equations

$$\sigma_{xx}\cos(n, x) + \sigma_{xy}\cos(n, y) = P_x;$$
$$\sigma_{xy}\cos(n, x) + \sigma_{yy}\cos(n, y) = P_y, \qquad (9)$$

where P_x, P_y are the projections of application of forces on axes x and y.

For the part of boundary where mixed boundary conditions Γ_u are set

$$\Delta U_x = \Delta U_x^0; \quad \Delta U_y = \Delta U_y^0. \qquad (10)$$

A proper combination of conditions (9) and (10) provides mixed conditions in part of boundary Γ_{Pu}. Equations (5)−(10) at known value of $\psi(x, y, t)$ completely determine differential formulation of a boundary-value problem on calculation of σ_{ij}, ε_{ij} and U_i.

A variation formulation of this problem is considered that is important in realizing of solution by finite-element method. For this the functional is used:

$$E_1 = -\frac{1}{2}\int_S \{(\sigma_{xx} + Y_{xx})\Delta\varepsilon_{xx} + (\sigma_{yy} + Y_{yy})\Delta\varepsilon_{yy} +$$
$$+ 2(\sigma_{xy} + Y_{xy})\Delta\varepsilon_{xy}\}dxdy + \int_\Gamma P_i\Delta U_i d\Gamma. \qquad (11)$$

It follows form studies [7, 8] that an absolute minimum E_1 for kinematically possible $\Delta\varepsilon_{ij}$ meets an actual distribution of the strain increments $\Delta\varepsilon_{ij}$ and corresponding to them increments ΔU_i which are the solutions of boundary-value problem (5)−(10).

The area integral S taking into account expression (11) is substituted by sum of the finite element integrals ΔS, strain $\Delta\varepsilon_{ij}$ are expressed through ΔU_i and stresses σ_{ij} are shown through $\Delta\varepsilon_{ij}$. The derivatives in (6) for each ΔS are expressed through ΔU_i in the nod points. The similar is done with integral in Γ. Thus, functional E_1 will be shown by quadratic form through unknown values of ΔU_x and ΔU_y in mesh nods.

Minimization of $\partial E_1/\partial\Delta U_x = 0$, $\partial E_1/\partial\Delta U_y = 0$ provides the system of algebraic equations being linear relatively to ΔU_i (at known function ψ).

$\Delta\varepsilon_{ij}$ and σ_{ij} are calculated after determination of ΔU_i. The function ψ is specified by obtained values of σ_{ij}. Different iteration processes are possible for this purpose among which a process, described in studies [7, 8], being sufficiently effective.

Thermo-physical and mechanical characteristics of titanium aluminide, given below, were used for calculation of elastoplastic stresses, occurring in the samples from γ-TiAl aluminide titanium at the moment of running of SHS reaction in the nanolayered foil.

Coefficient of heat conductance of plate
material λ, J/(m^3·K) [9] 0.25
Coefficient of volumetric heat capacity of plate
material $c\gamma$, J/(m^3·K) [9] 0.8
Yield strength $\sigma_{0.2}$, MPa [10] 510
Young's modulus E, MPa [11] .... 1.2·10^5
CTLE α_T, °C^{-1} [12] .... 10.8·10^{-6}

Coefficients λ and $c\gamma$ for titanium aluminide were taken as an average from given values for titanium and aluminide. Character of change of stressed state and level of microstrains of the surface layer of joined materials at running of SHS reaction in the nanolayered foil is shown in Figure 2. It can be seen from Figure that a jump in compression stresses ($\sigma_{xx} = 240$ MPa) takes place at rapid increase of temperature up to 1200 °C in the joint. They are changed by tensile ones which reach 575 MPa for 0.3 s. Running
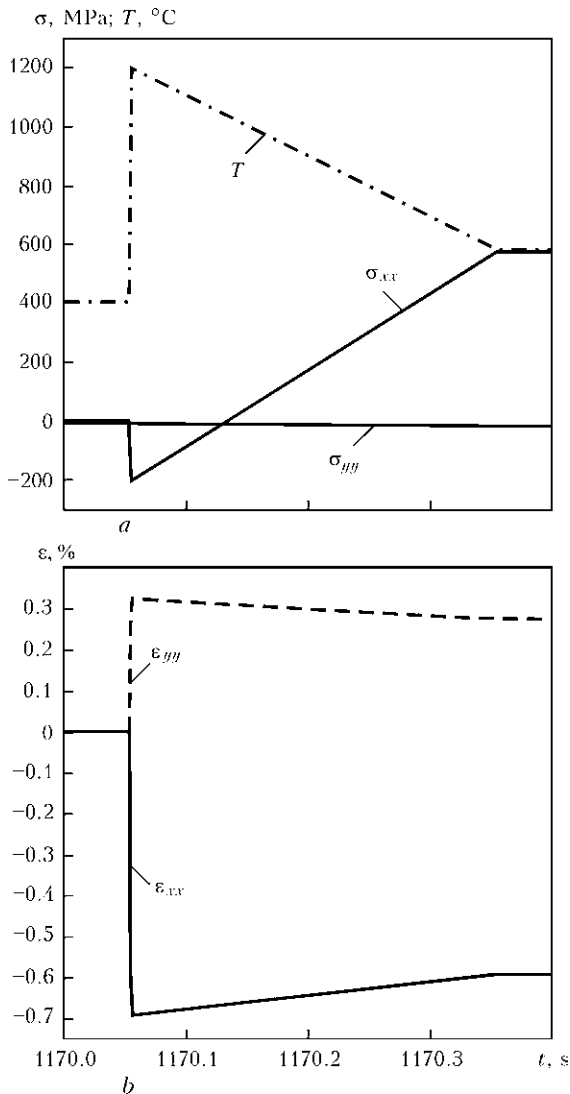
Figure 2. Curves of stresses σ_{xx} and σ_{yy} (*a*) and strains ε_{xx} and δ_{yy} (*b*) in near-contact volumes of the welded plates at running of SHS reaction

of SHS reaction also results in a rise of σ_{yy} from 8 to 18 MPa that exceeds the value of pressure of preliminary contraction more than 2 times. The calculated values of microstrains of the near-contact surface layer ($\delta \sim 20$ μm) make not more than 0.7 % (Figure 2, *b*).

Therefore, obtained calculation results indicate that running of SHS reaction in the interlayer results in a significantly intensive dynamic deformation effect on the welded surfaces. A thermal «hit» together with local increase of temperature activates the diffusion processes in the surface layers of welded materials and provides conditions for formation of permanent joints from difficult to weld materials.

1. Ustinov, A.I., Falchenko, Yu.V., Ishchenko, A.Ya. et al. (2009) Producing permanent joints of γ-TiAl based alloys using nanolayered Ti/Al interlayer by vacuum diffusion welding. *The Paton Welding J.*, **1**, 12–15.
2. Kharchenko, G.K., Mazanko, V.F., Ustinov, A.I. et al. (2009) Study of diffusion processes in welded joints of titanium aluminide (TiAl). *Visnyk ChDTU. Series Technical Sciences*, **37**, 117–119.
3. Elkina, N.A., Nosyrev, A.N., Khvesyuk, V.I. (2006) Investigation of processes for producing of foils of TiAl intermetallides from multilayer binary systems by method of self-propagating high-temperature synthesis. In: *Proc. of 33rd Int. Conf. on Plasma Physics and Controlled Thermonuclear Synthesis* (Zvenigorod, 13–17 Febr. 2006). *www.fpl./ Zvenigorod/XXXIIIPt/ru/BL-Khvesyuk.doc*.
4. Rogachev, A.S., Grigoryan, A.E., Illarionova, E.V. et al. (2004) Gas-free burning of multilayer bimetallic nanofilms of Ti/Al. *Fizika Goreniya i Vzryva*, 40(**2**), 45–51.
5. Meshkov, Yu.Ya., Gertsriken, D.S., Mazanko, V.F. (1996) On problem of mechanism of accelerated mass transfer in metals under conditions of pulsed loads. *Metallofizika*, 18(**4**), 52–53.
6. Gertsriken, D.S., Mazanko, V.F., Tyshkevich, V.M. et al. (1999) *Mass transfer in metals at low temperatures in conditions of external action*. Kiev: IMF NANU.
7. Makhnenko, V.I. (1976) *Computational methods for study of kinetics of welding stresses and strains*. Kiev: Naukova Dumka.
8. Makhnenko, V.I., Velikoivanenko, E.A., Pochinok, V.E. et al. (2001) Numerical methods of the predictions of welding stresses and distortions. In: *Welding and Surfacing Rev.*, Vol. 13, Pt 1. Ed. by B.E. Paton. Harwood Acad. Publ.
9. (1967) *Physical properties of steels and alloys used in power engineering*: Refer. Book. Ed. by B.E. Neumark. Moscow; Leningrad: Energiya.
10. Polkin, I.S., Kolachev, B.A., Iliin, A.A. (1997) Titanium aluminides and alloys on their base. *Tekhnologiya Lyog. Splavov*, **3**, 32–39.
11. Gorban, V.F., Kharchenko, G.K., Falchenko, Yu.V. et al. (2009) Investigation of joints of titanium aluminide with titanium alloy VT8 produced by diffusion welding. *The Paton Welding J.*, **12**, 7–9.
12. Bartolotta, P., Barrett, J., Kelly, T. et al. (1997) The use of cast Ti–48Al–2Cr–2Nb in jet engines. *J. Minerals, Metals and Materials Soc.*, 49(**5**), 48–50.

PECULIARITIES OF THE INFLUENCE OF COMPLEX ALLOYING ON STRUCTURE FORMATION AND MECHANICAL PROPERTIES OF WELDS ON LOW-ALLOYED HIGH-STRENGTH STEELS

V.V. GOLOVKO, V.A. KOSTIN and **G.M. GRIGORENKO**
E.O. Paton Electric Welding Institute, NASU, Kiev, Ukraine

Influence of technological factors (oxygen potential of the flux, welding wire–base metal combination, and cooling rate) on mechanical properties of the studied welds on high-strength low-alloyed 12KhN2MDF and 09G2FB steels was analyzed. Derived results are in agreement with the type of microstructure, composition and distribution of non-metallic inclusions, and features of austenite decomposition in the studied weld metal. It is shown that addition of finely-dispersed refractory inclusions of titanium and zirconium oxides to the weld metal allows achievement of high values of strength ($\sigma_t = 700-710$ MPa) and impact toughness ($KCV_{-20} = 80-100$ J/cm^2).

Continuously growing requirements to metal structures necessitate mastering new steel grades with an increased level of mechanical properties. Alongside low-carbon steels, high-strength low-alloyed (HSLA) steels are ever wider accepted in metallurgical production. Their alloying system envisages an increased content of elements strengthening the solid solution at simultaneous lowering of carbon content [1–3].

The main task in welding HSLA steels is formation of such a microstructure of weld metal, which would ensure both high mechanical properties of the weld proper and equivalent strength of joining of the weld with the base metal. Combination of high values of strength, ducility and toughness can be achieved at formation in weld metal structure of a high content of low-temperature forms of ferrite with fine-grained morphology, namely acicular ferrite (AF) [4, 5].

A rather wide spectrum of microstructures form in weld metal of HSLA steels: AF, polygonal ferrite (PF), Widmanstatten ferrite (WF), ferrite with an ordered (FOS) and disordered (FDS) second phase, as well as microphases (MAC-phase), which form during austenite decomposition. Optimum combination of such strength and ductility properties of weld metal of low-alloyed steels is achieved as a result of a favourable combination of the entire complex of ferrite-cementite structures.

It is known [4, 6] that in this complex AF structure has the highest properties in terms of brittle fracture resistance that is due to its morphological features: AF predominantly forms inside primary crystallites; AF needles have the length of 2–8 μm and thickness of 1–2 μm; their length-width ratio is equal to 1:3–1:10; high-angle boundaries with more than 20° angle of disorientation form between the needles; microphases (carbides or MAC-phase) are observed on the interfaces between the ferrite grains; high dislocation density forms inside AF grains ($\rho = 10^{12}$ cm^{-2}).

AF formation is affected by a whole range of factors, namely: weld metal composition, cooling rate in the temperature range of 800–500 °C, oxygen content in the weld, size of primary austenite grain, composition, size and distribution of nonmetallic inclusions.

At the same time, analysis of published data shows that in a number of cases it is impossible to achieve a high cold resistance of weld metal of HSLA steels, despite the presence of AF structure in them [6, 7]. According to their results, a decrease of impact toughness is possible, despite the presence of a high content of AF in the weld (above 70 %). It should be noted that such a lowering is observed in welds with carbon content of 0.12–0.15 %, that is, possibly, related to the influence of unconsidered structural factor.

In terms of further increase of the values of strength, ductility and impact toughness of the metal of welds and welded joints, bainite structures should form in the weld, preferably, lower bainite. This should be promoted by addition of alloying elements to the melt, which form carbides with melting temperature above that of weld pool metal in the amount that does not exceed their limit solubility in austenite. Such alloying elements as molybdenum, vanadium and niobium satisfy these conditions to the greatest degree.

Niobium dissolved in austenite promotes lowering of A_{c_3} temperature that causes a slowing down of the diffusion processes and promotes formation of rack bainite and martensite structures. Vanadium and molybdenum carbides, while concentrating on the boundary of $\gamma \rightarrow \alpha$ transformation, promote refinement of the forming ferrite grains.

The purpose of this work consisted in selection of metallurgical (oxidizing potential of the flux, flux

Table 1. Composition of base metal and welding wires, wt.%

Steel, wire	C	Mn	Si	S	P	Ti	Ni	Mo	Al	V	Nb	Cu
GNM series												
12KhN2MDF	0.088	0.44	0.253	0.005	0.010	–	2.16	0.27	0.011	0.015	0.005	0.47
Sv-08G1NMA	0.080	1.01	0.050	0.012	0.009	–	1.24	0.25	–	–	–	0.05
GNM-FB series												
09G2FB	0.090	1.70	0.220	0.004	0.008	–	<0.01	0.01	0.035	0.060	0.035	0.01
Sv-10GNMDTA	0.010	1.41	0.220	0.009	0.012	0.08	1.10	0.20	–	–	–	0.45

alloying by refractory element oxides) and technological (combination of base metal and welding wire, cooling rate) factors, ensuring a high level of mechanical properties of welds on HSLA steels.

Investigations envisaged assessment of the influence of weld metal alloying by molybdenum, vanadium and niobium on the structure and properties of weld metal.

To solve the defined task two series of weld metal samples were prepared. Weld metal alloying by molybdenum was performed with welding wires Sv-08G1NMA and Sv-20GNMDTA, and in order to add vanadium and niobium to the weld pool plates of low-alloyed pipe steel 09G2FB were used as base metal.

Chemical composition of base metal and welding wires is given in Table 1. Table 2 gives the results of determination of chemical composition of weld metal obtained in welding with Sv-08G1NMA wire of butt joints of 12KhN2MDF steel (GNM series) and of butt joints produced in welding of 09G2FB steel (GNM-FB series) with Sv-10GNMDTA wire.

Welding was performed using three experimental fluxes with different levels of oxygen potential: acid (flux 13, $\lg a_O = -0.83$), neutral (9, $\lg a_O = -1.25$) and basic (19, $\lg a_O = -1.70$). Oxygen potential of the flux was calculated by the formula

$$a_O = RTP_{O_2} \ (\text{kJ/mol}),$$

where R is the absolute gas constant, equal to 8.31 J/(mol·K); T is the temperature, K; P_{O_2} is the partial pressure of oxygen over the slag melt.

Slag base of experimental fluxes was based on Al_2O_3–MgO–SiO_2–CaF_2. In order to study the possibilities for controlling the dimensions of ferrite grains in one of the test series (GNM-TiO_2), titanium oxide was added to the flux charge, and in the other (GNM-ZrO_2) it was zirconium oxide.

The following welding modes were used in the experiments: reverse polarity direct current $I_w = 700-720$ A; $U_a = 35-36$ V; $v_w = 6.9-7.0$ mm/s.

Influence of technological factors (oxygen potential of the flux, welding wire–base metal system, cooling rates) on the mechanical properties of the studied welds is shown in Table 3.

Use of welding wire Sv-08G1NMA in welding of 12KhN2MDF steel gives quite low values of yield point (473–500 MPa) and impact toughness, particularly at low testing temperatures of −20 °C (16–20 J/cm^2). Reduction of oxygen potential of the flux ($\lg a_O$: $-0.83 \rightarrow -1.25 \rightarrow -1.70$) practically does not affect these characteristics. Application of Sv-10GNMDTA wire in welding 09G2FB steel leading to weld alloying by vanadium and niobium, increases both the total level of weld metal strength (yield point of 520–545 MPa), and their impact toughness (13–58 J/cm^2). Here, the most favorable is application of a neutral flux with oxygen potential level $\lg a_O = -1.25$ (weld of GNM09FB series), that allows achieving the level of impact toughness of about 60 J/cm^2 at testing temperature of −20 °C.

The best combination of strength and impact toughness is characteristic of samples of weld metal obtained with a similar combination of welding wire

Table 2. Composition of the metal of studied welds, wt.%

Weld series	C	Mn	Si	S	P	Cr	Ni	Mo	Al	Ti	V	Nb	O
GNM13	0.070	0.51	0.382	0.009	0.012	0.18	1.67	0.26	0.010	0.001	0.005	0.002	0.120
GNM09	0.063	0.53	0.265	0.009	0.013	0.20	1.52	0.25	0.014	0.001	0.007	0.002	0.522
GNM19	0.058	0.58	0.152	0.008	0.013	0.21	1.51	0.25	0.016	0.001	0.009	0.002	0.351
GNM13FB	0.087	1.38	0.453	0.009	0.016	0.08	0.38	0.10	0.021	0.013	0.023	0.013	0.152
GNM09FB	0.081	1.45	0.331	0.004	0.015	0.06	0.39	0.11	0.026	0.017	0.027	0.015	0.035
GNM19FB	0.087	1.59	0.247	0.002	0.015	0.06	0.37	0.12	0.033	0.021	0.040	0.020	0.023
GNM-TiO_2	0.059	1.40	0.533	0.011	0.015	0.25	0.46	0.53	0.019	0.019	0.040	0.006	0.071
GNM-ZrO_2	0.052	1.39	0.499	0.010	0.014	0.24	0.46	0.53	0.020	0.026	0.040	0.006	0.078

Table 3. Mechanical properties of the metal of studied welds (average value from three measurements)

Weld series	$\sigma_{0.2}$, MPa	σ_t, MPa	δ_5, %	ψ, %	KCV, J/cm^2, at T, °C		
					20	0	−20
GNM13	473.45	617.65	21.50	53.25	38.6	24.3	16.5
GNM09	491.80	603.20	23.50	62.90	48.2	26.7	20.7
GNM19	500.85	620.50	23.25	66.10	48.5	40.4	16.9
GNM13FB	534.15	667.85	26.20	58.85	54.4	35.8	25.9
GNM09FB	545.45	681.55	26.15	68.85	176.8	112.6	58.7
GNM19FB	523.70	688.80	23.85	69.90	45.9	22.6	13.5
GNM-TiO$_2$	631.45	712.25	26.50	64.95	125.7	99.5	79.5
GNM-ZrO$_2$	627.85	706.75	25.85	64.00	114.5	109.9	102.8

and base metal, using ceramic flux of basic type with additives of titanium and zirconium oxides (GNM-TiO$_2$ and GNM-ZrO$_2$ series), that allowed achieving the yield strength of 700−710 MPa and impact toughness of 80−100 J/cm^2 at testing temperature of −20 °C.

Results of assessment of the influence of cooling rate on the features of austenite decomposition in the metal of the studied welds are given in Figure 1. Investigations conducted in Gleeble 3800 system for simulation of the physical condition of welding showed that at low cooling rates (1 °C/s) of weld metal in the temperature range of 800−500 °C in welds of GNM-FB series austenite decomposition occurs in the region of high transformation temperatures (650−750 °C). With increase of cooling rate (10 °C/s) the region of austenite decomposition shifts into the region of 570−650 °C temperatures. In welds of GNM-TiO$_2$ and GNM-ZrO$_2$ series, even at low cooling rates (1 °C/s) austenite decomposition occurs in the region of 550−650 °C (see Figure 1), i.e. in the region of intermediate transformation.

Investigation of the structure and weld metal composition was performed for interpretation of the obtained results. Table 4 gives the quantity of structural constituents in weld metal.

Microstructures of welds of the studied samples are given in Figure 2. Microstructures of welds of GNM series (Figure 2, *a*, *b*), irrespective of the level

of oxygen potential in the base metal, consist of coarse-acicular ferrite formations and extended PF precipitates along primary crystallite boundaries.

Microstructure of welds alloyed with molybdenum, vanadium and niobium made using acid flux GNM13FB (Figure 2, *c*) consists of a large quantity (up to 72 %) of classical AF at moderate content of PF and polyherdral ferrite (PHF). Weld made using neutral flux GNM09FB has the highest content of AF (80 %) in the weld metal, and the lowest content of PF, respectively. Microstructure of the series of GNM19FB weld (Table 4) consists of various structural components: AF, PHF, PF, plate-like ferrite (PlF), upper (UB) and lower (LB) bainite, with AF fraction being small (up to 20 %).

Microstructures of welds of GNM-TiO$_2$ and GNM-ZrO$_2$ series almost completely consist of finely-dispersed AF, with minimum amount of PF observed (Figure 2, *e*, *f*; Table 4).

In connection with the fact that the weld structure is strongly affected by nonmetallic inclusions, analysis of the composition (Table 5, Figure 3), volume fraction (Table 5) and distribution of nonmetallic inclusions by size (Figure 3) was performed, which showed that with increase of oxidizing potential of the used flux, the volume fraction of nonmetallic inclusions in the weld metal increases (Table 5), while inclusion size decreases to 0.3−0.5 μm (Figure 3, *c*, *d*).
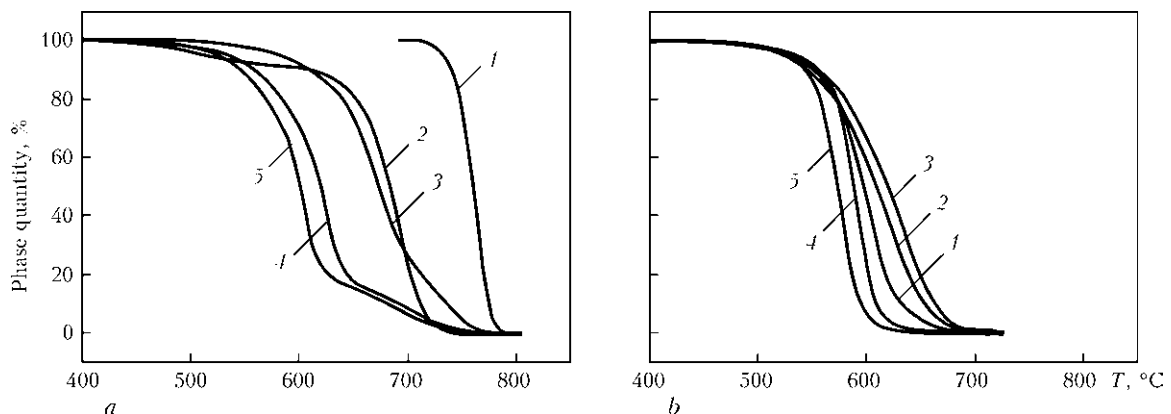

Figure 1. Influence of cooling rate of 1 (*a*) and 10 (*b*) °C/s on the nature of austenite decomposition in the studied welds: *1* — GNM09FB; *2* — GNM19FB; *3* — GNM13FB, *4* — GNM-ZrO$_2$; *5* — GNM-TiO$_2$
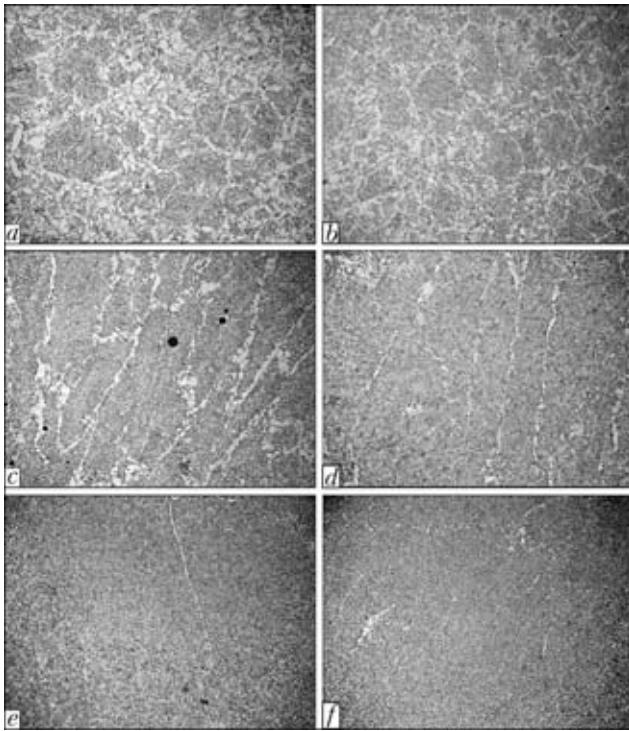
Figure 2. Microstructures (×200) in the center of sample weld: a — GNM13; b — GNM19; c — GNM13FB; d — GNM19FB; e — GNM-TiO$_2$; f — GNM-ZrO$_2$

Table 4. Quantity of structural components in the studied welds, %

Weld series	AF	PHF	PF	PlF	LB	UB	Austenite grain size, µm
GNM13FB	72	17	11	–	–	–	400
GNM09FB	80	9	11	–	–	–	350
GNM19FB	20	18	10	7	6	24	300
GNM-TiO$_2$	95	3	2	–	–	–	50
GNM-ZrO$_2$	97	1	2	–	–	–	50

Analysis of the results of mechanical testing of studied weld metal showed the non-rationality of application of Sv-08G1NMA welding wire in welding of 12KhN2MDF steel, as irrespective of the level of flux oxygen potential rather low values of yield point (473–500 MPa) and impact toughness are achieved, particularly at low testing temperatures of –20 °C (16–20 J/cm^2). Analysis of the conducted metallographic investigations showed that this is related primarily to formation of coarse-acicular ferrite and large amount of PF along the boundaries of primary crystallites (see Figure 2, a, b). This is due to considerable content in the metal of welds of this series (GNM, see Table 2) of nickel (1.5–1.6 %), molybdenum (0.25–0.26 %) at insignificant content of titanium (0.001 %), vanadium (0.005–0.009 %) and niobium (0.002 %). Thus, metal of the studied welds turned out to be «over-alloyed» by nickel and molybdenum. The forming coarse (more than 1.5 µm) nonmetallic inclusions also had a negative influence.

A more favorable combination is that of 09G2FB steel and Sv-10GNMDTA wire. Application of Sv-10GNMDTA welding wire in welding of 09G2FB steel leads to the level of nickel (0.37–0.39 %) and molybdenum (~0.1%) content in the weld metal turnig out to be much lower than in the previous combination of materials (see Table 2). Moreover, weld metal alloying by titanium (0.01–0.02 %), vanadium (0.02–0.04 %) and niobium (0.01–0.02 %) increases that results in an increase of both the total level of weld metal strength (yield point of 530–545 MPa), and their impact toughness (13–58 J/cm^2). The best values of mechanical properties were achieved at application of neutral flux (lg a_O = –1.25, GNM09FB weld series), which allowed achieving the level of about 60 J/cm^2 at testing temperature of –20 °C.

Obtained results found an explanation during analysis of microstructure of metal of GNM-FB series welds.

Analysis of the structural condition of the studied welds showed that the high contamination of GNM13FB weld (acid flux) by nonmetallic inclusions of more than 1 µm size promotes formation of solid precipitates (fringes) of PF along the grain boundaries.

Microstructure of the weld of GNM09FB series consists of finely-dispersed AF (~80 %) and small amount of PF, which is what ensures the high mechanical properties of the weld. Optimum content of dispersed titanium carbides (6.86 %) and fine inclusions of oxide type (9.68 %, see Table 5) in the microstructure allowed ensuring a fabourable combination of the values of strength, ductility and toughness

Table 5. Composition, total fraction of nonmetallic inclusions, V_{NMI}, fraction of finely-dispersed inclusions ($V_{<0.3}$) in the metal of studied welds

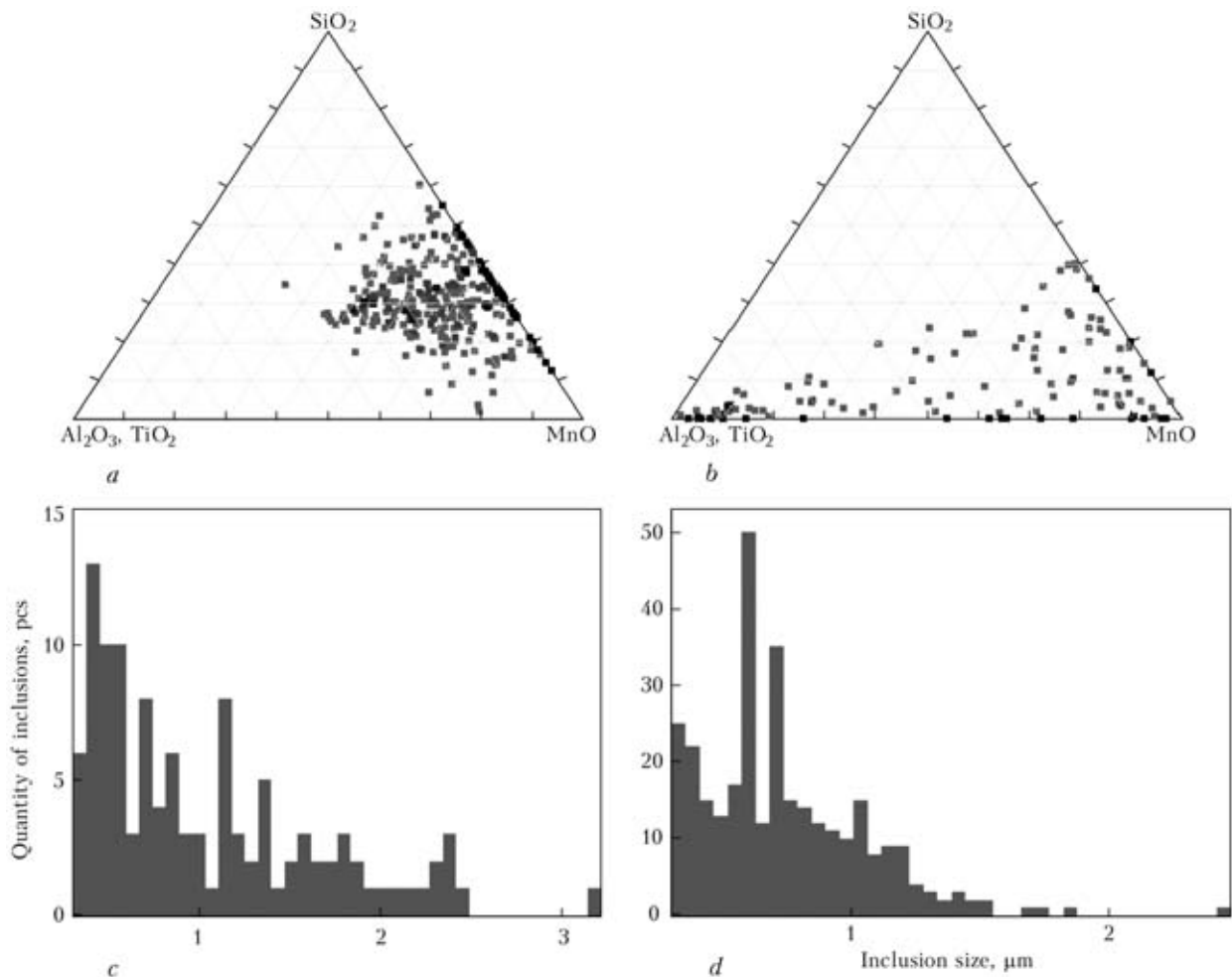| Weld series	Elemental content in inclusions, wt.%						V_{NMI}, %	$V_{<0.3}$, %
	O	Al	Si	S	Ti	Mn		
GNM13FB	25.05	5.27	15.56	1.86	3.57	48.69	0.86	11.40
GNM09FB	38.74	24.09	3.17	1.07	6.86	26.07	0.21	9.68
GNM19FB	43.81	29.39	1.08	0.79	5.82	19.12	0.10	21.56
GNM-TiO$_2$	28.44	6.62	13.56	3.34	5.47	42.56	0.33	80.34
GNM-ZrO$_2$	35.05	6.61	8.15	1.83	13.05	35.30	0.47	85.72

Figure 3. Nature of distribution of nonmetallic inclusions by composition (*a*, *b*) and dimensions (*c*, *d*) in GNM-TiO$_2$ (*a*, *c*) and GNM09FB (*b*, *d*) welds

in the metal of GNM09FB series weld, produced when welding with neutral flux (see Table 3). Here, not the dispersion, but grain boundary strengthening started having the leading role in ferrite matrix strengthening, its distinctive feature being its positive influence on increase of both the values of strength and toughness of the metal.

At formation of mechanical properties of metal in the structure of GNM19FB series weld the contribution of dispersion strengthening turned out to be too high, which is caused by a high content of finely-dispersed (< 0.3 μm, see Table 5) inclusions in the weld structure. X-ray spectral analysis of these inclusions showed that they contain a considerable amount of chromium carbides and titanium carbonitrides, which promotes formation of plate-like forms of ferrite, as well as UB, characterized by higher hardness.

Lowering of the temperature of the end of bainite transformation, formation of carbide-free bainite, combination of the content of oxide nonmetallic inclusions of up to 1.0 μm size and dispersed carbides of up to 0.3 μm size, which was ensured by the appropriate level of oxygen potential of flux 9 (lg a_O = = −1.25), promoted formation of a large amount of AF in GNM09FB weld metal. As a result, the level

of impact toughness of weld metal increased in the entire temperature range of testing (see Table 3).

Analysis of mechanical properties of welds of GNM-FB series showed that although the level of strength and ductility increased somewhat (see Table 3), compared to welds of GNM series, impact toughness values still remain on a rather low level, particularly in the field of negative temperatures. All that necessitated a search for new combinations of welding wire compositions and types of welding fluxes, in order to simultaneously ensure high values of strength, ductility and impact toughness by redistribution of alloying elements (nickel, molybdenum, titanium, vanadium and niobium) between the base metal, welding wire and flux.

In this connection, two more welds were made in the same system of base metal−welding wire. Proceeding from analysis of agglomerated fluxes currently applied in pipe-welding plants of the countries of the European Union, Russian Federation and Ukraine, their welding was performed using test flux of aluminate-basic type ((CaO + MgO) %, (Al$_2$O$_3$ + MnO) %, SiO$_2$ %, CaF$_2$ %). In one of the variants titanium oxide was added to the flux charge (weld of GNM-TiO$_2$), in another variant it was zirconium oxide (weld
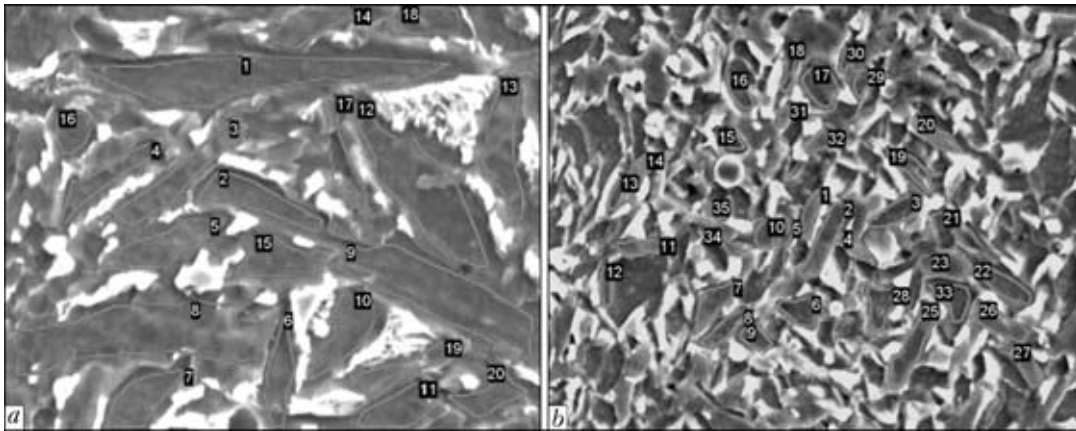
Figure 4. Comparison of AF morphology (×2000) in welds of GNM19FB (*a*) and GNM-TiO$_2$ (*b*) series (numbers show microanalysis regions)

of GNM-ZrO$_2$ series) in order to study the possibilities of improvement of mechanical properties of the weld through control of the kinetics of ferrite grain growth.

Analysis of mechanical properties of welds made with additives of titanium and zirconium oxides (see Table 3) showed that addition of TiO$_2$ and ZrO$_2$ refractory oxides to the weld pool allowed increasing the ultimate strength up to 700−710 MPa and impact toughness up to 80−102 J/cm^2 at the test temperature of −20 °C.

It was possible to interpret the obtained results when studying their microstructure. Analysis of the structural state of welds of GNM-TiO$_2$ and GNM-ZrO$_2$ series showed that the welds developed an almost completely (95 %) AF structure (see Table 4 and Figure 2, *e*, *f*).

Change of the temperatures of phase transformations during austenite decomposition in GNM-TiO$_2$ and GNM-ZrO$_2$ welds, compared to welds of GNM-FB series, was manifested in the principal difference in the type of AF formed in these welds (Figure 4).

AF forming in the weld of GNM-TiO$_2$ series is much finer (up to 1 μm) than in the weld of GNM19FB series (5−10 μm) with more chaotically located needles. This is obviously related to the influence of both primary titanium and zirconium oxides, and the possibility of initiation of ferrite needles on the secondary oxides precipitating from the melt. MAC-phase forming between the needles is finer, and has a smoothed shape (without sharp angles) and is uniformly distributed. Analysis of the content of alloying elements showed a lower content of manganese and silicon and

higher content of titanium and carbon in the ferrite needles.

Addition of TiO$_2$ and ZrO$_2$ to the flux charge leads to a considerable increase of the quantity of nonmetallic inclusions of not less than 1 μm size, compared to welds of GNM-FB series (see Figure 5, *b*, *c* and Table 5) promoting AF formation [8].

Analysis of the influence of complex alloying of weld metal on the kinetics of austenite decomposition (see Figure 1) showed an essential difference made by finely-dispersed inclusions of titanium and zirconium oxides in this process. A very gently sloping part of the curve of austenite decomposition in the temperature range of 750−650 °C indicates that in these welds austenite decomposition in the region of diffusion-induced ferrite transformation practically does not take place, whereas the main part of decomposition occurs at temperatures of 600−500 °C, i.e. in the region of low-temperature bainite (intermediate) transformation.

Increase of the cooling rate in the temperature range of 800−500 °C from 1 up to 10 °C/s, shifts austenite decomposition temperature into the region of lower temperatures, leveling off the differences in the nature of decomposition for all the studied welds (see Figure 1).

Complex alloying of weld metal by elements stabilizing the austenitic phase (manganese, nickel, molybdenum), as well as vanadium and titanium, which form carbides unstable at high temperatures, leads to formation of coarse (300−400 μm) primary austenite grains and formation of secondary structure with in-
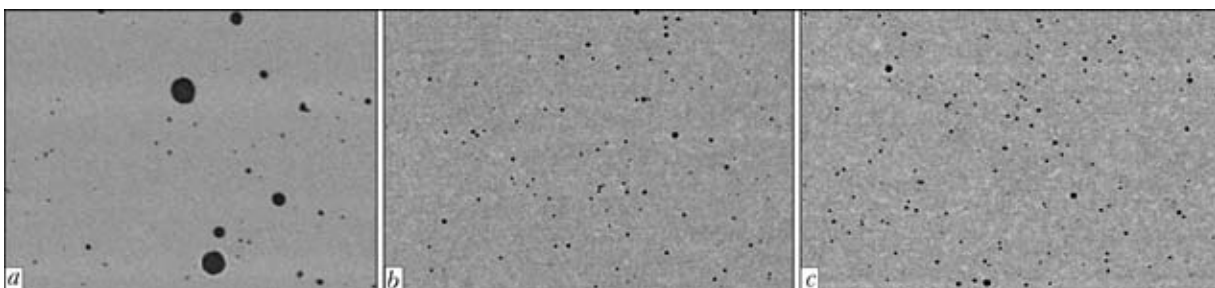

Figure 5. Microstructures (×1000) of nonmetallic inclusions in studied welds of GNM13FB (*a*), GNM-TiO$_2$ (*b*), GNM-ZrO$_2$ (*c*) series

creased content of brittle structural components. Addition of finely dispersed refractory inclusions of titanium and zirconium oxides to the weld metal allowed a considerable reduction of the size of primary austenite grain (to 50 μm) and shifting the transformation region into the low temperature zone, thus promoting formation of AF (up to 95−97 %). In this case weld metal has an optimum combination of the values of strength, ductility and toughness to the level corresponding to the requirements made of metal of welds of strength grade K65 ($\sigma_{0.2} > 570$ MPa, $\sigma_t > 620-700$ MPa, $KCV_{-20} > 98$ J/cm^2 according to specification of Khartsyzsk Pipe Plant) and higher.

Thus, in order to ensure a combination of high values of strength, ductility and impact toughness, secondary microstructure of the metal of welds of the studied alloying system should form in the low-temperature region of bainite transformations and should contain more than 50 % of structural components of higher toughness (carbide-free bainite, AF). Size of ferrite grains of such a structure should not be higher than 100 μm (up to 50 μm is optimal). To achieve a fine-grained structure it is necessary to add niobium and vanadium to the weld metal and ensure their carbide formation. Complex alloying of the weld (nickel, molybdenum, titanium, vanadium and niobium) is limited to the requirement, in keeping with which solid-solution strengthening of the structure should be lower than grain-boundary and dispersion strengthening. Parameters of welding consumables should ensure formation of finely-dispersed nonmetallic inclusions and carbides (carbonitrides) of alloying elements (titanium, vanadium, molybdenum) in the weld metal.

CONCLUSIONS

1. Investigations confirmed the advantages of application of agglomerated (ceramic) fluxes in welding HSLA steels. Ceramic fluxes of aluminate-basic type should be used to improve the mechanical properties of the metal of welds of HSLA steels that will allow simultaneous improvement of strength, ductility and impact toughness of weld metal.

2. It is not rational to use Sv-08G1NMA welding wire in welding of 12KhN2MDF steel, as the achieved strength ($\sigma_t = 473-500$ MPa) and impact toughness ($KCV_{-20} = 16-20$ J/cm^2) values are rather low, irrespective of the level of flux oxygen potential.

3. To ensure high mechanical properties in welding 09G2FB steel with Sv-10GNMDTA welding wire, it is rational to use neutral flux with the level of oxygen potential lg $a_O = -1.25$. Complex alloying of weld metal allows achieving high values of strength ($\sigma_t = 680$ MPa) and impact toughness ($KCV_{-20} = 58$ J/cm^2).

4. Oxygen potential and complex alloying ability of welding consumables should be selected so as to ensure formation of nonmetallic inclusions consisting predominantly of dispersed oxides (of up to 1.5 μm size) and finely-dispersed carbides and carbonitrides (of up to 0.3 μm size) in the weld metal. Composition and volume fraction of the oxide phase determine the conditions of formation of AF structure, carbides and carbonitirdes control formation of bainite structures.

5. Addition of finely-dispersed refractory inclusions of the type of titanium and zirconium oxides to the weld metal allows a considerable lowering of the size of primary austenite grain (to 50 μm) and shifting the transformation region into that of low temperatures, promoting formation of a completely acicular structure (up to 95−97 %). High values of strength ($\sigma_t = 700-710$ MPa) and impact toughness ($KCV_{-20} = 80-100$ J/cm^2) are achieved as a result of complex alloying of weld metal and adding titanium and zirconium oxides to the metal.

1. Goldshtejn, M.I., Farber, V.M. (1979) *Dispersion strengthening of steel*. Moscow: Metallurgiya.
2. Lagneborg, R., Sivetsky, T., Zayats, S. et al. (2001) *Role of vanadium in microalloy steels*. Ekaterinburg: Mariya.
3. Khajsterkami, F., Khulka, K., Matrosov, Yu.I. et al. (1999) *Niobium-containing low-alloy steels*. Moscow: Internet Engineering.
4. Pokhodnya, I.K., Golovko, V.V., Denisenko, A.V. et al. (1999) Effect of oxygen on formation of acicular ferrite structure in low-alloy metal of welds. *Avtomatich. Svarka*, **2**, 2−10.
5. Ito, G., Nakanishi, M. Study on Charpy impact properties of weld metals with submerged arc welding. *IIW Doc. XI-A-113−75*.
6. Svensson, L.-E., Gretoft, B. (1990) Microstructure and impact toughness of C−Mn weld metals. *Welding Res. Supp.*, Dec., 454−461.
7. Evans, G.M. The effect of carbon on the microstructure and properties of C−Mn all-weld-metal deposits. *IIW Doc. II-A-546−81*.
8. Cole, W., Colvin, P. (1971) Submerged arc welding of higher tensile steels. *Metal Constr. and British Welding J.*, **3**, 131−135.

DAMPING OF WELDING CURRENT FLUCTUATIONS IN ROBOTIC ARC WELDING

G.A. TSYBULKIN

E.O. Paton Electric Welding Institute, NASU, Kiev, Ukraine

The possibility of damping undesirable current fluctuations in welding circuit was considered. A criterion was derived which allows assessment of damping properties of welding circuit directly by its parameters.

The character of dynamic processes running in welding circuit in consumable electrode arc welding is defined, as is known, by parameters of the circuit itself. One of the fundamental requirements for the choice of these parameters is providing stable dynamics for a wide range of modes being applied. Therefore the issues of stability have always been of a proper attention. In particular, the conditions of stability for the case of fixed parameters were profoundly studied and corresponding criteria were obtained [1–4]. The results of further investigations [5–8] regarded issues of stability in mechanized and automatic arc welding. In the recent time the influence on stability of parametric disturbances, caused by electric current fluctuations in arc column [9] and non-controlled change of contact resistance in current conducting tip of a torch in welding process, was investigated [10]. The influence on stability of so-called small parameters, in particular, lag of arc discharge [11] was also investigated.

Therefore it is necessary to note that in manual arc welding the conditions of stability are practically fulfilled in the whole range of applied welding currents. It is predetermined, first of all, by the fact that steepness of external characteristics of welding current source is selected as a rule as steep falling, and welding electrodes are used of rather large diameter. Such combination of parameters, as is shown below, provides not only stable but also aperiodic mode, at which transition processes in welding circuit are running without free (natural) fluctuations, which favorably affects the quality of welding process itself.

Somewhat different characteristics are peculiar for robotic arc welding. Its distinctive feature is application of consumable electrode wire of small diameter and welding current sources with more rigid external characteristics. Namely in that case the so-called loss of aperiodicity can occur and, as a consequence, fluctuation processes can occur in welding circuit due to different disturbances (especially at the beginning of welding) not contributing to the quality of welding performance. To damp undesirable fluctuations of

welding current one should know the conditions (criteria) first of all which result in running only aperiodic processes in welding circuit.

Thus, it turns out to be necessary to define the aperiodicity criterion itself which could be used at preparation of equipment for robotic arc welding. In the present work such criterion has been derived.

Let us examine welding circuit as a system with negative feedback by the rate of electrode melting. Due to this feedback the rate of electrode melting, arc length and welding current in welding process are automatically maintained at the specified level (in literature this effect is known as arc self-adjustment).

According to [12] the system under consideration can be introduced in dynamic relation by a one «folded» link with the operator transferring function

$$W(D) = \frac{\Delta v_m(t)}{\Delta v_e(t)} = \frac{1}{T_e T_s D^2 + T_s D + 1}, \qquad (1)$$

where $D = \mathrm{d}/\mathrm{d}t$ is the operator of differentiating; t is the current time; $\Delta v_m(t)$, $\Delta v_e(t)$ are the deviations of rate of melting and feed of electrode from nominal values, respectively; T_e, T_s are the constants of time, defined by relations

$$T_e = \frac{L}{R_*}, \qquad (2)$$

$$T_s = \frac{R_*}{EM}. \qquad (3)$$

Here L is the inductance of welding circuit; E is the intensity of electric field in arc column; $M \equiv \partial v_m/\partial i$ is the steepness of characteristics of electrode melting at nominal value of welding current i; R_* is the total resistance of a circuit, calculated according to the formula

$$R_* = R + S_a - S_s, \qquad (4)$$

where R is the summed resistance of current-carrying wires, electrode stickout and sliding contact in the torch nozzle; $S_a \equiv \partial u_a/\partial i$, $S_s \equiv \partial u_s/\partial i$ is the steepness of volt-ampere characteristics of arc and source of welding current, respectively, at nominal value of a current i; u_a, u_s is the arc voltage and output terminals of welding current source, respectively.

Having used the following relation from the work [13]:

$$M = P / d^2,$$

where P is the parameter characterizing thermal physical properties of electrode material (density, temperature of melting and boiling, specific heat capacity and work of electron outlet); d is the diameter of consumable electrode, let us write the expression (3) as a function of R_* and d:

$$T_s = \frac{R_* d^2}{EP}. \tag{5}$$

Now disposing the dependencies (2) and (5) as a criterion of aperiodicity one can accept the relation

$$T_s > 4T_e, \tag{6}$$

at the performance of which the both roots of distinguishing equation corresponding to denominator of transfer function (1) are substantial, different and negative [14, 15]. Consequently, in this case welding circuit represents aperiodic link in structural relation. Violation of the condition (6) transfers this link to the fluctuating one. Therefore, the constant of time T_s defining lag of welding circuit is at the same time a damping factor, as with increase of T_s the decrease of natural fluctuations in welding circuit until their complete disappearance occurs.

Substituting the (2), (5) into inequality (6), we shall obtain the expression

$$R_* d > 2 \sqrt{PLE}, \tag{7}$$

which is the criterion of aperiodicity for the processes running in welding circuit. The criterion (7) considering the expression (4) can be presented in the form of

$$S_s < - \frac{2\sqrt{PLE}}{d} + (R + S_a). \tag{8}$$

On the right side of the inequality (8) all values of parameters, except d, are constant and known beforehand. Consequently, to define the field of aperiodicity of processes in welding circuit it is enough to plot a diagram of dependencies $S_s = S_s(d)$ at preset values of the rest parameters.

In the Figure, a curve $S_s(d) = - \frac{2\sqrt{PLE}}{d} + (R + S_a)$ at $P = 0.53$ mm^3/(A·s), $L = 10^{-3}$ H, $E = 2$ V/mm, $R = 0.015$ Ohm, $S_a = 0.005$ Ohm, $d = 0.2{-}6.0$ mm is presented. It represents a boundary between regions of aperiodicity and damping fluctuating processes. It is seen form the Figure that for electrodes of large diameters the aperiodic character is preserved practically at any slope of falling external characteristic of welding current source. With the decrease of the value d the margin of aperiodicity is sharply decreased. Therefore, at small values of d, which are used as a rule in robotic arc welding, the appropriate value of steepness S_s applied for welding current source should
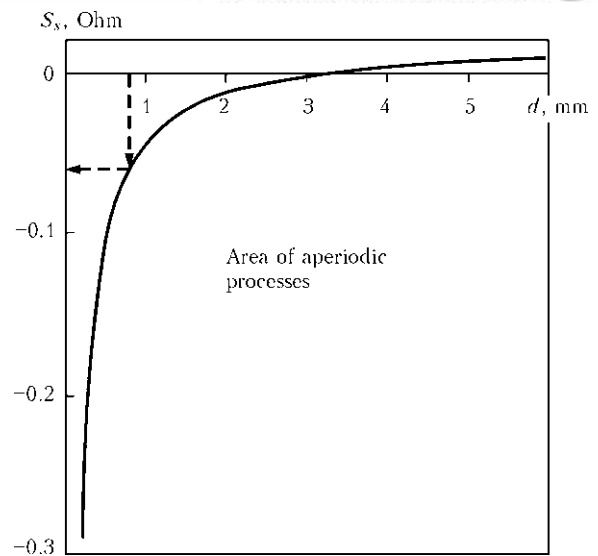
Boundary between areas of aperiodic and fluctuating processes

be preliminary calculated according to the formula (8) for damping of undesired fluctuations. For example, if the steepness S_s is selected larger (according to the absolute value) than $|S_s| = 0.07$ Ohm at $d = 0.8$ mm and mentioned values of other parameters (see the Figure) are considered, only aperiodic processes will run in welding circuit.

Thus using criterion of aperiodicity (8) one can easily calculate the necessary slope of external characteristics of welding current source for any diameter of consumable electrode, at which the welding circuit itself will provide damping of undesired fluctuations in robotic arc welding.

1. Nikitin, V.P. (1934) *Electric machines and transformers for arc welding*. Moscow; Leningrad: Energoizdat.
2. Paton, B.E. (1951) Stability of arc burning in welding circuit containing inductance with saturated steel magnetic core. *Automatich. Svarka*, **2**, 56−63.
3. Paton, B.E. (1952) Self-adjustment of arc in consumable electrode welding. *Ibid.*, **1**, 38−45.
4. Rabinovich, I.Ya. (1964) Some problems of theory of stability of power sources and adjustment systems for arc welding. In: *New problems of welding technique*. Kiev: Tekhnika.
5. Lenivkin, V.A., Dyurgerov, N.G., Varukha, E.N. (1981) Increase in arc stability during consumable electrode welding with straight polarity current. *Svarochn. Proizvodstvo*, **12**, 28−30.
6. Sudnik, V.A., Erofeev, V.A., Logvinov, R.V. (1999) Investigation of stability of shielded arc welding process. *Izvestiya TGU*. Series Computer Technologies in Joining of Materials. Ed. by V.A. Sudnik. Tula: TGU.
7. Tsybulkin, G.A. (2002) To the question of GMAW stability. *The Paton Welding J.*, **5**, 14−16.
8. Dyurgerov, N.G., Sagirov, Kh.N. (2009) Stability of system of arc self-adjustment in mechanized and automatic welding. *Svarochn. Proizvodstvo*, **2**, 13−14.
9. Tsybulkin, G.A. (2002) About effect of electric field fluctuations in arc column on arc welding process stability. *The Paton Welding J.*, **6**, 38−39.
10. Tsybulkin, G.A. (2003) Effect of sliding contact in current conductor of torch on stability of arc welding process. *Ibid.*, **12**, 37−38.
11. Tsybulkin, G.A. (2008) On the influence of small parameters on MIG/MAG welding stability. *Ibid.*, **8**, 22−25.
12. Tsybulkin, G.A. (2010) Evaluation of quality of the arc self-adjustment process. *Ibid.*, **2**, 11−13.
13. Korinets, I.F. (1995) Mathematical model of electrode wire melting in arc welding. *Automatich. Svarka*, **10**, 39−43.
14. Jury, E. (1979) *Innory and stability of dynamic systems*. Moscow: Nauka.
15. Polyak, B.T., Tsypkin, Ya.Z. (1994) Robust aperiodicity. *Doklady AN SSSR*, 335(**3**), 304−307.

PECULIARITIES OF FORMATION OF STRUCTURE IN THE TRANSITION ZONE OF THE Cu–Ta JOINT MADE BY EXPLOSION WELDING

B.A. GRINBERG[1], **O.A. ELKINA**[1], **O.V. ANTONOVA**[1], **A.V. INOZEMTSEV**[1], **M.A. IVANOV**[2],
V.V. RYBIN[3] and **V.E. KOZHEVNIKOV**[4]

[1]Institute of Metal Physics, RAS Ural Division, Ekaterinburg, Russia
[2]G.V. Kurdyumov Institute for Metal Physics, NASU, Kiev, Ukraine
[3]A.M. Prokhorov Academy of Engineering Sciences, St-Petersburg, Russia
[4]OJSC «Ural Chemical Engineering Factory», Ekaterinburg, Russia

Structure of the transition zone in a joint of metals having no mutual solubility was studied. It was determined that surface of the explosion welded Cu–Ta joint is not smooth, but contains protrusions with a size of about 5–10 μm. The transition zone of the joint consists of chaotically distributed non-melted regions of copper and tantalum, as well as zones of local melting of copper containing tantalum nanoparticles 30–50 nm in size. Two processes, i.e. formation of protrusions at the interface and local melting zones, determine stirring of the materials having no mutual solubility.

At a wide variety of materials and welding conditions, an important problem in explosion welding is stirring in the transition zone near the interface in the welded joints. It is structure of the transition zone that determines the possibility of adhesion of two materials. Stirring is a complex process for different pairs of the materials joined, especially for the metal–intermetallic pair, as well as for metals having no mutual solubility.

Difficulties in welding metals to intermetallics are caused by the fact that, firstly, the latter are high-temperature chemical compounds with strong interatomic bonds, and, secondly, they are characterised by increased brittleness. Nevertheless, explosion welding provided a joint between titanium and orthorhombic titanium aluminide [1–9].

The problem of stirring is not less important for metals having no mutual solubility. To find out how important the presence of mutual solubility of the initial materials is the pair of copper and tantalum, which have no mutual solubility and form immiscible suspensions in liquid state, was chosen for explosion welding. The principle of formation of such suspensions is investigated in this study.

Tantalum of grade TVCh and copper M1 were used as initial materials. Welding was performed at Open Joint Stock Company «Ural Chemical Engineering Factory» (Ekaterinburg, Russia) by using different schemes and different parameters. After that the joints were selected for further investigations. The parallel arrangement of plates was used. Thickness of the tantalum plate was 1 mm, and that of the copper plate was 4 mm, the gap between the plates being 1 mm. The copper plate was a flyer plate with respect to the tantalum one, which lay on a support plate of titanium and steel with thickness of 4.5 + 20 mm. The detonation velocity was 2680 m/s. The plates collided at an angle of 5.22° at a velocity of 234 m/s. The choice of the welding parameters corresponded to a lower limit of weldability. These welding conditions traditionally applied by «Khimmash» are most cost effective because of a smaller charge and, hence, lower expenses for explosives. Moreover, this diminishes the impact of the detonation wave on the surrounding facilities.

Metallographic analysis was performed by the optical microscopy (OM) method using optical microscope «Epiquant» equipped with computation system SIAMS. Microstructure of the welded joints was examined by the transmission electron microscopy (TEM) method using transmission electron microscopes «JEM 200CX» and «CM-30 Super Twin», by the scanning electron microscopy (SEM) method using scanning electron microscopes «Quanta 200 3D» and «Quanta 600» with a maximal resolution of about 2 nm, as well as by using ion gun «Faschione 1010 ION MILL».

It can be clearly seen in microstructures of transverse sections of the transition zone of the Cu–Ta joint that the interface is heterogeneous (Figure 1, *a*) and has thickness of about 5–10 μm (Figure 1, *b*, *c*). It turned out that the interface of the investigated joint is not wavy but corrugated, which can be readily seen in microstructure of a longitudinal section of the Cu–Ta joint interface (Figure 2). Instead of parallel bands characteristic of the corrugated interface, the microstructure consists of spots of three colours: white, black and gray. This is indicative of the fact that the transition zone comprises chaotically distributed regions of three types. These regions in the longitudinal section of the Cu–Ta interface (see Figure 2) have
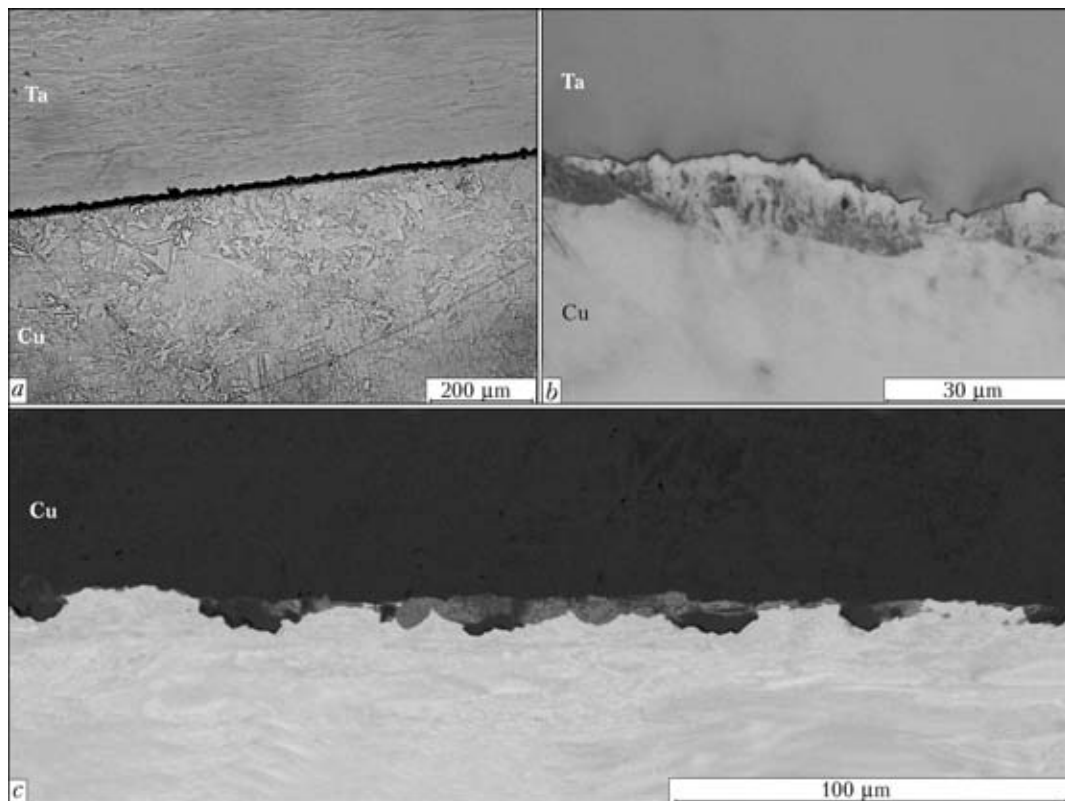
Figure 1. OM (*a, b*) and SEM (*c*) microstructures of transverse section of the Cu−Ta joint interface

approximately identical sizes (30−50 μm). Also, they can be seen in microstructure of the transverse section of the interface (see Figure 1, *c*).

In the Cu−Ta joint, the titanium to aluminide interface is not smooth. It comprises protrusions that can be readily seen in Figure 1 at different magnifications. Supposedly, it is these protrusions that determine the shape of the interface (see Figure 1, *a*) in the transverse section of the Cu−Ta joint interface and presence of regions of the three colours in the longitudinal section (see Figure 2). The protrusions (see Figure 1, *c*) are about 5−10 μm in size. Earlier [5] the protrusions were detected in the transition zone of the titanium−orthorhombic titanium aluminide joint. The depth of their penetration from one material into the other was tens of micrometres.

The data on chemical composition of the regions of three colours, which form the transition zone, were obtained by SEM on the basis of numerous measurements. It was determined that the white colour corresponds to the tantalum zone and black colour — to copper. Particular attention was given to a region of the gray colour, which was hereafter referred to as the gray zone. Figure 3 is extremely important for revealing its structure. This Figure shows at different magnifications the longitudinal section of the transition zone after complete etching out of copper. Tantalum particles having mostly nanometric sizes can be seen on the surface of tantalum (Figure 3, *b*).

In cases where copper was not etched out, it was detected at a magnification of 5000 that the concentration of both metals in the gray zone was approxi-

mately the same. However, as can be seen at a higher magnification (12,000), structure of the gray zone is heterogeneous and the concentration of both metals is different, i.e. some regions contain more copper, and other regions contain more tantalum. At the same time, the internal structure of the gray zone remains indiscernible until a higher magnification is used. Structuring of the gray zone begins at a magnification of 25,000 (Figure 4, *a*). The white zone of tantalum and the black zone of copper can be seen nearby. The microheterogeneous structure of the gray zone is even more pronounced in the microstructure revealed at a high magnification (Figure 4, *b*). This type of the structure evidences that the gray zone is a zone of stirring. The alternating microvolumes of the white
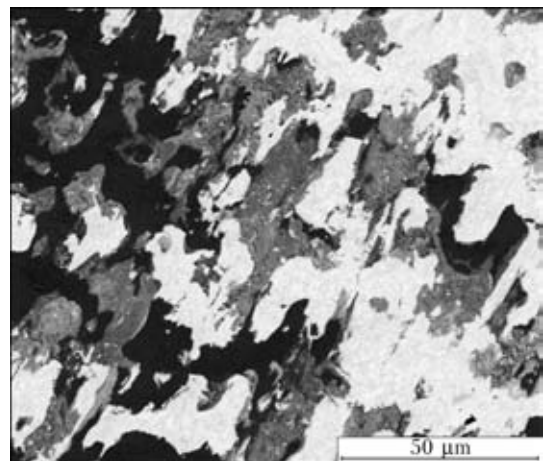

Figure 2. SEM microstructure of longitudinal section of the Cu−Ta joint interface (white spots — tantalum, black spots — copper, gray spots — mixture of tantalum and copper)
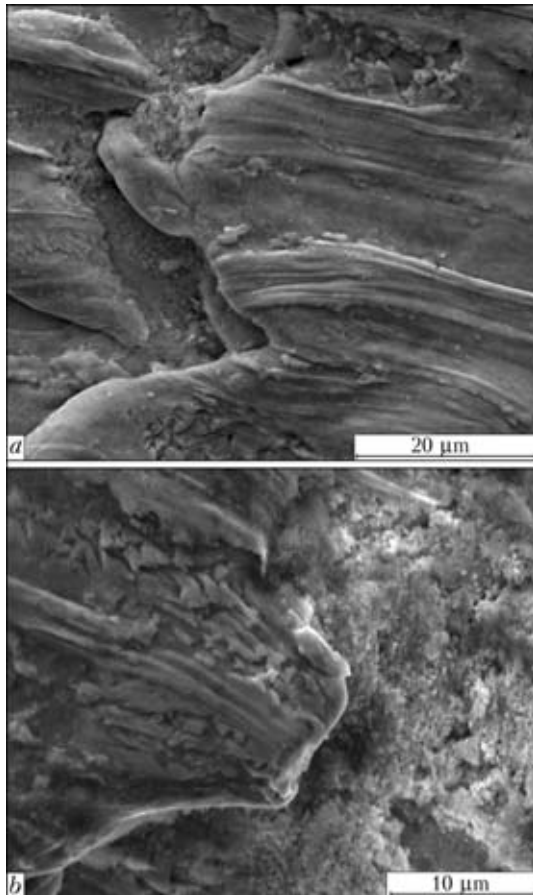
Figure 3. SEM microstructures of longitudinal section of the Cu–Tal joint transition zone (copper is fully etched out)

Figure 4. SEM microstructures of longitudinal section of the Cu–Ta joint at different magnifications

and black colours inside the gray zone are different. Only the black regions (copper) are elongated.

Examination of the Cu–Ta joints by the TEM method involves difficulties. Selection of reagents to prepare foils for such dissimilar materials is very complicated, as copper might be fully etched out under the effect of the reagents suitable for tantalum. In this connection, for this study the foils were made by using an ion gun.

Microstructure of the gray zone revealed by TEM gives an idea of the above microvolumes. Note that tantalum is of a dark shade in these images. Many dark particles with a shape close to the spherical one, the sizes of which are approximately 30–50 nm, can be seen in the light-field image (see Figure 5, *a*). Figure 5, *b* clearly shows a system of rings consisting of separate reflexes, which were decoded to belong to tantalum. Intensive spot-like reflexes are reflections of copper. It can be considered that nanoparticles of tantalum remain on its surface after etching out of copper (see Figure 3). Figure 6, *a*, *b* shows a light-field image of the gray zone at different magnifications. The dark particles can be seen here, like in Figure 5. Figure 6, *c*, *d* shows the dark-field images of the same joining zone as in Figure 6, *b*, in reflex <111> Cu and reflex <110> Ta, respectively. The particles of tantalum can be seen in both dark-field images. Electron-diffraction pattern reveals a substantial disorien-

tation of both tantalum and copper particles, as well as the presence of individual amorphous interlayers having a characteristic microdiffraction, which consists of two diffusion rings.

Figure 7 also shows the particles of copper oxides. As indicated by the calculation of interplanar spacings, they sufficiently accurately coincide with the values obtained for Cu_2O. The possible cause of formation of copper oxides is as follows. When the plates collide, a shock-compressed gas saturated with fine copper particles is formed in the welding gap ahead of the contact point. It can be suggested on the basis of the data of study [10] that copper oxides are formed as a result of their burning. The surface layer of tantalum participating in formation of the joint has a higher thermal conductivity than copper, and is heated to a much lower temperature than copper. Possibly, this is a cause of the absence of tantalum oxides.

In addition to the gray zone, the transition zone comprises the above-mentioned zones of copper and tantalum (see Figure 2). As indicated by the analysis performed by the TEM method, all these zones do not experience melting and have a structure typical of intensive plastic deformation: both materials are characterised by the presence of a band structure and recrystallised regions. The size of grains in these regions is about 100–300 nm, which is several orders of mag-
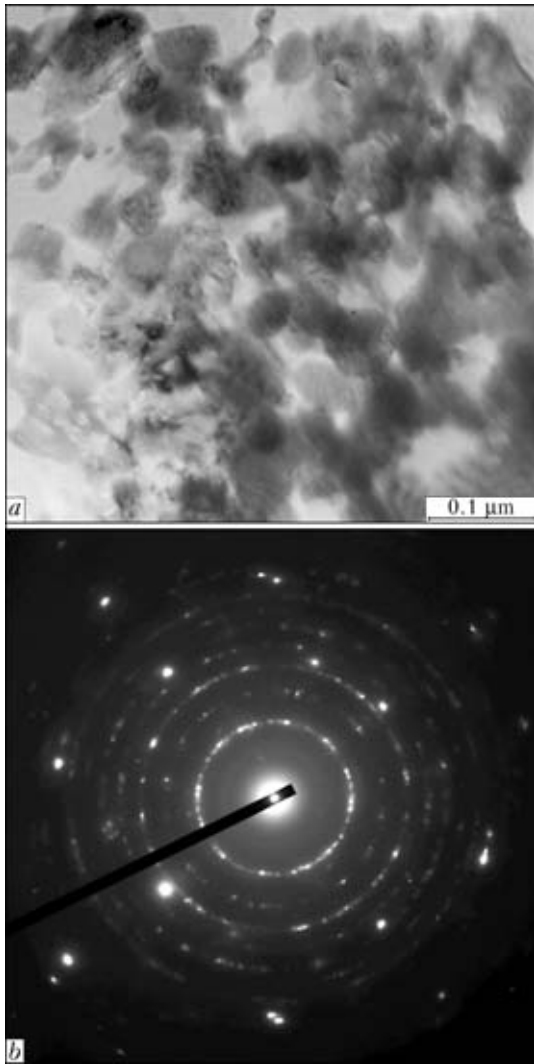
Figure 5. TEM microstructure of gray zone of the Cu–Ta joint: *a* — light-field image; *b* — microdiffraction pattern
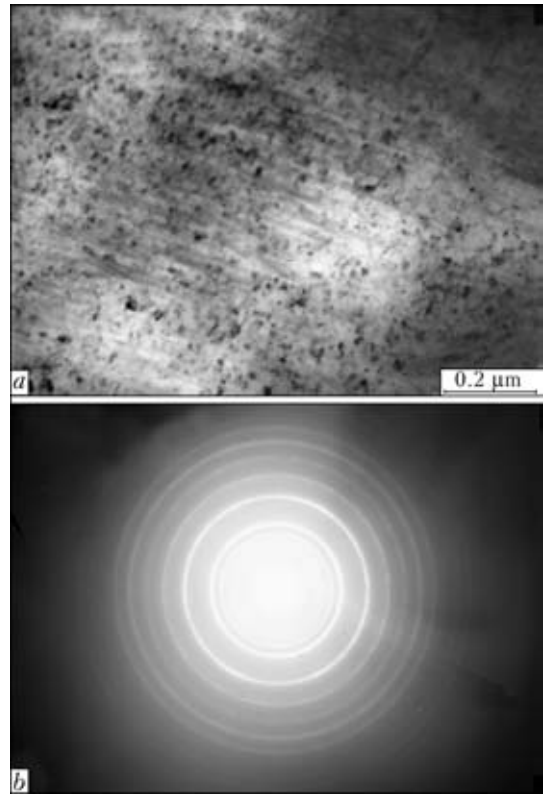
Figure 7. Light-field TEM image of copper oxides in the Cu–Ta joint (*a*) and microdiffraction pattern (*b*) [8]

nitude smaller than the initial size (approximately 100 μm). Also, a high density of dislocations and twins is fixed.

Different notions of the mechanisms of weldability are available [11]. According to one of them, the process of formation of a welded joint requires only atomic-pure and atomic-smooth surfaces. Moreover, because of a high pressure the process occurs in a solid state
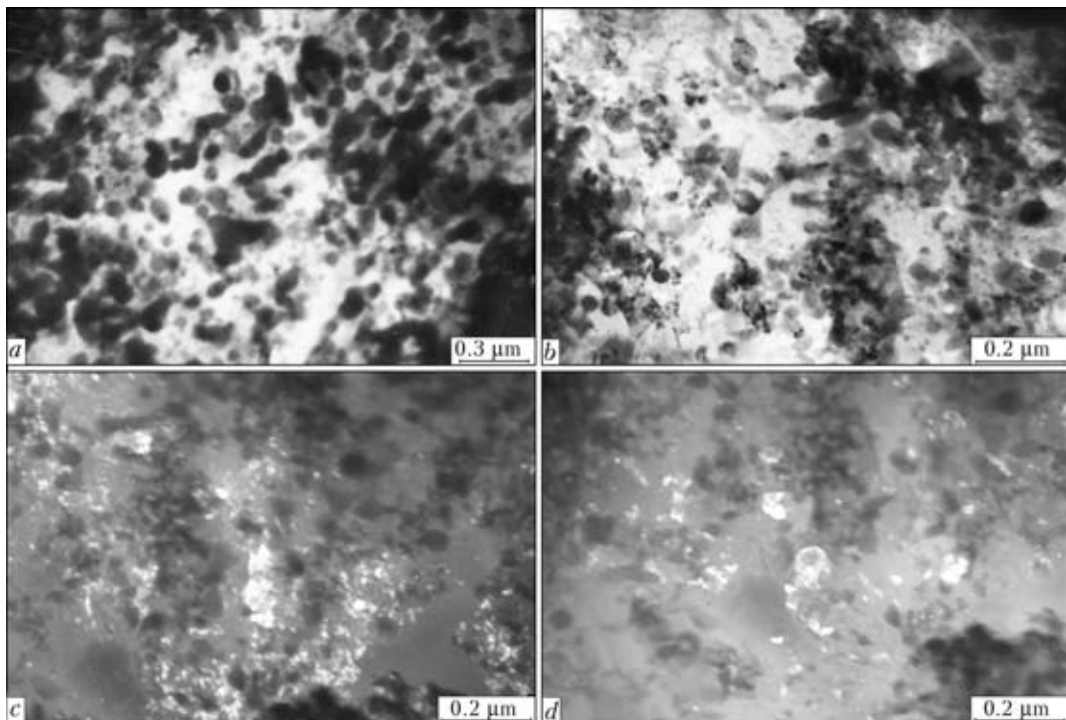
Figure 6. TEM microstructure of gray zone of the Cu–Tal joint (*a–d* — see in the text)

and excludes melting. According to other notions, good weldability is provided by formation of a continuous submicron layer, which solidifies extremely rapidly. Study [11] contains descriptions of numerous models of stirring, and some of them are discussed in study [5].

We think that stirring at the atomic level does not take place in materials having no mutual solubility. Otherwise they could form true solutions. This fact forms the basis of further development of the notion of colloidal systems in regions of local melting, which was confirmed by the structural examination results obtained in this study. Furthermore, the notion that the weldability requires only atomic-smooth surfaces does not agree with the presence of protrusions at the interface (see Figures 1 and 2). Formation of protrusions near the interface, compared to natural roughness of the initial samples, proves that they are formed particularly during the welding process. As a result, regions filled with any of the materials welded can be found on each side near the interface, which is indicative of their interpenetration. In fact, protrusions act as «nails» providing adhesion of the surfaces. It's true, especially if we allow for a high microhardness of tantalum (about 3000 MPa), which is 3 times as high as that of copper. The protrusions are formed as a result of a strong external effect of a number of factors: high plastic deformation (including pressure, shear components, turning moments of stresses, heterogeneity of deformation, etc.), friction of the surfaces, effect of the cumulative jet, etc.

The developed plastic deformation is characterised by the fact that it always occurs in bursts [12]. So, we suggest the following scenario of formation of gray zones as regions of local melting in locations where the external effect is strongest. Here there is no continuous molten layer, which was mentioned above. We give just the rounded values of temperature, as we know its different values, which differ because of composition and methods used to produce materials. At a normal pressure the boiling temperature of tantalum is $T_b^{Ta} = 5700$ K, its melting temperature is

Figure 8. SEM image of vortices in the Cu−Ta joint

$T_m^{Ta} = 3300$ K, while the boiling temperature of copper is $T_b^{Cu} = 2800$ K, and its melting temperature is $T_m^{Cu} = 1400$ K. At a high pressure the characteristic temperature values increase, but it can be assumed that their sequence persists: $T_b^{Ta} > T_m^{Ta} > T_b^{Cu} > T_m^{Cu}$.

Assume that in explosion welding the temperature that is a bit higher than T_m^{Ta} is achieved in some individual regions, thus causing melting of tantalum [13]. Boiling of copper (so-called boiling with forced circulation) occurs at the said temperature, leading to formation of a vapour, which contains the scattered tantalum droplets having a spherical shape, this minimising their surface energy. The vapour may also contain a small amount of the copper droplets. In transition to a temperature below T_m^{Ta}, the tantalum droplets will immediately solidify, and will not change thereafter. Below T_b^{Cu}, neither vapour nor droplets of copper are formed, but only its uniform melt is produced. Because of a short duration of the welding process, these transitions occur during a time of about a microsecond. In transition through T_m^{Cu} the copper melt solidifies at a residual temperature.

Vortices similar to those taking place in many joints could be formed in the copper melt. The titanium−orthorhombic titanium aluminide joint, which we investigated earlier, contains local zones with a laminated structure in the form of concentric rings that copy in shape the contour of a cavity wherein melting occurred. The size of the vortex zones is about 50−100 μm. Optical microphotographs of the vortex zones are given in studies [5, 6, 8]. However, no vortices are seen in optical microphotographs of the Cu−Ta joint. The vortices are seen in the SEM microphotographs obtained at high magnification (Figure 8), but they do not look like the above vortices either in shape or in size (about 0.5 μm), and appear very rarely. The issue of their origin is unstudied as yet.

The key assumption used as a basis of our scenario is the possibility of melting of tantalum. This possibility is really implemented in many joints on refractory metals, such as Mo−Fe, Mo−Cu, Nb−Ti and Nb−Zr [14]. Note the following fact [14]: vortices are formed in welding of niobium to titanium alloys, which evidences melting of niobium.

What is important is that in the case investigated the gray zone is a dispersed system, the different stages of formation of which are characterised by changing of the dispersed medium and dispersed phase (this fact was mentioned above). In any case, the dispersed phase is a finely scattered material (tantalum) with linear sizes smaller than 100 nm, whereas the dispersed medium is a homogeneous material (copper) with the dispersed phase distributed in it. Dispersed systems with such characteristics are usually called colloidal [14]. They take an intermediate position between true solutions, on the one hand, and coarse-dispersed systems (emulsions and suspensions), on the other hand.
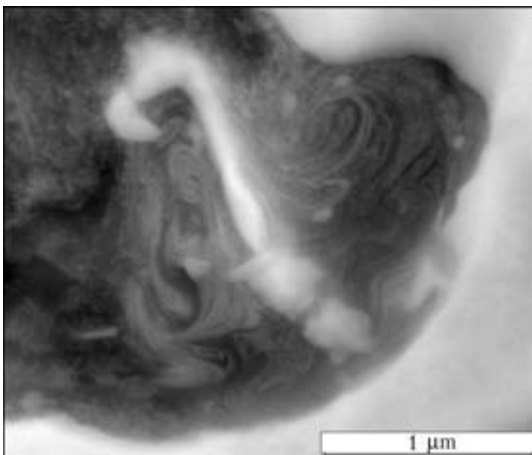
Therefore, the gray zone is a solidified colloidal system consisting of two immiscible phases.

Nevertheless, there is an alternative version of the scenario — scattering of tantalum in solid state into particles, which is a case of explosion welding of orthorhombic titanium aluminide to titanium. Figure 7 shows a fragmented layer consisting of the orthorhombic aluminide particles, and Figure 8 shows penetration of these particles into the zone of local melting of titanium. Comparison of the two joints clearly indicates a difference between the aluminide and tantalum particles. Thus, the aluminide particles, unlike the tantalum particles, have an irregular shape, rather than the spherical one. Moreover, they have micron and submicron sizes, this being an order of magnitude larger than size of the tantalum particles, which in fact are nanoparticles. It is the spherical shape of the tantalum particles and their small sizes that allow us to prefer the first version of the scenario.

Therefore, the choice of the scenario is reduced to the choice between two versions of formation of the tantalum particles, i.e. from the molten or solid phase.

To explain why scattering of tantalum in the solid state is difficult, it should be taken into account that brittleness of the materials leads to their refining under a strong external effect. Tantalum is a ductile material, capable of deforming to a high degree of deformation (approximately by 45 %, tension at room temperature). In this connection, mechanical refining of tantalum to nanoparticles can hardly be expected, considering that even a more brittle orthorhombic aluminide does not transform into a powder during explosion welding. In addition, we conducted a simulation experiment. Plates of tantalum and orthorhombic titanium aluminide (alloy VTI-1) were subjected to forging. Omitting details of the experiment, note that we used pneumatic hammer M-413 with impact energy of 5300 J, and placed both plates into one jacket of titanium foil. When we opened the jacket, we found out that the tantalum plate became flat and the aluminide plate crumbled.

The data obtained allow a conclusion that the transition zone of the joint consists of the copper and tantalum regions that experienced no melting, as well as zones of local melting of copper, which contain tantalum nanoparticles in the form of solidified droplets.

The local zones, where the external effect was strongest, require special consideration, as strength of the joints is determined particularly by these zones. Melting is one of the efficient processes leading to dissipation of the kinetic energy of the flyer plate. The local melting zones are «inserts» in the transition zone, having a different structure compared to the surrounding. It can be assumed that the resulting structure of the zones provides strengthening of the entire joint, rather than causing its brittleness. Microhardness was measured at different points of the transition zone, and it was established that microhard-

ness of copper and tantalum increased insignificantly compared to the initial values. However, microhardness of the gray zone is over 4000 MPa, which is approximately 1000 MPa higher than that of tantalum. The observed effect is a result of dispersion hardening of copper due to the tantalum nanoparticles.

The process of formation of protrusions at the interface and local melting zones is determined by stirring of the materials having no mutual solubility. Mutual solubility is not required for interpenetration of one material into the other by way of formation of protrusions. Interpenetration of the materials in the local melting zones is provided by their scattering into droplets and intensive stirring owing to circulation of the melt, which prevents separation of the colloidal system into components during the time period required for solidification of the refractory liquid.

Electron microscopic examinations were carried out at the Electron Microscopy Shared Use Centre of the Ural Division of the Russian Academy of Sciences (Ekaterinburg, Russia).

1. Greenberg, B.A., Rybin, V.V., Antonova, O.V. (2005) Microstructure of bimetallic joint of titanium and orthorhombic titanium aluminide (explosion welding). In: *Severe plastic deformation: toward bulk production of nanostructured materials.* New York: Nova, 533–544.
2. Rybin, V.V., Semenov, V.A., Sidorov, I.I. et. al. (2009) Bimetallic joint of orthorhombic titanium aluminide and titanium alloy (diffusion welding, explosion welding). *Voprosy Materialovedeniya,* 59(**3**), 17–31.
3. Rybin, V.V., Grinberg, B.A., Antonova, O.V. et al. (2009) Formation of vortices in explosion welding (titanium—orthorhombic titanium aluminide). *Fizika Metallov i Metallovedenie,* 108(**4**), 371–384.
4. Grinberg, B.A., Rybin, V.V., Ivanov, M.A. et al. (2009) Nanostructure of vortex during explosive welding. In: *Proc. of 4th NANOSMAT Conf.* (Rome, 2009), 220.
5. Rybin, V.V., Grinberg, B.A., Ivanov, M.A. et al. (2010) Structure of transition zone in explosion welding (titanium—orthorhombic titanium aluminide). *Svarka i Diagnostika,* **3**, 26–31.
6. Grinberg, B.A., Ivanov, M.A., Rybin, V.V. et al. (2010) Processes of melting, vortex formation and fragmentation in explosion welding. *Ibid.,* **6**, 34–38.
7. Rybin, V.V., Grinberg, B.A., Ivanov, M.A. et al. (2010) Structure of joining zone between titanium and orthorhombic titanium aluminide. Pt 1: Interfaces of different types. *Deformatsiya i Razrush. Materialov,* **11**, 27–33.
8. Grinberg, B.A., Ivanov, M.A., Rybin, V.V. et al. (2010) Structure of joining zone between titanium and orthorhombic titanium aluminide. Pt 2: Zones of local melting. *Ibid.,* **12**, 27–35.
9. Rybin, V.V., Greenberg, B.A., Ivanov, M.A. et al. (2011) Nanostructure of vortex during explosion welding. *J. Nanoscience and Nanotechnology,* **11** (to be publ.).
10. Pervukhina, O.L., Pervukhin, L.B., Berdychenko, A.A. et al. (2009) Features of explosion welding of titanium to steel in a shielding atmosphere. *The Paton Welding J.,* **11**, 18–22.
11. Lysak, V.I., Kuzmin, S.V. (2005) *Explosion welding.* Moscow: Mashinostroenie-1.
12. Vladimirov, V.I., Romanov, A.E. (1986) *Disclinations in crystals.* Leningrad: Nauka.
13. Deribas, A.A. (1980) *Physics of strengthening and explosion welding.* Novosibirsk: Nauka.
14. Summ, B.D. (2009) *Principles of colloid chemistry.* Moscow: Akademiya.

^{137}Cs AND ^{90}Sr PHASE TRANSITIONS IN SURFACING OF RADIOACTIVELY CONTAMINATED METAL STRUCTURES

A.A. ENNAN[1], **S.A. KIRO**[1], **M.V. OPRYA**[1], **V.E. KHAN**[2], **B.I. OGORODNIKOV**[2], **V.A. KRASNOV**[2], **A. de MEYER-VOROBETS**[3], **L. DARCHUK**[3] and **B. HOREMENCE**[3]

[1]Physical-Chemical Institute for Environmental and Human Protection, NASU, Odessa, Ukraine
[2]Institute for Problems of Nuclear Power Plants Safety, NASU, Chernobyl, Ukraine
[3]University of Antwerp, Antwerp, Belgium

The paper presents the results of investigation of phase transitions of ^{137}Cs and ^{90}Sr radionuclides from the surface of contaminated metal structures into the solid component of welding aerosol (SCWA), slag crust and deposited metal in metal surfacing with stick electrodes. It is shown that SCWA radioactivity is due to adsorption of thermolysis products of Cs_2CO_3 (Cs_2O, Cs_2O_2, Cs), slag (its contamination by ^{90}Sr and ^{137}Cs), deposited metal surface (formation of cesium monoferrite ($CsFeO_2$) and/or polyferrites ($Cs_2O \cdot 6Fe_2O_3$ and $CsFe_{11}O_{17}$)). The established empirical dependence of specific activity of ^{137}Cs in SCWA composition on ^{137}Cs surface activity can be used in forecasting the radioactive contamination or air in the working zone and rating the need for personal protective gear for respiratory organs.

Service experience of ChNPP object «Ukrytie» shows that despite the taken measures (monitoring and essential reduction of emissions of radioactive aerodispersed particles into the environment), its radioecological hazard remains high. A characteristic example of air contamination inside and outside object «Ukrytie» is formation of radioactive aerosols during performance of building-mounting operations, in particular, at cutting and repair of damaged and welding of new metal structures of shielding barriers and constructions [1].

In this connection investigations of the regularities and mechanism of phase transitions of radionuclides from the surface of contaminated metal structures are of theoretical and practical interest. It is obvious that for monitoring of radioactive situation in service of object «Ukrytie», and forecasting the effectiveness of application of personal and collective protective means for respiratory organs of personnel it is also important

to know the intensity of formation, dispersion, as well as chemical composition of the forming SCWA [2, 3].

This work presents the results of investigation of phase transitions of ^{137}Cs and ^{90}Sr radionuclides into SCWA, slag crust and deposited metal in stick electrode arc surfacing of radioactively contaminated metal plates. 25 years after the accident in the 4th reactor of ChNPP the above-mentioned beta-emitting radionuclides are exactly the particles responsible for surface contamination of metal structures in the premises and local zone of object «Ukrytie».

Investigations were performed using plates of low-carbon steel St3 of $400 \times 150 \times 8$ mm size, on which single-pass surfacing was performed with 4 mm ANO-4 and UONI-13/45 electrodes applied for welding low-carbon and low-alloyed structural steels.

To simulate radioactive contamination of metal structures of object «Ukrytie», alkali-carbonate liquid radioactive wastes (LRW) taken from water accumulated in the premises at the lower marks of object «Ukrytie» (rooms 012/7 and 014/2) were uniformly applied onto the plate surface by dripping method. According to the current classification, LRW belong to the category of medium radioactive wastes, ^{137}Cs and ^{90}Sr isotopes making the greatest contribution to their radioactivity (furtheron referred to as activity). After LRW drying, a rust layer forms on the plate surface.

Data on the initial value of surface activity of plates, A_s, prepared for investigations, are given in Table 1.

Electrode metal deposition on the plates was performed in a cabinet of 0.7 m^3 volume (Figure 1, *a*) at two values of welding heat input E_i (electric power consumed per a unit of weld length $E_i = IU/v$, where I is the reverse polarity direct current; U is the voltage;

Table 1. Initial surface activity of plates, Bq/cm^2

Plate number	^{137}Cs	^{90}Sr
1	17	3
2	160	56
3	146	51
4	20	3.5
5	200	70
6	22	3.7
7	100	35

v is the electrode displacement speed): 0.8 kJ/mm ($I = 110$ A, $U = 24$ V, $v = 3.3$ mm/s) and 1.3 kJ/mm ($I = 200$ A, $U = 33$ V, $v = 5$ mm/s). Electrode position relative to the plate is vertical. SCWA plume was localized using a hood installed at 0.4 m above the arc. Here the rate of feeding gas-air mixture by a flexible hose (0.06 m diameter) into the sampling chamber (1.9 m high and 0.19 m in diameter) (Figure 1, b) was equal to 75 dm³/s.

Air flow velocity in the points of taking representative SCWA samples was equal to 2.7 ± 0.2 m/s, SCWA concentration in the chamber was changed in the range of 50−200 mg/m³, depending on the welding mode and grade of applied electrodes. Simultaneous selection of SCWA samples: respirable fraction (SCWA$_{2.5}$) — particles with less than 2.5 μm aerodynamic diameter, penetrating into and depositing in the lung alveoli, was performed using low-pressure single-stage impactor LPI 2.5/10 dm³/min (Air Diagnostic and Engineering Inc., USA), fitted with filter (Teflon membrane filter TK15-G3M); for particles of 0.005−20,000 μm size (SCWA$_{tot}$) impactor of the same grade but without the separating plate was used. Sampling time was varied in the range of 10−60 s, filter weighing before and after sampling was performed with the accuracy of $5 \cdot 10^{-6}$ g under similar conditions (not less than 48 h conditioning time, $T = 20\pm1$ °C, air humidity of 50 ± 5 %).

^{137}Cs activity in the samples was determined using gamma-spectrometer with germanium detector GL2020 with input beryllium window of 0.5 mm thickness with energy resolution of 1.6 keV for gamma-quantum energy of 1.33 MeV of ^{60}Co. Minimum detectable activity of ^{137}Cs was equal to 0.1 ± 0.02 Bq per sample. Geniu-200 program was used for spectra interpretation. ^{90}Sr activity in the samples was determined using beta-spectrometer SEB-01 and low-background (background of 0.03 ± 0.01 pulse/s) alpha- and beta-counter Tesla NRR-610.

Results of gamma-spectrometric investigations of SCWA$_{2.5}$ and SCWA$_{tot}$ samples are given in Figure 2. Intensity of formation of SCWA$_{2.5}$ and SCWA$_{tot}$ at $E_i = 1.3$ kJ/mm, $G_{2.5}$ and G_{tot}, respectively, was as follows, mg/s:

	ANO-4	UONI-13/45
$G_{2.5}$	10.2	12.5
G_{tot}	13.1	15.3

As follows from Figure 2, dependence of specific activity of ^{137}Cs A_{sp} in SCWA composition on surface activity A_s of the plates is best described by the following exponential dependence:

$$A_{sp} = N(A_s)^n. \qquad (1)$$

Specific activity of SCWA$_{2.5}$ respirable fraction is by 20−30 % higher than that of SCWA$_{tot}$. The latter is quite explainable, considering that thermolysis of ^{137}Cs carbonate ($Cs_2CO_3 \rightarrow Cs_2O + CO_2$; $2Cs_2O \rightarrow$
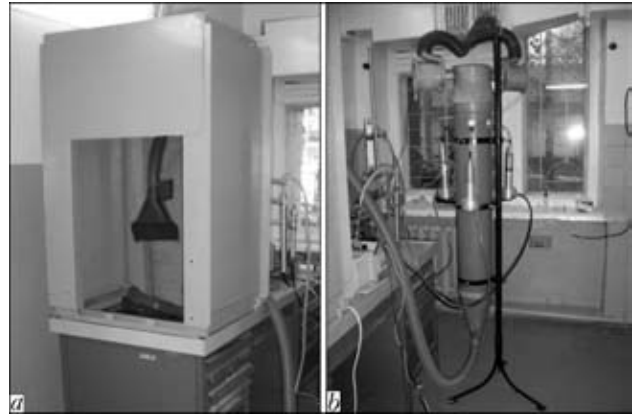
Figure 1. Experimental set up: a — welding cabinet with hood; b — sampling chamber fitted with impactors

$\rightarrow Cs_2O_2 + 2Cs$) occurs in an air atmosphere at $T \geq 880$ K, and in carbon dioxide gas atmosphere — at $T = 1065$ K it melts without noticeable decomposition, while its dissociation with CO_2 detachment occurs only at higher temperature [4], and assuming that the products of thermolysis of Cs_2CO_3 (Cs_2O, Cs_2O_2, Cs), evaporating from the plate area, where $T \geq T_{dis}$ of Cs_2CO_3 are sorbed by all the aerodispersed particles,
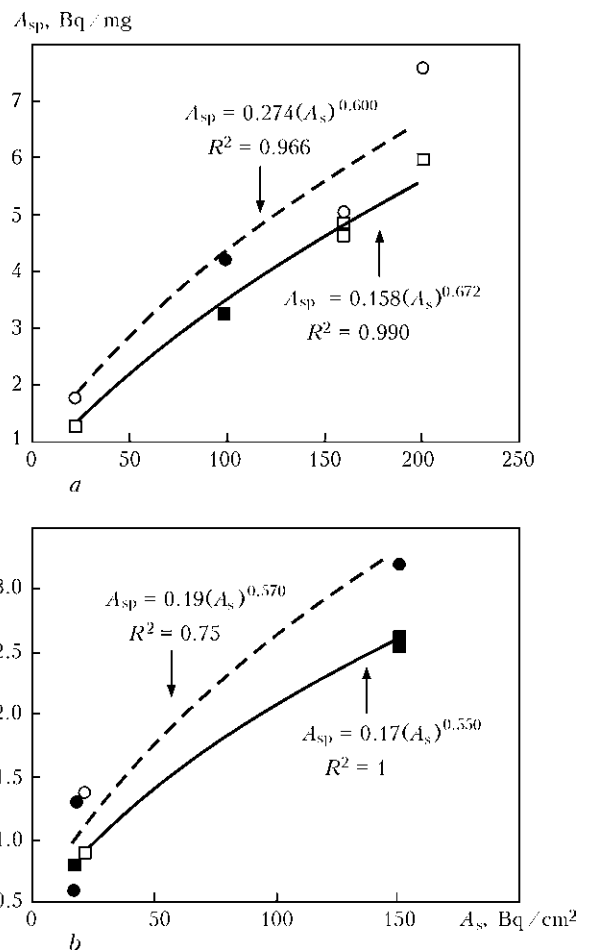
Figure 2. Dependence of ^{137}Cs specific activity A_{sp} in SCWA$_{2.5}$ (dashed curve) and SCWA$_{tot}$ (solid curve) on ^{137}Cs surface activity A_s of plates at application of electrodes ANO-4 (a) and UONI-13/45 (b): circles — SCWA$_{2.5}$; squares — SCWA$_{tot}$; light signs — at $E_i = 1.3$ kJ/mm; dark signs — at $E_i = 0.8$ kJ/mm

while radioactivity of sampled particles is proportional to their surface area [1].

Indeed, SCWA particles by their dispersion and formation mechanism are subdivided into nano-sized (less than 0.1 μm) forming as a result of condensation of vapours of welding consumables and metals being welded, disintegration and spattering of drops of electrode metal and slag melt of more than 0.5−1.0 μm size, and agglomerates in the form of stringers and clusters of varying density from nano-sized particles of more than 0.1−0.2 μm size [5, 6]. In stick electrode welding particles of the second and third types prevail in the welder's breathing zone at 0.4−0.5 m distance from the arc − 98−99 % of $SCWA_{tot}$ weight [7], in the range of particle sizes of 2.5−20 μm weight fraction of disintegration particles in $SCWA_{tot}$ is not higher than 70 % [8].

A considerable difference in the ratios of activities of ^{137}Cs and ^{90}Sr in SCWA and in the surfaced plates should be also noted. Under typical experimental conditions (at $E_i = 1.3$ kJ / mm) and sampling time (10−20 s) traces of ^{90}Sr (A_{sp} (^{137}Cs) / A_{sp} (^{90}Sr) = 135) were found in $SCWA_{2.5}$ composition only at metal deposition on plate 5, where A_s (^{137}Cs) / A_s (^{90}Sr) = = 2.86. At increase of sampling time for $SCWA_{2.5}$ samples up to 50−60 s ($m > 2$ mg) ^{90}Sr is found, as was expected, also at metal deposition on plates 1−4, 6 and 7.

Obtained results are due, in our opinion, to insignificant vapour pressure of strontium oxide (with boiling temperature of 3270 K) over the melt in the weld pool, where the average temperature is only by 100−200 K higher than iron melting temperature ($T_m \approx$ ≈ 1812 K) [9], although in the cathode spot area it may reach 2600 K [10].

Judging from the data given in Figure 2, under comparable conditions specific activity of $SCWA_{2.5}$ when using UONI-13 / 45 electrodes is on average by 45−65 % lower than in the case of ANO-4 electrodes, although the intensities of their formation differ by just 23 %. This difference is, probably, due to a large amount of carbon dioxide gas, forming at melting of the covering of UONI-13 / 45 electrodes [2], and the resultant retardation of the reaction of Cs_2CO_3 thermolysis [4].

It is obvious that the values of empirical coefficients N and n in equation (1) depend on the composition of electrode covering and the assumed changes of welding heat input by approximately 1.6 times have an only minor effect here. Indeed, proceeding from the general theoretical notions, N is functionally dependent on the ratio of increment rate of the zone of evaporation of ^{137}Cs and two of its oxides ($\Delta S / \Delta t =$ = Lv (here L is the width of the evaporation zone) to the intensity of SCWA formation G:

$$N = f\left(\frac{\Delta S / \Delta t}{G}\right).$$

On the other hand, in stick electrode welding a proportional dependence is found of the intensity of SCWA formation on arc power $G \approx IU = E_i v$ [2] and, as follows from [11], heating zone increment proceeded similarly, where $T \geq 880$ K depends on electric arc power at displacement of the linear heat source during metal deposition on a thin plate:

$$\Delta S / \Delta t \sim E_i v.$$

Thus, the width of the heating zone L_{880} on a plate limited by isotherm $T = 880$ K, under the experimental conditions ($E_i = 1.3$ kJ / mm, $v = 0.5$ cm / s, $I = 200$ A, $U = 33$ V) is equal to [11]

$$L_{880} = \frac{\sqrt{2/(\pi e)}\eta E_i}{c_\rho d \Delta T} \approx 2.2 \text{ cm},$$

where $\eta \approx 0.8$ is the efficiency of direct welding current source in stick electrode welding [10]; $d = 0.8$ cm is the plate thickness; $\Delta T = 880−300$ K is the temperature increment; $c_\rho \approx 5$ J / (cm^3·K) is the volumetric heat capacity of low-carbon steel.

In view of the above-said, it could be anticipated that at metal deposition on plate 5 ($A_s =$ = 200 Bq / cm^2) products of thermolysis of ^{137}Cs carbonate will come to the gas phase from its surface every second, their activity being equal to

$$A_{calc} = A_s L_{880} v \approx 220 \text{ Bq / s}.$$

Actually, SCWA activity experimentally established at application of ANO-4 electrodes ($G_{tot} =$ = 13.1 mg / s; $G_{2.5} = 10.2$ mg / s; A_{sp} ($SCWA_{2.5}$) = = 7.6 Bq / mg; A_{sp} ($SCWA_{tot}$) = 6 Bq / mg) is equal to

$$A_{exp} = G_{rot}A_{sp} (SCWA_{tot}) \approx$$
$$\approx G_{2.5}A_{sp} (SCWA_{2.5}) \approx 78 \text{ Bq / s},$$

i.e. A_{exp} is 2.8 times lower than A_{cacl}, and is approximately 1.4 times less than could have come from the deposited weld zone ($L_w = 1.1$ cm, where $T > T_m^{Fe}$):

$$A_w = A_s L_w v \approx 110 \text{ Bq / s}.$$

Judging by the values of A_{cacl}, A_{exp} and A_w it is obvious that Cs_2CO_3 thermolysis is accompanied by ^{137}Cs transition not only into the gaseous, but also other phases.

During decontamination of the deposited plates it was possible to establish that ^{137}Cs is contained in the slag, as well as surface layer of weld metal. Radioactive slag was removed mechanically, and decontamination of deposited metal surface layer was performed only as a result of acid etching of the weld surface.

Indirect confirmation of ^{137}Cs transition into the surface layer at metal deposition was obtained as follows. Cs_2CO_3 solution was applied on the surface of two rusted plates of 30 × 30 × 1.5 mm size from low-carbon steel St3 by dripping. The solution had been prepared using sample radioactive solution of ^{137}Cs
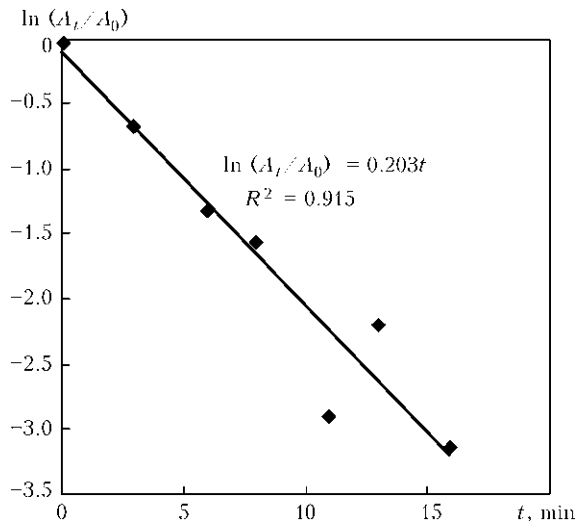
Figure 3. Dependence of ln (A_t/A_0) on duration of plate heating at $T = 1300$ K

Table 2. Dynamics of plate decontamination at baking at $T = 1300$ K

Cycle number	Plate 8 ($A_0 = 5700$ Bq)		Plate 9 ($A_0 = 870$ Bq)	
	Heating duration, min	A_t, Bq	Heating duration, min	A_t, Bq
1	3	2900	6	230
2	5	1200	5	48
3	5	630	5	38

(without carrier) in the chloride form. Dried plates (samples 8 and 9) with initial activity A_0 equal to 5700 and 870 Bq, respectively, were placed into a muffle furnace pre-heated up to 1300 K, and were baked at this temperature for a certain time. Then samples were taken out, cooled and activity A_t was measured. The above sequence of operations (cycles) was repeated thrice. Results of investigation of the dynamics of decontamination of plates 8 and 9 are given in Table 2 and in Figure 3.

It follows from the obtained data that the process of plate surface decontamination is quite well ($R^2 = 0.915$) described by the kinetic equation

$$\frac{A_t}{A_0} = \exp(-kt), \qquad (2)$$

where A_0 is the initial ^{137}Cs activity on a plate; $k = 0.203$ min^{-1} is the constant of the rate of evaporation of thermolysis products (plate decontamination) at $T = 1300$ K; t is the current baking time. Under the experimental conditions radioactivity of plate 8 decreased by 89 %, and that of plate 9 — by 95.6 %; for complete decontamination of the plates (after three cycles of their baking) it is enough to mechanically remove the easily removable layer from the contaminated surface.

Thus, investigation results obtained in Chernobyl are the first attempt to establish the regularities and mechanisms of phase transitions of ^{137}Cs and ^{90}Sr radionuclides from the surface of contaminated metal structures into SCWA at metal deposition by stick electrode surfacing.

Our results give grounds for an assertion that competing phase transitions take place in welding, surfacing and cutting of metal structures radioactively contaminated by ^{137}Cs and ^{90}Sr: G → T accompanied by formation of radioactive aerodispersed SCWA particles as a result of adsorption of vapours of products of Cs_2CO_3 thermolysis; G → T and T → T leading to radioactive contamination of slag by ^{90}Sr and ^{137}Cs and of surface layer of deposited metal by ^{137}Cs. In the latter case at the temperature of 950−1000 K, most probably, interaction of iron oxide ($T_m \approx 1830$ K) with cesium carbonate/oxide proceeds, and cesium monoferrite ($CsFeO_2$) and/or polyferrites ($Cs_2O \cdot 6Fe_2O_3$ and $CsFe_{11}O_{17}$) form [12, 13].

The established empirical dependencies can be used in forecasting the radioactive contamination of air in the working zone and rating the need for personal means of respiratory organ protection.

1. Ogorodnikov, B.I., Pazukhin, E.M., Klyuchnikov, A.A. (2008) *Radioactive aerosols of the object «Ukrytie»: 1986−2006.* Chernobyl: IPB AES NANU.
2. Pokhodnya, I.K., Gorpenyuk, V.N., Milichenko, S.S. et al. (1990) *Metallurgy of arc welding. Processes in arc and fusion of electrodes.* Kiev: Naukova Dumka.
3. Ennan, A.A. (2002) Physico-chemical principles of recovery, neutralizing and recycling of welding aerosols. In: *Proc. of 1st Int. Sci.-Pract. Conf. on Protection of Environment, Health, Safety in Welding Production* (Odessa, 11−13 Sept. 2002). Odessa: Astroprint, 10−37.
4. Plyushchev, V.E., Stepin, B.D. (1970) *Chemistry and technology of lithium, rubidium and cesium joints.* Moscow: Khimiya.
5. Zimmer, A.T., Biswas, P. (2001) Characterization of the aerosols resulting from arc welding processes. *J. Aerosol Sci.*, 32(**8**), 993−1008.
6. Jenkins, N.T., Pierce, W.M.G., Eagar, T.W. (2005) Particle size distribution of gas metal and flux-cored arc welding fumes. *Welding J.*, 84(**10**), 156−163.
7. Sowards, J.W., Lippold, J.C., Dickinson, D.W. et al. (2008) Characterization of welding fume from SMAW electrodes. *Welding Res.*, 81(**4**), 106−112.
8. Ennan, A.A., Oprya, M.V., Kiro, S.A. et al. (2010) About composition of inhalation particles of welding aerosol. In: *Proc. of 24th Sci. Conf. of CIS Countries on Dispersion Systems.* Odessa: Astroprint, 327−330.
9. Pokhodnya, I.K. (1972) *Gases in welds.* Moscow: Mashinostroenie.
10. Erokhin, A.A. (1973) *Principles of fusion welding. Physicochemical laws.* Moscow: Mashinostroenie.
11. Frolov, V.V., Volchenko, V.N., Yampolsky, M.V. et al. (1988) *Theory of welding processes.* Moscow: Vysshaya Shkola.
12. Kachalov, D.V., Stepanov, E.G., Kotelnikov, G.R. (2008) Investigation of processes of formation of catalytically active ferrites of alkaline metals. *Izvestiya Vuzov. Khimiya i Khimich. Tekhnologiya*, 51(**7**), 45−47.
13. Randhawa, B.S. (1995) Mossbauer study on thermal decomposition of cesium tris(oxalato)ferrate(III) dehydrate. *J. Radioanalytical and Nuclear Chemistry, Letters*, 201(**1**), 57−63.

SYSTEM FOR AUTOMATIC REGULATION OF POSITION OF TUNGSTEN ELECTRODE IN NARROW-GAP MAGNETICALLY CONTROLLED ARC WELDING OF TITANIUM

V.Yu. BELOUS and **S.V. AKHONIN**

E.O. Paton Electric Welding Institute, NASU, Kiev, Ukraine

A system is offered for automatic regulation of position of tungsten electrode in the groove in narrow-gap magnetically controlled arc TIG welding of titanium. The system uses direct measurement of voltage of the arc at its deflection to extreme positions. The experimentally established relationship between displacement of tungsten electrode from the groove centre and amplitude of fluctuations of the arc voltage is presented.

Keywords: *TIG welding, titanium alloys, tungsten electrode, displacement of tungsten electrode from the weld centre, tracking systems*

Narrow-gap TIG welding is a high-productivity and high-efficiency method for joining of titanium more than 16 mm thick. This welding method has certain technological advantages over V- or U-groove arc welding, such as decrease in width of the weld and HAZ, and decrease in weight of the deposited metal, which is particularly important for welding of titanium.

The E.O. Paton Electric Welding Institute developed the technology for narrow-gap magnetically controlled arc TIG welding of titanium and titanium alloys [1]. Application of the external controlling magnetic field provides redistribution of heat input to the welded joint by the arc, reliable fusion of vertical walls of the narrow groove and quality formation of the welded joints.

According to the above technology, welding is performed with the tungsten electrode lowered into the groove, the protective nozzle being located over the weld edges. This allows making the 10 mm wide groove. Magnetic core of the electromagnet is combined with the filler wire feed guide and is placed in the groove ahead of the tungsten electrode. The electromagnet generates the magnetic field, the force lines of which within the arc zone are directed mainly along the welding line. The value of magnetic induction amounts to 12 mT. This magnetic field is transverse with regard to the arc, and its direction changes into the opposite at a certain frequency.

Narrow-gap welding of longitudinal joints is accompanied by undesirable transverse displacements of the tungsten electrode with regard to the calculated central plane of the joint (weld centre). This can be caused by deviation of the actual welding direction from the calculated central plane of the joint, distortions of workpieces during welding under the effect

of the welding thermal cycle, etc. These displacements can be substantial, and can lead to short-circuiting of the tungsten electrode to the side wall of the groove. Displacement of the tungsten electrode from the weld centre in narrow-gap welding may cause violation of the uniformity of fusion of the side walls of the groove, which will lead to lacks of fusion and lacks of penetration in the weld, as well as to formation of a defective surface of the deposited layer.

Therefore, when developing a technology for narrow-gap magnetically controlled arc TIG welding, to provide a sound joint it is necessary to estimate the effect of displacement of the tungsten electrode from the weld centre on the welding process, i.e. on the distribution of the electric current in the side walls, arc voltage and weld formation. So, it seemed promising to use the welding arc moved under the effect of the external controlling magnetic field to monitor the electrode displacement from the weld centre.

This, in particular, was the purpose of this study. The authors proceeded from the fact that application of the external controlling magnetic field in narrow-gap welding should lead to redistribution of energy of the welding arc, which is introduced into a metal welded by alternately deflecting the arc to the side walls of the groove under the effect of the Lorentz force resulting from interaction of the magnetic field with the arc current. It causes deflection of the arc and shifts the anode spot to the vertical side wall of the groove. A change in distance between the tungsten electrode and side walls leads to a change in both height of shifting of the anode spot to the vertical wall and values of the electric current flowing through the vertical side walls. The effect of displacement of the tungsten electrode on the electric current flowing through the side walls of the groove, which was measured by the divided anode method [2], was studied to estimate violation of the symmetry of heating of the side walls in displacement of the tungsten electrode from the weld centre.
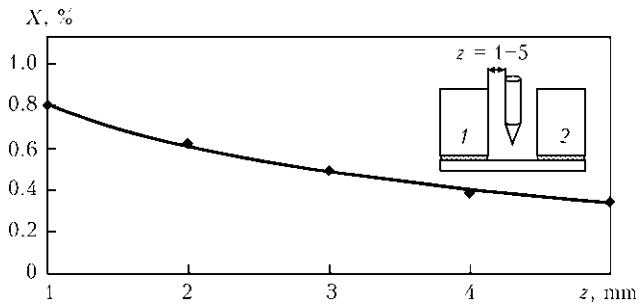
Figure 1. Change in share X of the current flowing through side wall of the groove I_s depending on distance z between the side wall and flat-tip electrode at $B_x = 11.4$ mT and $I_w = 400$ A ($X = I_s / I_w$)

It was experimentally determined that a change in distance between the electrode and side walls of the groove is accompanied by a change in the value of the electric current flowing through side walls *1* and *2* (Figure 1). Displacement of the tungsten electrode from the weld centre causes increase of the welding current flowing through near wall *1* of the groove, and decrease of the welding current flowing through distant wall *2*. It was established that displacement of the electrode to 1 mm leads to a 4–5 % decrease in share X of the current flowing through wall *1*, and a 15–25 % increase in the share of the current flowing through wall *2*. Hence, displacement of the tungsten electrode from the weld centre causes violation of the symmetry of heat input into the welded joints, thus leading to a different depth and different height of fusion of the side walls.

Therefore, to maintain symmetrical heat input into the side walls and their uniform fusion in narrow-gap magnetically controlled arc welding, it is necessary to ensure that the electrode be located at the weld centre.

In narrow-gap TIG welding of titanium by applying the external magnetic field, which is transverse with regard to the arc, a decrease in arc voltage U_a is fixed when the arc is deflected to the extreme position. This is related to the fact that distance L_1 between the tungsten electrode tip and side wall is shorter than arc gap length L_0 at the absence of deflection of the welding arc (Figure 2).

Displacement of the tungsten electrode from the weld centre causes decrease of the L_1 values (Figure 2,
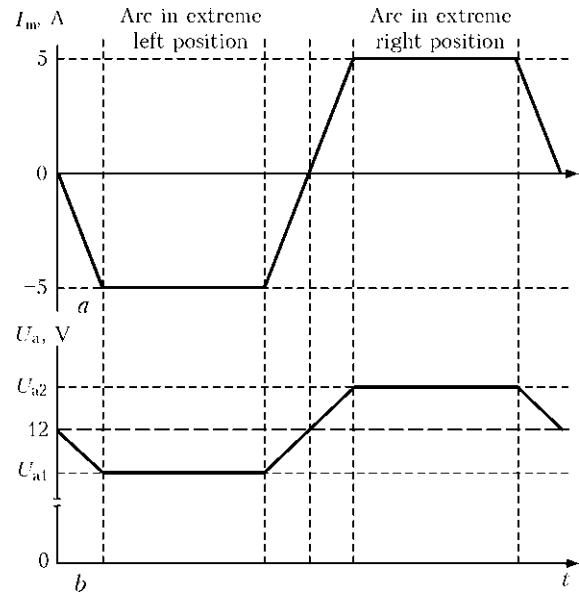

Figure 3. Effect of displacement of tungsten electrode on arc voltage U_a: a — diagram of current I_m flowing through the electromagnet coil; b — diagram of arc voltage

b) and increase of the L_2 values (Figure 2, c). Accordingly, arc voltage U_{a1} measured at deflection of the arc to the nearest wall of the groove (extreme left position) is lower than arc voltage U_{a2} measured at deflection of the arc to the distant wall (extreme right position). With alternate deflection of the arc to the opposite side walls of the groove the arc voltage changes at a frequency corresponding to the frequency of the reversing magnetic field, i.e. the arc voltage is imparted additional pulsations, whose amplitude ΔU is a difference between U_{a1} and U_{a2} (Figure 3):

$$U = U_{a1} - U_{a2}. \qquad (1)$$

It was determined that when welding is performed in a copper water-cooled groove by applying the reversing controlling magnetic field, if the tungsten electrode is placed at the weld centre, then $U_{a1} = U_{a2}$, and their values are proportional to arc gap length L_0. When welding is performed in the copper water-cooled groove by applying the reversing controlling magnetic field, and if the tungsten electrode is shifted from the groove centre, ΔU is directly proportional to displacement of the tungsten electrode from the
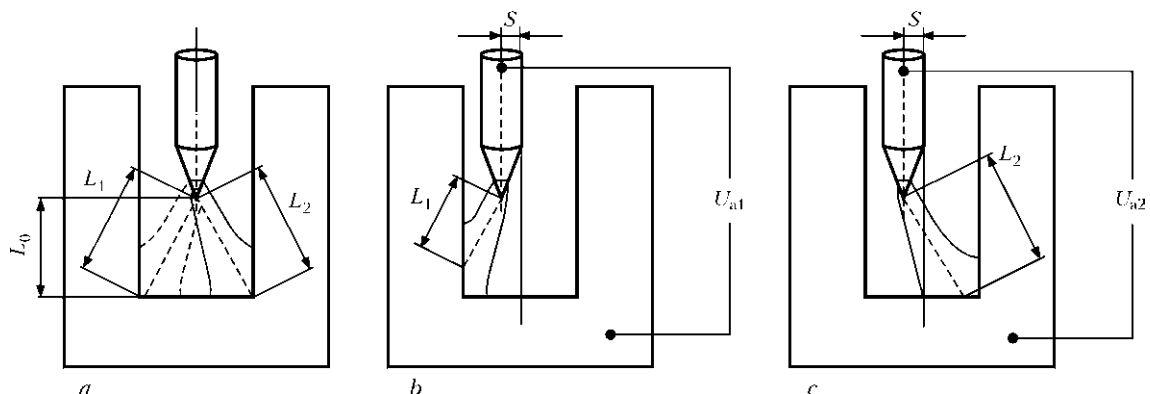

Figure 2. Schematic of deflection of welding arc at different positions of tungsten electrode: a — at the weld centre; b, c — displacement S of electrode from the weld centre to the left and right positions, respectively (see text for the rest of the designations)
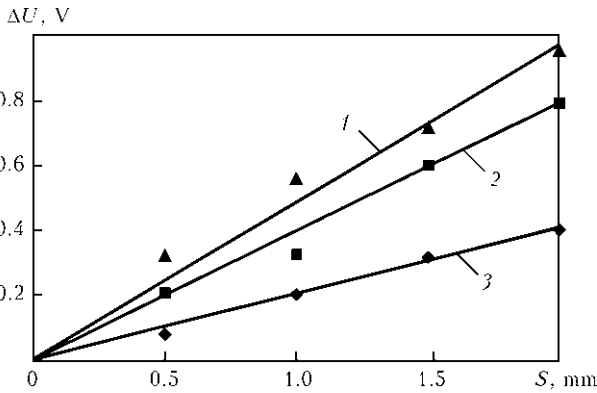
ΔU, V

Figure 4. Dependence of arc voltage pulsation amplitude ΔU on electrode displacement S from the weld centre in narrow-gap welding with water-cooled groove: $1 - L_0 = 5$; $2 - 4$; $3 - 3$ mm
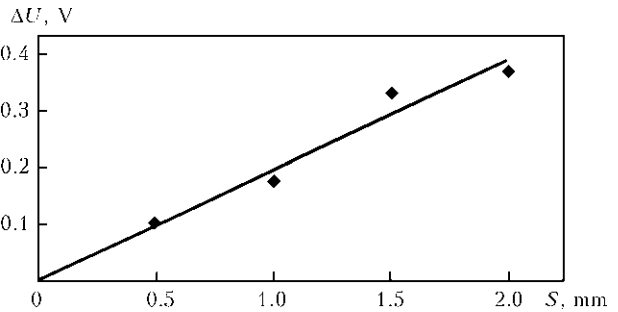
ΔU, V

Figure 5. Dependence of ΔU on electrode displacement S from the weld centre in narrow-gap welding of titanium alloy VT1-0 ($I_w = 400$ A; $U_a = 12$ V; welding speed $v_w = 8$ m/h; 2 mm diameter filler wire feed speed $v_f = 120$ m/h)
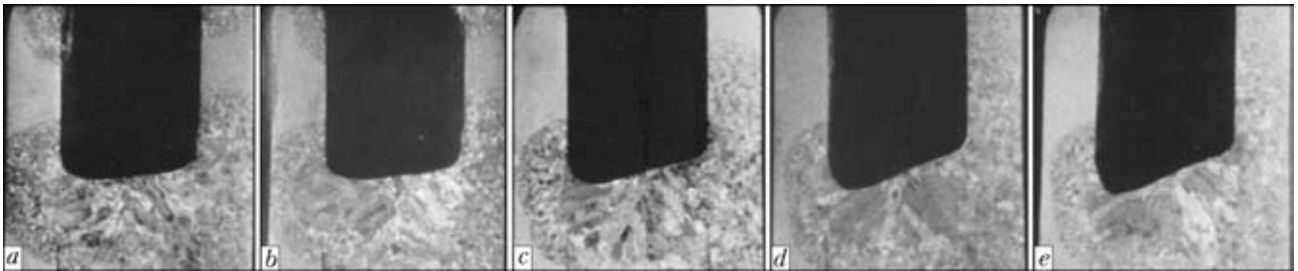

Figure 6. Formation of surface of the deposited layer at displacement of tungsten electrode from the weld centre to a distance of 0.2 (*a*), 0.5 (*b*), 0.7 (*c*), 1.0 (*d*) and 1.5 (*e*) mm

weld centre and depends on the length of the arc gap (Figure 4).

It was established that ΔU also depends on the groove material. For instance, in welding of titanium and titanium-base alloys the material is melted and the shape of the weld pool surface differs from the initial geometry of the groove, the ΔU value being decreased. Dependence of ΔU on the displacement of the tungsten electrode from the weld centre in narrow-gap magnetically controlled arc TIG welding of

Figure 7. Functional diagram of the system for tracking the arc voltage and position of tungsten electrode in the groove: *1* — electromagnet control device; *2* — programmable controller; *3*, *4* — drives for moving the electrode vertically and across the groove; *5* — arc power supply; *6* — collet with tungsten electrode; *M*1 and *M*2 — electric motors

titanium alloy VT1-0 by using 2 mm diameter filler wire of the VT1-00 grade is shown in Figure 5. Voltage pulsation ΔU amounts to 0.4 V at a 2 mm displacement of the electrode from the weld centre.

It was concluded as a result of analysis that in narrow-gap welding of longitudinal joints by applying the controlling magnetic field it is necessary to use tracking systems to correct transverse displacements of the tungsten electrode from the weld centre. Analysis of the welds made with different displacements of the tungsten electrode from the weld centre (Figure 6) showed that the quality formation of the joints can be ensured providing that the electrode displacement is no more than 0.5 mm.

Available are tracking systems based on the use of parameters of the welding arc [3, 4] or mechanical or optical sensors as a source of information on shifting of the line of elements being joined. Because of a small width of the groove, difficulties in viewing the welding zone and a limited access to it, the most promising tracking systems are those where parameters of the welding arc serve as sources of information on the electrode displacement. Study [5] suggested a seam tracking system based on the magnetic deflection of the welding arc and measurement of the instantaneous value of the welding current. As the external magnetic field is applied in narrow-gap magnetically controlled arc welding of titanium to provide reliable fusion of the side walls of the groove, it seemed expedient to use a tracking system based on the magnetic deflection of the welding arc and measurement of one of its parameters — arc voltage.
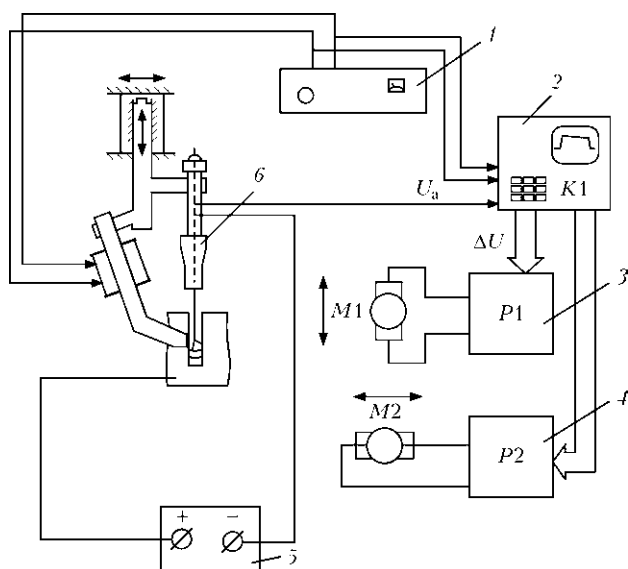
Investigation of the effect of the external magnetic field on the arc voltage in narrow-gap welding made it possible to offer a tracking system that uses one parameter of the welding arc, i.e. arc voltage, to monitor position of the electrode at the weld centre and length of the arc gap. Functional diagram of the developed system for tracking the arc voltage and position of the tungsten electrode in the groove is shown in Figure 7.

Controller $K1$ measures the voltage which is taken from a current conductor to the tungsten electrode. The signal proportional to $(U_{a1} + U_{a2})/2$ is fed to actuating mechanism $P1$, which provides vertical displacement of the tungsten electrode, filler wire and electromagnet to maintain the value of U_a at a constant level. The signal proportional to ΔU is fed to actuating mechanism $P2$, which provides transverse displacement of the tungsten electrode to keep the latter at the groove centre. To determine direction of the transverse displacement of the tungsten electrode, controller $K1$ measuring the value of ΔU is synchronised with the electromagnet control device.

The experiments conducted showed the efficiency of the offered system for automatic regulation of the arc voltage and position of the tungsten electrode in the groove, and confirmed the high quality of the produced welded joints even at the preliminarily set deviations of the tungsten electrode from the geometrical centre of the weld.

CONCLUSIONS

1. It was established that displacement of tungsten electrode from the weld centre in narrow-gap welding with the external magnetic field is a factor that has a considerable effect on the value of the current flowing through the side walls of the groove, symmetry of heat input into the joint and depth of penetration of the side walls of the groove. Displacement of the electrode to 1 mm leads to a 4–5 % decrease in the share of the current flowing through the distant wall and a 15–25 % increase in the share of the current flowing through the near wall. Also, it causes a change in the penetration depth.

2. It was experimentally proved that displacement of the electrode from the weld centre leads to a difference in levels of the arc voltage with the amplitude of up to 0.4 V at its deflection to the extreme positions, the frequency of oscillations of the arc voltage corresponding to the frequency of reversals of the controlling magnetic field. The value of the coefficient of proportionality between displacement of the tungsten electrode from the weld centre and amplitude of oscillations of the arc voltage in narrow-gap welding of titanium and titanium-base alloys was determined to be equal to 0.2 V/mm. The functional diagram of the system for automatic regulation of position of the tungsten electrode in the groove, using the direct measurement of the arc voltage, was offered.

1. Paton, B.E., Zamkov, V.N., Prilutsky, V.P. (1996) Narrow-groove welding proves its worth on thick titanium. *Welding J.*, **4**, 37–41.
2. Topolyansky, P.A., Khristofis, B.O., Ermakov, S.A. et al. (2005) Correlation between an integrated value of the effective power of an axisymmetric heat source on a segment and function of the radial heat flow density distribution. In: *Proc. of 6th Int. Pract. Conf.-Exhibition on Technologies for Repair, Restoration and Strengthening of Machine Parts, Mechanisms, Equipment, Tool and Technological Fitting* (St.-Petersburg, 13–16 April 2004). St.-Petersburg: SPbGPU, 3–9.
3. Paton, B.E., Lebedev, V.K. (1966) *Electric equipment for arc and slag welding*. Moscow: Mashinostroenie.
4. Tsybulkin, G.A. (1994) Side correction of a current position of the welding tool based on continuous measurement of the welding current. *Avtomatich. Svarka*, **7/8**, 28–31.
5. Lebedev, V.K., Chernysh, V.P. (1986) *Automation of welding processes*. Kiev: Vyshcha Shkola.

ELECTRON BEAM WELDING IN PRODUCTION OF STEEL-ALUMINIUM JOINTS OF TRANSITION PIECES OF DISSIMILAR METALS

A.A. BONDAREV, V.M. NESTERENKOV and **Yu.A. ARKHANGELSKY**

E.O. Paton Electric Welding Institute, NASU, Kiev, Ukraine

New design-technological solutions for producing of dissimilar welded joints of aluminium alloy–stainless steel materials by electron beam welding are presented. Variants of heavy-section welded joints, optimal parameters for their welding and examples of application in structures are given.

Keywords: welded structures, electron beam welding, steel-aluminium joints, bimetallic transition pieces, armor shielding, macrosections of joints

One of the priority trends in development of modern machine building is decrease of mass of structures and devices with simultaneous preservation of their technical characteristics and service reliability at the high level. Application of different grades of steels and aluminium alloys allows optimal reacting of a product to the effect of loadings, temperatures or aggressive environments existing under service conditions. During realization of modern design solutions the welding of aluminium and its alloys with other metals is widely applied.

In welded joints of dissimilar metals aluminium is one of the most hard-to-weld metals. At the same time manufacturing of welded structures of aluminum joined with other metals is especially rational, as it allows considerable decrease of mass of the product.

Nowadays many fields of industry are in growing need of reliable methods for joining dissimilar metals and alloys. Many specialists deal with the development and creation of aluminium-steel transition pieces. The result of many year investigations allowed creating different technologies for production of sheet bimetal aluminium-steel for manufacturing transition pieces in the structures of different purpose (Figure 1). The largest volume of bimetal production accounts for metallurgical industry where it is produced by rolling of two sheets. Bimetal is produced also by explosion treatment in spite of specific conditions for realization of this process, by diffusion welding, brazing, friction welding and resistance welding. However, all these processes are limited only by negligible volumes of production of aluminium-steel transition pieces.

A new welding method using high-speed impact finds also ever wider application [1]. Sometimes transition pieces are not used and the welding-in of aluminium parts to the steel ones is directly performed. However, to realize this welding process the edges of

steel to be welded should be previously subjected to aluminizing, i.e. to their coating with molten aluminium by dipping into a liquid melt.

In most cases the application of mentioned methods for production of bimetal concerns the application of thin-sheet components, i.e. in total the thickness of bimetal can reach 10 mm and a bit larger. It is more difficult to realize the process if the transition pieces of thickness, for example, of aluminium of 20 mm and larger are required.

Even more complicated problem for producing the bimetallic transition pieces is the presence of intermetallic brittle interlayers [2, 3] on the interface of two metals. These can be phases $FeAl$, Fe_2Al_5, as well as oxides and suboxides Al_2O_3, Al_2O, AlO which are always present on the surface of aluminium and its alloys.

All these compounds have high heat resistance and are not destroyed even during heating of the interface up to the temperature of 1600 °C and higher. The presence of such interlayer in the aluminium-steel joint of even 50–100 μm thickness considerably influences the embrittlement of a joint, the tearing strength of which decreases from 300–350 down to 50–100 MPa [2].

Application of such bimetallic transition pieces in welded structures [4], when other structure elements are welded to any of the metals using arc methods, results in high temperature heating of transition zone
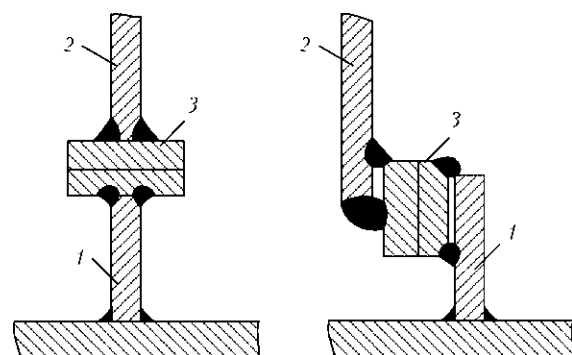

Figure 1. Variants of typical units in welded structures using transition pieces of dissimilar materials [2]: *1* — steel structure element; *2* — aluminium element; *3* — bimetallic aluminium alloy–steel transition piece
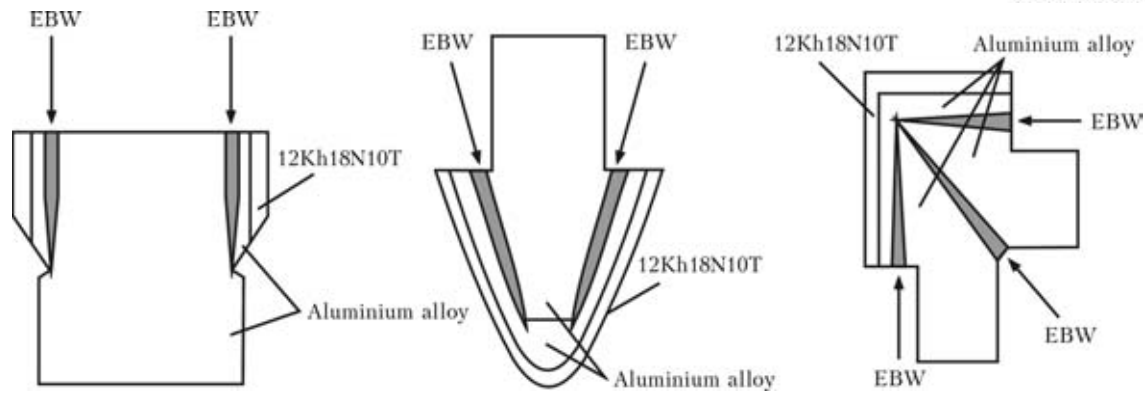
Figure 2. Schemes of welded joints of transition pieces of large thickness

which additionally increases the intermetallic interlayer. Moreover it becomes less dense and as a result not only its strength but also corrosion resistance decrease both under the influence of liquid and gas environment.

The solution for this situation can be application of bimetallic transition pieces produced using explosion welding. In explosion process of producing of bimetal in a certain range of flying speed parameters (2000 m∕s and higher) at the interface of metals being welded the wave-formed swirlings appear [5, 6]. Due to increase of impact toughness of near-surface metal layers, the crushing of intermetallic interlayer at the interface and their localization in single areas of metal swirlings occurs. Bimetallic transition piece produced according to this technology is not almost subjected to embrittlement and loss of strength during its further heating in welded joint with other metals.

Also the method of welding steel with aluminium alloys is known when application of bimetallic transition piece is not required [7]. The welding is performed directly by flashing of an edge of aluminium semi-product on the steel edge of a butt, which is previously subjected to coating of intermediate film of modifier elements. Coating of these elements is performed by depositing from the vapor phase in vacuum. These can be titanium, zirconium, nickel and other. The thickness of a film is usually 5−10 μm, but it has continuous metallic bond with a steel, and after flashing on the surface of aluminium edge the modifier elements transform into solid solution of liquid aluminium melt and strengthen it. The strength of these joints of steel with aluminium alloys is at the level of 300−350 MPa. In spite of all advantages of this method, its wide application is limited due to complexity of technological process and large economic costs.
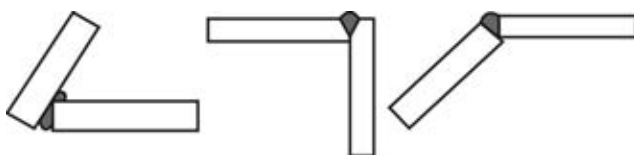

Figure 3. Variants of typical joints during manufacturing of transition pieces for heavy-loaded welded structures of dissimilar materials [3]

Therefore, in welding of products, when application of structure elements with large thickness of welded edges is required, the best variant to be considered is manufacturing of transition pieces using explosion technology. However even in this case in order to avoid at least partial formation of intermetalic solid interlayer along the interface of metals, the best further technology for joining will be the electron beam one. This solution is based on the fact that in electron beam welding the heat input is much lower than in other methods of fusion welding. Consequently in this situation the heating of the interface during welding will be the least. And possibility of welding edges of larger thickness using electron beam and for one pass prevents repeated heating of delimitation zone due to making beads using arc methods on the groove.

During development of design-technological solutions for creation of transition peaces of a large thickness, their further application in the certain structures of products was also considered.

In Figure 2 the variants of typical transition pieces in the structures with an aluminium body and steel framing are presented. Such transition pieces can be applied for example in aircraft building. In heavy transport aircrafts, wear-resistant guides for moving the loads should be located along the floor of fuselage. Except of wear resistance these elements should not increase the weight of a structure in general, therefore it would be more reasonable to produce them in a bimetallic variant.

Another kind of problems appeared during creation of large-sized transport means manufactured of aluminium armor in army subdivisions. These machines of light type are in popular demand especially when using at swampy, sandy soils or in the jungle. Figure 3 shows variants of typical welded joints produced in different spatial positions at a large thickness of elements being welded. Naturally it is necessary to perform welding by multi-pass welds, which is accompanied by considerable overheat of the interface while using bimetallic transition pieces. There is also one more problem to be solved while creating structures of that type. Welded joints of high-strength aluminium alloys, including armor plates, have impact
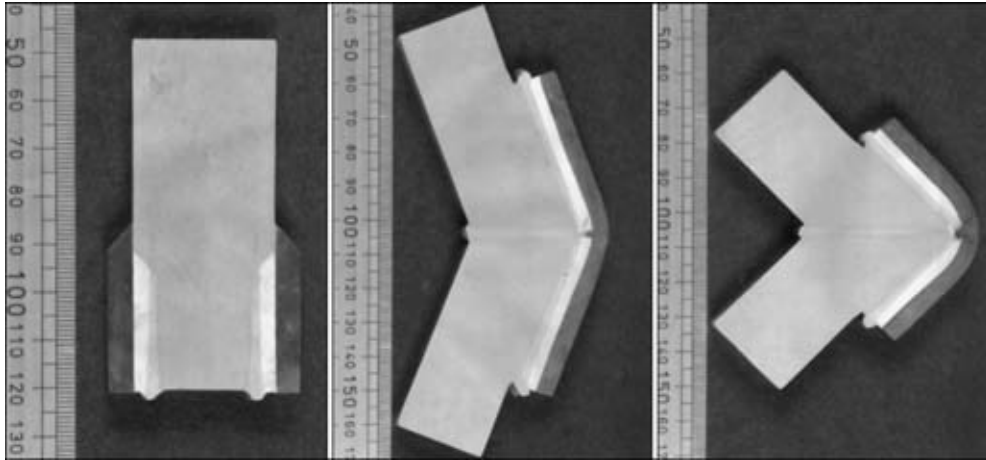
Figure 4. Macrosections of transition pieces manufactured according to new technology using electron beam welding

Conditions of EBW of bimetallic transition pieces of alloy D16

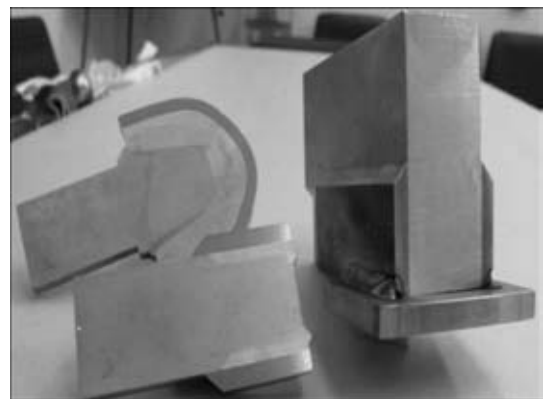| Penetration depth, mm	Welding current I_w, mA	Focusing current I_f, mA	Welding speed v, mm/s	Amplitude of circular scanning A, mm
33	128	618	12	2
41	175	618	12	2
44	185	618	12	2
40	170	618	12	2

Figure 5. Macrosections and appearance of an assembly after welding-on of transition piece to steel structure elements

toughness of the joints almost twice lower than that of base metal. In this case at local loading of a weld, for example, during hit of a bullet or a shell, a weld is cracked reaching a very large length from the place of loading. Therefore to provide high design strength of these products, the steel armor shield of welds of aluminium armor along the whole length [8] is required. The solution of this task is possible using bimetallic transition pieces shown in Figure 2.

In Figure 4 macrosections of transition pieces of a large thickness of aluminium elements are given manufacturing of which was performed using electron beam in vacuum. The power source with accelerating 60 kW voltage was applied. Welding conditions of transition pieces with different thickness of aluminium edges are given in the Table. Figure 5 shows macrosection of a joint in welding-in of transition pieces to steel structure elements.

The application of principally new solutions for using transition pieces for joining of dissimilar metallic materials in welded structures will provide solution of the problems in many cases during designing and manufacturing of highly-loaded products of light alloys.

CONCLUSIONS

1. The radically new design-technological solutions during manufacturing of steel-aluminium transition pieces as-applied to creation of welded assemblies and products of dissimilar materials of a large thickness have been developed.

2. The variants of typical assemblies and joints of semi-products of aluminium alloys to the steel parts and assemblies during creation of complex heavy-loaded welded structures are given.

1. Ryabov, V.R., Pervukhin, L.B., Volferts, G.A. et al. (1995) Influence of explosion welding parameters on strength and plastic properties of steel-aluminium joints. *Avtomatich. Svarka*, **12**, 32–34.
2. Oryshchenko, A.S., Osokin, E.P., Pavlova, V.I. et al. (2009) Bimetal steel-aluminium joints in shipbuilding hull structures. *The Paton Welding J.*, **10**, 35–38.
3. Paton, B.E., Gordonny, V.G. (2002) Works of the E.O. Paton Electric Welding Institute of the NAS of Ukraine in the field of military tank construction. *Ibid.*, **2**, 33–39.
4. Ryabov, V.R. (1969) *Fusion welding of aluminium with steel*. Kiev: Naukova Dumka.
5. Dobrushin, L.D. (2004) State-of-the-art and prospects for development of welding by explosion and high-velocity impact (Review). *The Paton Welding J.*, **9**, 45–51.
6. Fadeenko, Yu.I., Dobrushin, L.D., Illarionov, S.Yu. (2005) Mechanisms of joint boundary shaping in explosion welding. *Ibid.*, **7**, 13–16.
7. Paton, B.E., Bondarev, A.A. (2004) State-of-the-art and advanced technologies of electron beam welding of structures. *Ibid.*, **11**, 20–27.
8. Vaskovsky, M.I. (2004) Concept of system of individual protection of armored machines from high-precision arms. *Artiller. i Strelk. Vooruzhenie*, **4**, 38–42.

ASSESSMENT OF THE EFFECTIVENESS OF COMPOSITE BANDS FOR RECONDITIONING OF DEFECTIVE SECTIONS OF PIPELINES

E.F. GARF[1], **V.A. NEKHOTYASHCHY**[1], **R.I. DMITRIENKO**[1], **Yu.V. BANAKHEVICH**[2],
A.V. SAVENKO[3] and **I.N. OLEJNIK**[3]

[1]E.O. Paton Electric Welding Institute, NASU, Kiev, Ukraine
[2]SC «Ukrtransgaz», Kiev, Ukraine
[3]«Kailas» Ltd, Kiev, Ukraine

The paper gives the results of testing 720 × 10 and 530 × 8 mm pipes with composite-polymer bands in sections with defects simulating local corrosion damage. Joint work of the band and pipe at static and cyclic loading caused by inner pressure is shown. Effectiveness of reinforcement of defective pipeline sections by composite-polymer bands is established and features of fracture of a banded pipe are noted.

Problem of ensuring reliability of pipelines, which have been in service for a long time, requires availability of design solutions and technologies for their implementation aimed at increasing the reliability of individual damaged sections. This problem is particularly urgent for Ukraine, in the territory of which more than 42,000 km of just the main oil-, gas- and product pipelines are in operation.

Repair of pipeline sections with local corrosion-mechanical damage can be performed using design-technological solutions, realized either with application of welding, or with application of high-strength non-metallic materials [1]. Often here one of the conditions is performance of repair operations without interruption of pipeline operation. Under field conditions, far from power sources, application of bands from non-metallic materials is usually preferred for liquidation of local defects. Simplicity of the technology of band mounting with application of high-strength non-metallic materials and their small weight are the decisive advantages at selection of the technology of pipeline repair in mountainous regions on rocky soil.

In the world practice investigations in the field of application of composite materials at repair of oil- and gas pipelines have been performed during the last 20 years [2]. There are research programs funded by companies operating the pipelines and pipe manufacturers, the realization of which enabled including composite materials into pipeline repair technologies. A normative base was developed for pipeline repair by non-metallic composite systems under field conditions [3]. The range of the used composite materials is becoming wider [2].

In Ukraine local repair of pipelines is performed using composite bands PPS of «Polipromsintez» Company based on glass-fiber-plastic and polyester resin. A large scope of research was performed on calculated evaluation of the strength of pipeline — composite band system, studying mechanical properties of the composite band, development of design-technological schematics of reinforcement of pipeline defective sections. Unfortunately, application of composite materials based on glass-fiber-plastic and polyether resins does not have a well-established and stable technology. The wide range of composites and techniques, high sensitivity of mechanical properties to the change of technological parameters requires allowing for the technological features of materials and special features of repair operation performance when designing the composite bands [1].

In Russia composite polymer bands (CPB) are becoming applied for local repair of pipelines. The codes [3] specify defects in pipes repairable with CPB, materials recommended for defects filling and used as adhesives, materials taking the load applied by inner pressure, and fillers. Specifications for these materials and technologies of CPB application have been defined.

On the other hand, increased number of design-technological solutions on reinforcement of pipelines by CPB and widening the range of the used materials is not accompanied by an increase of the scope of investigations of joint work of the pipe and band. An essential difference in the moduli of elasticity, as well as mechanical and deformation properties of pipe and composite materials requires a more profound study of their joint work, particularly in the elasto-plastic and plastic deformation fields.

The purpose of this work was studying on full-scale pipe fragments and on samples the features of joint work of the pipe with a local defect and reinforcing
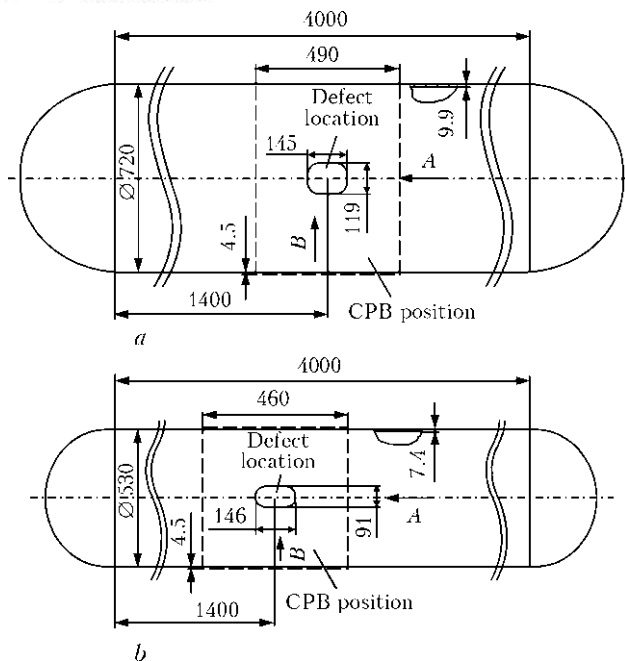
Figure 1. Samples-stands Dn 720 (*a*) and Dn 530 (*b*) with artificial defects and CPB

CPB, as well as assessment of the effectiveness of CPB application to increase pipeline strength under static and dynamic loading by inner pressure.

Investigations were performed on fragments of Dn 720 × 10 pipe made (TU 14-31573−96) from steel of 13G1S-U grade, and Dn 530 × 8 pipe made (TU 14-8-20−99) from steel of 17G1S-U grade. Semispherical caps were welded to 4 m pipes. Artificial defects were made on pipe outer surface with an abrasive wheel, the defect dimensions are given in Figures 1 and 2.
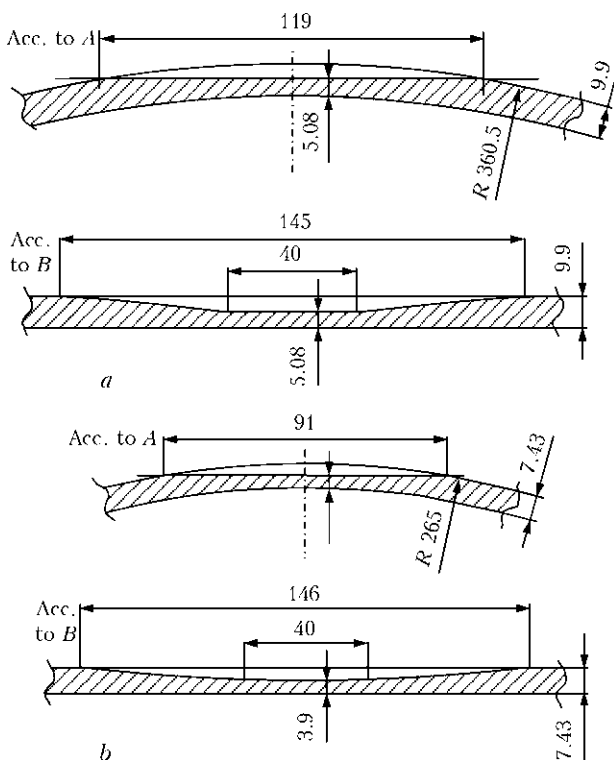

Figure 2. Geometrical dimensions of defects on samples-stands: *a* — Dn 720; *b* — Dn 530

Coefficients of lowering of the pipe load-carrying capacity were determined, proceeding from the pre-requisite, that the defect influence is similar to that of an isolated through-thickness hole at equality of the areas of the defect and hole in the longitudinal direction [4−6]. Proceeding from the actual dimensions of defects, strength coefficients were equal to: for Dn 720 × 10 pipe — 0.72, for Dn 530 × 8 pipe — 0.617.

Defective sections were reinforced by applying a multilayer band. Technology of CPB application envisages preparation of the pipe surface by sand-blasting, as well as filling the defects and smoothing the roughnesses, in particular, in the presence of reinforcement in the weld, using REM-Steel composite material, the specification of which is given in TU 2257-005-00396558−98. After polymerization of REM-Steel and surface cleaning in keeping with VRD 39-1.10-013−2000 CPB was applied. For both pipes the band consisted of seven layers of glass net, and its thickness was equal to approximately 4 mm. Band width for Dn 720 pipe was equal to 490 mm, and for Dn 530 pipe it was 460 mm. All the operations on band mounting were performed at excess pressure of 4.94 MPa in pipes, that corresponds to 70 % of the working pressure. After complete polymerization of the band pipe testing began.

Testing program envisaged determination of the actual mechanical properties of metal of Dn 720 and 530 pipes; measurement of the actual wall thickness in the studied pipe fragments; investigation of the stress-strain state of samples-stands at the elastic stage of loading; testing of sample-stand Dn 530 at cyclic loading; testing of samples-stands by inner pressure to fracture; investigation of joint work of pipe wall with REM-Steel; and testing a shell with CPB for flattening.

Mechanical properties of pipe metal were determined on standard samples cut out of reference-shells cut off the pipe, and on samples made from the pipe after its failure. Testing results meet the specification requirements both for Dn 720 pipe and for Dn 530 pipe.

Measurement of wall thickness was conducted by ultrasonic thickness meter TUZ-2 in order to establish its actual value and scatter region on 4 m pipe. For sample-stand Dn 720 measurement results were in the range of 9.77−10 mm at the average value of wall thickness of 9.9 mm. For Dn 530 the range of wall thickness measurement was 7.36−7.53 mm at average value of 7.43 mm.

Stress-stain state of samples-stands was studied in order to determine the joint work of the pipe and band at all the loading stages, corresponding to pipeline operation. Relative deformations were measured using wire strain gauges of 5P1-20-200-B12 type with 20 mm base and static deformation measurer ISD-3. Deformations on the pipe wall and bands in defect locations

and at a distance from them were measured in the longitudinal and circumferential directions. Figure 3 gives the transducer layout.

It should be noted that transducers were pasted to the pipe in the absence of inner pressure, and on the band — at the pressure equal to 70 % of working pressure. Deformations were measured at stage-by-stage pressure lowering to zero and subsequent increase of inner pressure to 9.81 MPa. Results of deformation measurement in the circumferential and longitudinal directions are given in Figure 4.

As is seen, zero deformations in the band correspond to 4.94 MPa pressure in the pipe. Zero deformations in the pipe are found in the absence of inner pressure. Compressive deformations are found in the band.

The given data indicate that band deformation occurs simultaneously with the pipe both at pressure lowering and at its increase. Deformation gradient in the defect zone (transducers 2 and 3) and in the zone of the longitudinal weld (transducer 1) is higher. This is less pronounced in sample-stand Dn 530. Circumferential and longitudinal deformations in the pipe body and on the band outside the zone of the defect and weld (transducers 5 and 7) are practically the same. At 9.81 MPa pressure a deviation of deformations from the linear law is found that is related to achievement of yield stresses in the pipe.

The band starts taking up part of the forces after the pressure rises above that at which it was applied.

An important element of checking the joint work of the pipe and band was testing for cyclic load of sample-stand Dn 530. Loading was performed by ex-
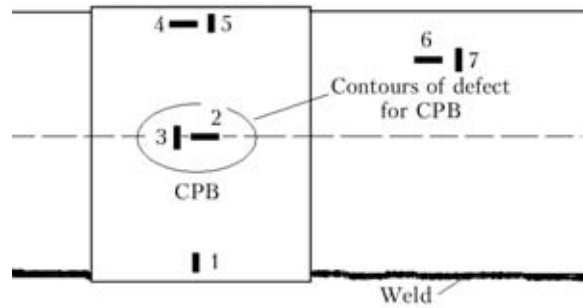
Figure 3. Layout of transducers (strain gauges) on samples-stands Dn 720 and Dn 530

cess hydraulic pressure of 0.4—7.5 MPa. The period of stress cycle was equal to about 36 s. Fatigue life of 10^4 cycles was taken as the test base that corresponds to 33 years of pipeline operation. Load was applied by PTR 1-1-400 hydraulic machine with 1000 l/h efficiency. Control of loading process was performed in the automatic mode. Loading parameters were controlled by highly accurate manometer and Metran 100-DI pressure sensor. Maximum cycle stresses were equal to about $0.6\sigma_y$, i.e. testing was performed in the elastic region. After 2500, 5000 and 8000 cycles, as well as after completion of testing (10,036 cycles) the pipe and band were examined. No delaminations or cracks in the band, or band delaminations from the pipe body were found.

Testing to fracture was performed on samples-stands Dn 720 and Dn 530. Dn 530 sample-stand was first subjected to cyclic testing. Load was increased in steps with 10 minute holding after each step and visual examination of the pipe and band. Loading steps envisaged: working pressure; 1.5 times working
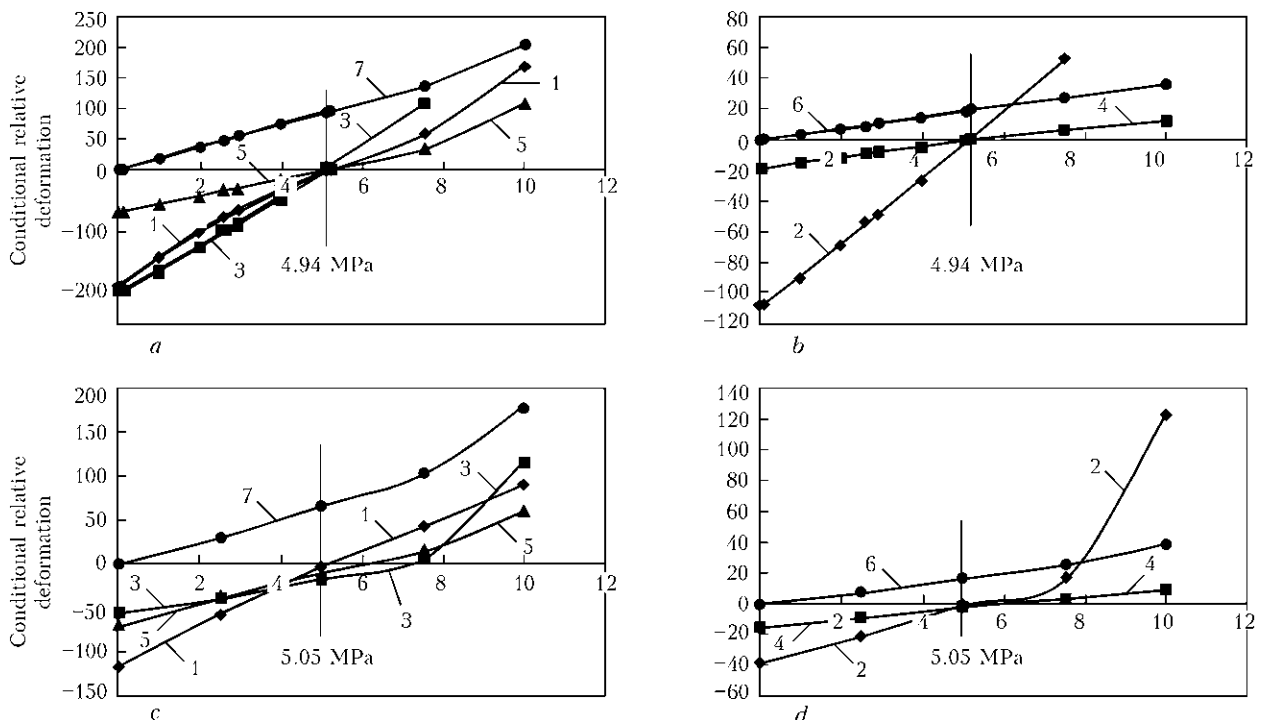
Figure 4. Results of measurement of circumferential (*a*, *c*) and axial (*b*, *d*) deformations of sample-stand Dn 720 (*a*, *b*) and Dn 530 (*c*, *d*): *1—7* — numbers of transducers of strain gauges
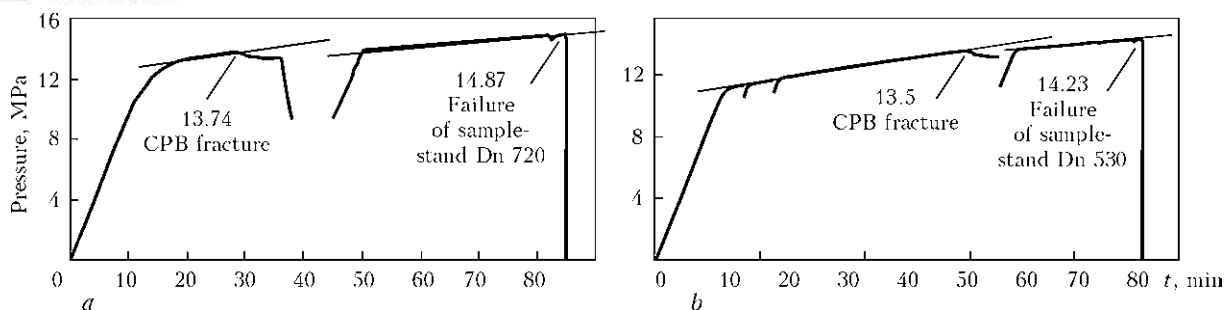
Figure 5. Diagrams of hydraulic testing of samples-stands Dn 720 (*a*) and Dn 530 (*b*) by inner pressure to fracture

pressure, pressure corresponding to material yield point; breaking pressure of sample-stand. Testing sequence required additional stops in the plastic region of pipe operation that is related to band fracture, which was observed before pipe failure. Complete diagrams of testing samples-stands are given in Figure 5.

Failure of a pipe reinforced by CPB has its special features. At loads inducing plastic deformation of the pipe, a field of deformation concentration starts forming in the defect location. When deformations have reached critical values for the band, its rupture occurs, which does not cover the entire width of the band, but just one part of it located above the defect. Here no delamination of the band from the pipe is observed. At the moment of band rupture the pressure in the pipe drops somewhat, and then starts rising again, and exceeds the level of initial band rupture. At this stage the angle of inclination of loading diagram decreases somewhat which is indicative of slowing down of load increment, and more intensive strain increase. Failure of sample-stand Dn 720 (Figure 6) is tough,

Figure 6. Appearance of failed sample-stands

and it occurred at inner pressure of 14.87 MPa. Here, a longitudinal crack formed, which ran through defect center. Immediately before pipe failure, band delamination occurred in the defect zone accompanied by characteristic crackling.

Testing of sample-stand Dn 530 was conducted by the same schematic as that of Dn 720. At the pressure of 13.5 MPa the first rupture of part of the band occurred (about 30 % of its width). Pipe failure occurred at the pressure of 142.3 MPa (Figure 6, *b*).

Generalization of the results of testing samples-stands Dn 720 and Dn 530 is given in the Table.

A criterion for assessment of CPB effectiveness can be comparison of strength coefficients of band-reinforced pipe, and coefficients of pipe wakening by the defect. Strength coefficient of a pipe reinforced by a band is considered proceeding from partial fracture of the band and complete failure of the pipe with the band.

Sample-stand Dn 530 demonstrated a slightly lower effectiveness of the band. It is possible that the result may have been affected by its preliminary testing by cyclic load, as well as application as initial mechanical properties of the results obtained on samples, cut out of the pipe after its testing to fracture. It is also possible that the band effectiveness is somewhat decreased with increase of pipe weakening by the defect.

As is seen, the effectiveness of band application is significant, even if partial rupture of the band is taken as the limiting state. On the other hand, it is clear that 100 % restoration of pipe strength requires such a considerable increase of band thickness which will be not cost-efficient.

Coefficients of pipe weakening, given in the last column of the Table, were derived proceeding from minimum values of ultimate strength of steels given in the pipe specification. This characteristic is quite conditional, as the specified values of pipe mechanical properties are below the actual value.

To get an idea of joint deformation of the metal of the pipe and REM-Steel tensile testing of samples with a layer of REM-Steel applied on them was conducted. Samples were cut out of a reference-shell Dn 720. Three samples were tested to varying degrees of plastic deformation.

Loading in the first sample was taken to its necking. Stresses here were equal to 568.8 MPa that prac-
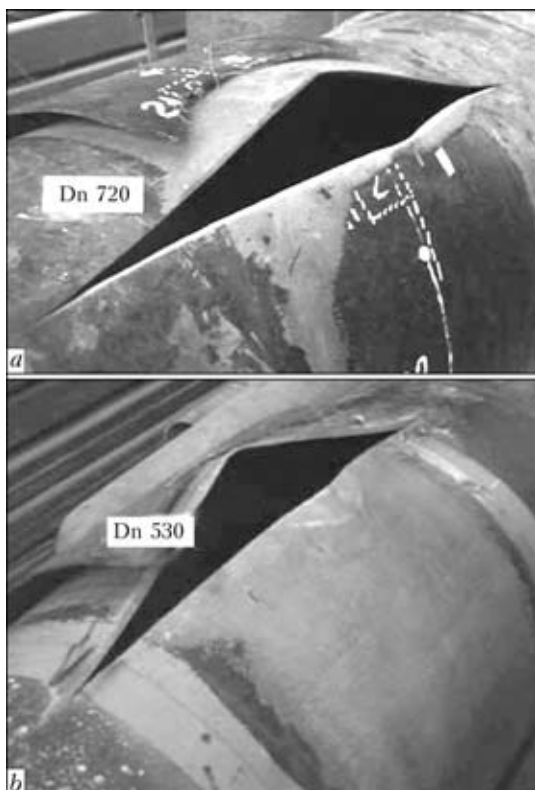
Results of testing samples-stands Dn 720 and Dn 530 to failure

Pipe Dn	Minimum wall thickness (actual), mm	Strength properties of steel				Stresses in the pipe at band fracture, MPa	Pipe breaking stresses, MPa	Coefficient of weakening of defective pipe φ	Coefficients of weakening of pipe reinforced by a band	
		Acc. to TU (min), MPa		Test, MPa					Against actual properties	Against specification requirements
		σ_y	σ_t	σ_y	σ_t					
720 × 10	9.77	380	540	388.20	560.60	518.93	540.5	0.720	0.927 / 0.964	0.961 / 1
530 × 8	7.36	360	510	391.65[*]	560.65[*]	479.30	504.2	0.617	0.864 / 0.910	0.940 / 0.989

[*]Minimum mechanical properties obtained on samples cut out of the pipe after its testing.

tically corresponds to ultimate strength of steel. Relative elongation in the sample, measured after relieving of the load, was equal to 17 %. Cracking and delamination of REM-Steel was recorded at stresses of 505 MPa.

At testing of the second sample stresses reached 538.6 MPa, residual deformations were equal to 4.25 %. Start of delamination in this sample was recorded at the stress of approximately 505 MPa.

In the third sample, when stresses reached 468.8 MPa, loading was interrupted. Here, residual elongation was 1.5 %. No traces of delamination or cracking of REM-Steel were found in this sample.

This testing confirmed that at elastic and elasto-plastic deformations REM-Steel works together with the pipe metal. Delamination and cracking are found when plastic deformations are equal to 2−3 %.

If these results are transferred to the pipeline, one can see that delamination of REM-Steel occurs at the very final stage of pipe loading, when the site of deformation concentration is determined.

Joint work of the pipe and band at deformation was checked by testing the shell with the band for flattening. Testing was aimed at determination of the relative deformation, at which the joint work of the metal and the band is disturbed. Band rupture took place at flattening of Dn 530 shell with the band up to 220 mm distance between the outer walls. At load relieving this distance increased to 265 mm. Relative deformation of metal, at which band cracking occurred, was equal to about 7.8 %. This result is another confirmation of the joint work of the band and the pipe at quite high local plastic deformations.

On the other hand, tensile testing of samples in the form of bands 44 mm wide, cut out after fracture of sample-stand from the band section, removed from the fracture point, showed that the band material works in the elastic region right up to fracture. Relative elongation of samples is practically zero. However, at simultaneous work with the pipe, band fracture occurs, as was noted above, at sufficiently high plastic deformations in the pipe. This is attributed to the fact that the composite modulus of elasticity is more than two orders of magnitude lower than that of steel, the band is applied onto a loaded pipe and the band is capable of taking up plastic deformations of the pipe partly at the expense of the filler ductility.

CONCLUSIONS

1. Results of testing fragments of pipes reinforced by CPB in defective locations showed that deformations in the bands are proportional to pipe deformations. This is indicative of simultaneous work of the pipe and the band not only in the elastic region at tensile and compressive stresses in the band, but also in the region of elasto-plastic deformations in the pipe.

2. Pulsed cycle testing with maximum cycle stresses corresponding to working pressure in the pipe, showed the joint work of the pipe and band in the entire testing base (10^4 cycles) and did not induce any fatigue cracks.

3. At the given combination of geometrical dimensions and mechanical properties of the pipe, defect dimensions and conditions of placing the band, fracture of the latter precedes exhaustion of the pipe load-carrying capacity. Band rupture occurs in the defect location at the stage of concentration of plastic deformations in this zone is of a local nature and is not accompanied by delamination of the band from the pipe.

4. Results of testing samples-stands Dn 720 and Dn 530 showed that band fracture occurs at stresses which are equal to 86.4−92.7 % and pipe failure — at 91.0−96.4 % of values of tensile strength of pipe metal. This is indicative of the fact that the band significantly increases the strength of a defective pipe.

1. Becker, M.V., But, V.S., Govdyak, R.M. et al. (2008) *Repair of main pipelines under pressure*. Kyiv: Kyj.
2. Alexander, C., Francini, B. (2006) State of the art assessment of composite systems used to repair transmission pipe lines. In: *Proc. of 6th Int. Pipeline Conf.* (25−29 Sept. 2006, Calgary, Alberta, Canada).
3. *ASME B 31.4, ASME B 31.8*: Classes of ASME boiler and pressure vessel code. Date 10.05.90.
4. *PNAE G-7-002−86*: Codes of strength analysis of equipment and pipelines of nuclear power units. Moscow: Energoizdat.
5. *OST 108.031.08−85*: Stationary boilers and steam and hot water piping. Codes of strength analysis. Introd. 01.07.87.
6. Garf, E.F., Netrebsky, M.A. (2000) Assessment of the strength and residual life of pipelines with erosion-corrosion damage. *The Paton Welding J.*, **9/10**, 13−18.

DEVELOPMENT OF A SENSOR FOR ESTIMATION OF THE RATE OF CORROSION OF WELDED METAL STRUCTURE UNDER ATMOSPHERIC CONDITIONS

S.A. OSADCHUK, L.I. NYRKOVA, S.G. POLYAKOV, S.L. MELNICHUK and **N.A. GAPULA**

E.O. Paton Electric Welding Institute, NASU, Kiev, Ukraine

A two-electrode sensor with co-surface electrode position was developed for measurement of the instantaneous rate of corrosion of structural steels and welded joints in thin electrolyte films. Performance of the sensor was demonstrated for measurement of the rate of atmospheric corrosion at different temperatures, 100 % air humidity with and without moisture condensation. It was established that under conditions simulating the atmospheric ones the developed sensor can be used to measure the corrosion rate in the $1 \cdot 10^{-6}$–10 mm/year range.

Atmospheric corrosion is the most common type of corrosion, as about 80 % of metal structures operate under the atmospheric conditions. Atmospheric corrosion of metals is mainly of an electrochemical nature and occurs in thin films of the moisture, which is condensed on the metal surface. Corrosion in atmosphere is a long-duration process. The time to complete fracture of a metal structure is from 5 to 16 years. However, it would be wrong to think that the process of corrosion in atmosphere is always slow and occurs at a lower rate than when metal is immersed into the bulk of electrolyte. While the mean rate of corrosion in sea water is i_c = 0.10–0.15 mm/year, the rate of corrosion of piles in a zone of cyclic wetting, e.g. in the Caspian oil fields, is 0.5–0.6 mm/year. The rate of atmospheric corrosion (i_c, mm/year) in living and industrial premises is given below [1]:

```
kitchen and bathroom ............................. 0.0025–0.0100
laundry ......................................................... 0.0075
bleachery ...................................................... 0.0430
sulphuric acid factory ........................................ 0.0480
paper mill .................................................... 0.0680
locomotive depot .............................................. 0.0800
etching shop at metallurgical works ............... above 0.450
```

Corrosion of the unprotected surface of steel and its welded joints in atmosphere depends on the climatic conditions of specific surroundings. The main causes of atmospheric corrosion are humidity and temperature of air, temperature differences, wetting–drying cycles, and presence of sulphur dioxide (industrial atmosphere) or sodium chloride (sea atmosphere) in air.

The rate of corrosion during the first year of operation of welded metal structures is 0.19 mm/year, which is the upper limit for the most aggressive atmospheres (category C5) according to standard ISO 12944–2. Corrosion may occur at low humidity values in the presence of contaminants or hygroscopic salts.

It is a known fact that the key factor inducing the atmospheric corrosion is water [1], which leads to formation of a moisture film on the surface of metal. At a relative air humidity of no more than 60 % no traces of moisture are fixed on the metal surface. In this case corrosion occurs by the chemical mechanism.

At a relative air humidity of 60–70 %, which is called critical, the moisture condensation process begins, and a thin continuous adsorption water film forms on the metal surface. Critical humidity of the industrial atmosphere is 60 % on the average. The rate of the atmospheric corrosion considerably increases at a relative humidity that is higher than the critical one.

This important fact was first demonstrated by Vernon in a series of his classical experiments [1]. He demonstrated that corrosion in clean air at a relative humidity below 100 % occurs at a rate of not more than 0.001–0.002 mm/year, whereas the presence of an insignificant concentration of such impurities as sulphur dioxide may cause a 100 times increase in the rate of corrosion even at the absence of visible traces of moisture. For this it is enough that the relative humidity exceeds some critical (even comparatively low) value, which depends on the nature of the atmospheric pollution, but is 70–80 % at the presence of sulphur dioxide. If humidity is below the critical value, the rate of corrosion is lower than 0.001 mm/year even in the polluted air.

It is well known that the thin film on the metal surface affects the course of the corrosion processes, while the rate of corrosion depends in a certain way on the thickness of this film. Thin films can be of two types: adsorption films that are formed at a relative air humidity of 60 to 70 %, and phase films that are visible to the naked eye and formed at an air humidity close to 100 %, which may be or may not be accompanied by the condensation of moisture on the surface.

At present no procedure is available for monitoring of durable welded metal structures under the atmos-
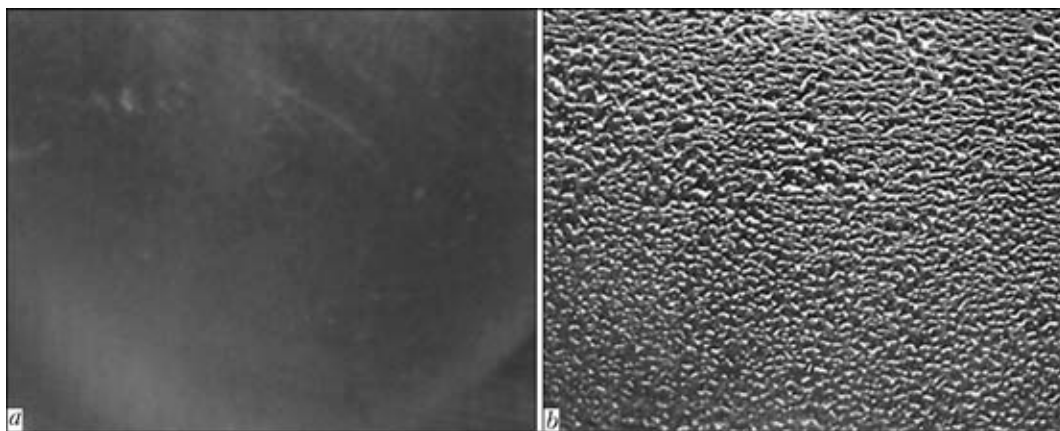
Figure 1. Appearance of the moisture film formed on the surface of steel St3 and its welded joints at $T = 24$ °C without moisture condensation (a) and at $T = 50$ °C with moisture condensation (b)

pheric corrosion conditions. Development of such a procedure is impossible without development of reliable and unfailing corrosion control means, i.e. sensing devices or sensors with a high sensitivity level, which allow measuring the instantaneous rate of corrosion over a period of a diurnal cycle on durable facilities, such as storage or industrial rooms, including the new safe confinement at the Chernobyl NPP.

The two-electrode sensor with co-surface position of electrodes, the sensing element of which is made from steel St3, was developed to measure the instantaneous rate of corrosion of structural steels and their

welded joints in thin electrolyte films. To obtain more reliable data on the rate of corrosion, it is planned that the sensing element of the sensor will be made from the same material as the material of a metal structure. To increase the accuracy of measurements, the sensing element is placed on the anodised plate, with the help of which the sensor is secured to the metal structure being monitored. The operation of the sensor is based on the polarisation resistance method, the theoretical principles of which are described in study [2].

Specifications of the sensor

Range of measurement of atmospheric corrosion
rate, mm/year .... $1 \cdot 10^{-5} - 5$
Measured polarisation resistance, Ohm .... $10^2 - 10^7$
Service conditions:
    temperature, °C .... $-40 - +70$
    relative air humidity, % .... $80-100$
Measurement error, % .... no more than 20

Investigations were conducted to study the peculiarities of corrosion of carbon steel St3 and its welded joints under conditions simulating the atmospheric ones at an air temperature of 24, 50 and 70 °C, and at a relative humidity of 100 %. For this the corrosion rate sensors and samples of the welded joints were placed horizontally to let the moisture films form on their surfaces. The measurements were made under the temperature-controlled conditions. The investigations were carried out by creating the atmospheric conditions, under which the moisture condensed on the metal surface, but the condensation of the moisture on the surface was not yet completed, and then the thickness of the formed film was estimated (Figure 1).

Figure 2. Kinetics of corrosion rate i_c on structural steel St3 under conditions simulating the atmospheric ones with (a) and without (b) moisture condensation on the metal surface at $T = 24$ (1), 50 (2) and 70 (3) °C, which was determined with the help of the corrosion rate sensor

Rate of corrosion of structural steel and its welded joints (i_c, mm/year) determined by the polarisation resistance method under conditions simulating the atmospheric ones

T, °C	With moisture condensation	Without moisture condensation
24	$1.4 \cdot 10^{-3}$	$1.4 \cdot 10^{-3}$
50	$3.9 \cdot 10^{-3}$	$2.3 \cdot 10^{-4}$
70	$2.0 \cdot 10^{-2}$	$7.5 \cdot 10^{-6}$

Figure 3. Appearance of the surface of sensors after exposure ($t = 3$ h) to conditions simulating the atmospheric ones with (a–c) and without (d–f) moisture condensation on the sensor surface at $T = 24$ (a, d), 50 (b, e) and 70 (c, f) °C
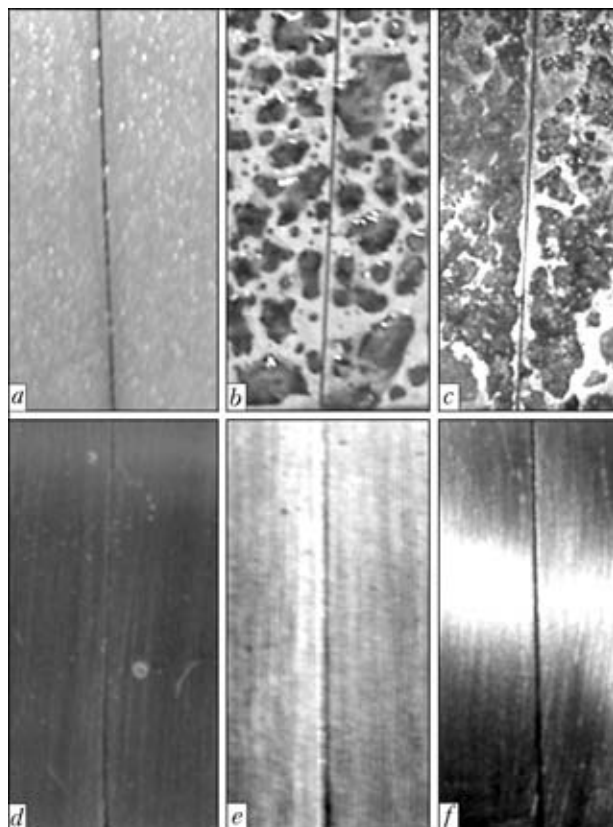

Figure 4. Dependence of i_c of structural steel St3 on temperature under conditions simulating the atmospheric ones with (1) and without (2) moisture condensation on the sensor surface, determined by using the corrosion rate sensor

It was determined that a very thin film from 0.6 to 3.0 μm thick formed on the sample surfaces at a temperature of 24 °C for 20 min under the moisture condensation conditions (see Figure 1, a). At $T > 40$ °C under the moisture condensation conditions the visible phase layers of moisture and water droplets formed on the samples surfaces. Thickness of the moisture layer ranged from 17 to 45 μm (see Figure 1, b).

The instantaneous corrosion rate was estimated under laboratory conditions simulating the atmospheric ones (for 3 h). The results obtained are given in the Table and in Figures 2–4.

It can be noted as a result of analysis of the obtained data that the rate of corrosion of steel St3 and its welded joints in thin moisture films grew with increase in temperature of the humid air because of intensification of the process of moisture condensation and formation of moisture layers of different thicknesses. Corrosion in these layers occurred by different mechanisms: in layers less than 30 μm thick it occurred by the diffusion mechanism, and in layers more than 30 μm thick — by the convection mechanism [1, 2].

At $T = 24$ °C the moisture condensation was slower than at a higher temperature. In this case the moisture film from 0.6 to 3.0 μm thick formed on the metal surface. Corrosion was of a continuous character and occurred at a rate of no more than 0.005 mm/year (Figure 2, a, curve 1; Figure 3, a).
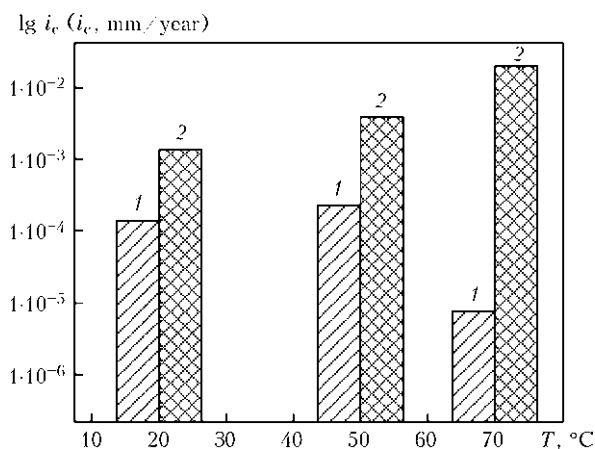
Because of formation of a non-uniform layer of moisture on the surface of the sensors, corrosion acquired a hot-spot character with increase in temperature (Figure 3, b, c). The highest corrosion rate was fixed under the moisture droplets. Increase in the local corrosion rate was promoted by the formed corrosion products, which were hygroscopic in their properties and kept the moisture on the sensor surface.

The rate of corrosion of steel St3 and its welded joints at the absence of the condensation of moisture on the sensor surface also grew with increase in temperature from 24 to 50 °C, and was 0.00014 mm/years at $T = 24$ °C (Figure 2, b, curve 1; Figure 3, d) and 0.00023 mm/year at $T = 50$ °C (Figure 2, b, curve 2; Figure 3, e). These values of the rate of corrosion evidenced that metal behaved as the «absolutely corrosion-resistant one» according to the five-point scale of corrosion resistance [2]. Further increase in temperature to 70 °C led to decrease in the rate of corrosion (Figure 2, b, curve 3; Figure 3, f). This phenomenon can be explained by heating of the sensor and, as a result, drying of the formed phase layer, which probably led to a change in the corrosion mechanism from the electrochemical to chemical one, and to a substantial decrease of the rate of corrosion.

It is planned to continue the research efforts on investigation of atmospheric corrosion of structural steels and their welded joints by the polarisation resistance method on the laboratory scale and under service conditions at different temperatures and at the air humidity close to the critical one. It is intended to develop systems for continuous monitoring of the corrosion state of welded metal structures.

CONCLUSIONS

1. Peculiarities of corrosion of carbon steel St3 and its welded joints under conditions simulating the atmospheric ones (air temperature 20, 50 and 70 °C, and relative humidity 100 % with and without moisture condensation) were investigated. It was estab-

lished that in thin moisture films the rate of corrosion grows with increase in temperature of the humid air because of intensification of the moisture condensation process and formation of the layers of different thicknesses.

2. Thickness of the moisture film formed on the metal surface under different conditions was estimated. It was shown that thickness of the moisture layer on the sensor surface at a temperature of 24 °C under the moisture condensation conditions was 0.6−3.0 μm, and increased to 17−45 μm with increase in temperature to more than 40 °C.

3. Performance of the sensor for measuring the rate of atmospheric corrosion at different temperatures, air humidity of 100 % with and without moisture condensation was studied. It was determined that the sensor can measure the rate of corrosion over a range of $1 \cdot 10^{-6}$−10 mm/year.

1. Rosenfeld, L.I. (1960) *Atmospheric corrosion of metals*. Moscow: AN SSSR.
2. Chviruk, V.P., Polyakov, S.G., Gerasymenko, Yu.S. (2007) *Electrochemical monitoring of man-made environments*. Kyiv: Akademperiodyka.

NEWS

NEW INTERACTIVE ELECTRIC WELDING LABORATORY

PWI RC SKAE completed development of a new facility for welder's training during the real process. Arc welder's trainer (DTS-06) is designed for on-line analysis of the level of professional skills of arc welding specialists. Interactive electric welding laboratory allows accelerating the process of training in welding technologies (and reducing the cost, respectively), improving the quality of specialist training due to application of modern interactive technologies when learning practical skills of the welding process. Welder's trainer is a unique local development of PWI specialists.

The trainee is able to conduct preliminary trials and welding process under the instructor's guidance for familiarization with the training facility. Then test welding can be performed for assessment of welder's professional level. Various calculation procedures are used for calculation assessment for each welding process type. Welder's training and testing are performed for real processes of MMA, MIG/MAG and TIG welding.

The laboratory includes: tabletop personal computer, tabletop block of technological interface with specialized electrode holder, welding table; and welding power source.

Main functions of the trainer:
• entering the task for selected welding process (from the panel or earlier saved task file);
• measurement, processing, calculation and real-time representation of the following welding process parameters and auxiliary signals: welding current; arc voltage; arc length; welding speed; heat input; horizontal angle of electrode inclination (turning along the arm axis); vertical angle of electrode inclination (up and down movement of the wrist); deposit cross-section; deposited metal weight; gas flow rate; electrode position on the sample; filler wire feed signal; calculation assessment of the quality of performed welding (several welding passes can be performed within one assessment);

• viewing graphs of recorded welding processes after assessment;
• preservation in the form of operating system files of tasks for assessment of various kinds of welding processes for fast setting up of the training facility for a specific process;
• preservation in the form of operating system files of resulting data of assessment for possible subsequent analysis.

The training facility can be used in training establishments, specializing in arc welders' training; large welding enterprises for certification or re-certification of welder personnel or in a specialized organization involved in supervision, training or re-training of arc welding specialists.

INTERNATIONAL SPECIALIZED EXHIBITION «WELDING, CUTTING, SURFACING»

In the period of May 23–26, 2011 the International exhibition «Welding, Cutting, Surfacing» took place in Moscow in the Central Exhibition Complex «Expotsentr» at Krasnaya Presnya. It was organized for the fourth time together with the companies «Messe Essen GmbH» and «Messe Duesseldorf Moscow Ltd» and supported by the constant business partners of German welding society (DVS) and National agency for control and welding (NAKS). At the same time exhibitions on similar subjects as «Metal treatment», «Wire of Russia», «Pipes of Russia», «Metallurgy-Litmash», «Aluminium-Tsvetmet» were held providing nice opportunities for complex solution of problems by welders-specialists in very different fields of industry.

The Russian market is attractive for many enterprises. That is why German companies (more than 20 expositions), Chinese representatives (about 15 stands), Russian enterprises (about 30 stands) took active part at the exhibition. Participation at the exhibition is an important investment to the future. According to the survey results of the Eastern Committee and the German-Russian Chamber of Commerce, on the eve of holding the exhibition 57 % of companies-respondents accounted for positive development of the economy in Russia. New working places and new investments are already planned. For the enterprises represented in Russia excellent opportunities are opened in finding reliable partners and customers. It was confirmed by the survey carried out in AUMA e.V (Association of the German Trade Fair Industry of the German economy): 91 % of enterprises-respondents noted that the main stimulus for their participation in the specialized exhibition was the search for new customers, and their purpose was to build up their personal reputation; 89 % supposed that the ex-

position of the exhibition was very favorable to keep contacts with available customers, and 86 % said that new products and services were provided.

According to the forecast assessments the economic growth in Russia for 2011 will amount 4–5 %. It is supposed that in nearest years it will be maintained on that level due to growth of industrial production. For Russia, whose economy was formerly based on the production of raw materials these are the revolutionary changes which recently resulted in the highest demand on goods and services related with technologies for joining materials.

The expositions presented on the exhibition included demonstration of arc equipment for welding-in studs, electron beam welding, MIG/MAG welding, including narrow-gap welding, tandem welding, equipment for welding plastic, including welding using heated tool and high-frequency welding; automated and mechanized equipment for production lines, including robots; equipment for workshops and worksites (tables for welding and cutting, charging rotation devices); means of labor protection (systems for extraction of welding fumes, welding cabins, curtains, screens, filters and filter systems); means of individual protection (shields, glasses, filters); devices of combined function (rotary tables, manipulators), electrodes for resistance welding and TIG welding. The exposition of welding and filler materials looked rather simple (four stands) and included electrode metallic and flux-cored wires for arc welding in shielding gases, covered electrodes, sticks for TIG welding.

Among the famous world brands in the field of welding production the following participants can be mentioned: «Boehler Welding Holding GmbH», «Kjellberg Finsterwalde Plasma GmbH», «Kemper GmbH», «Cloos» (Germany), «GRPZ», «Mezhgosmetiz Mtsensk», «ITS», «Linde Gaz Rus», «NAKS», «Shtorm» and «Shtorm-Lorch Ltd.» (Russia), E.O. Paton Electric Welding Institute (Ukraine), «Panchmanal Steel Limited» (India), «Hoeganaes» (Sweden). The latter is the world leader in production of metallic powders for coatings and brazing alloys as well as plasma and laser deposition.

The exposition of the E.O. Paton Electric Welding Institute showed main trends of scientific searches of the Institute, achievements in solution of actual tasks of the Ukrainian economy, demonstrated production of its pilot plants. The visitors had a keen interest to the recent achievements of the Institute. A number of proposals for scientific and technical cooperation was followed.

Prof. N.P. Alyoshin (RAS) (*second on the left*), and Prof. L.M. Lobanov (NASU) (*in the centre*) at the Exhibition

The held exhibition was featured by the fact that a number of expositions of «welding» profile was presented not in the welding hall of the exhibitions, but, for example, in the exhibition «Metal treatment». Namely in that place welding process and its performance were considered as a basic tool in technological multilinked production of different kinds of products.

During exhibition the one-day International Conference «Welding – look into the future 4», organized by NAKS and DVS, took place. Nine reports were delivered in the plenary form.

At the opening of the Conference Prof. N.P. Alyoshin (RAS), stated that this exhibition-fair was the offspring of the global family of exhibitions headed by the Essen one. Nowadays it is regularly held in China, India, Russia, and since 2011 in Brazil. Everywhere it plays a role of an expert giving an impetus to development of business in many regions of the world. The next speaker Mr. K. Middeldorf, executive director of DVS, said it was a really good chance to discuss problems of welding and related technologies. The situation after crisis becomes stabilized. The market of welding technologies in Russia is estimated at 100 mln Euro, the volume of consumed welding materials reaches 200,000 t. Two third of the surveyed German companies see challenges at the Russian market. There is a common problem: lack of highly-skilled welders. Therefore, constant care about optimization of the technologies, welding consumables, equipment and everything necessary for welding production is of great importance. DVS and NAKS share a common vision of this problem. The exhibition and seminar contribute to the discussion of burning tasks, elaboration of requirements for the joints of the future.

The report of Prof. L.M. Lobanov on the subject «Activities of the E.O. Paton Electric Welding Institute in the field of development of new welding methods» was of substantial interest. In particular it highlighted the last achievements of the Institute in a number of technological developments which were highly estimated at the practical applications. Among them:

• resistance welding of armature at reconstruction of the Olympic stadium in Kiev;

• restoration of large crankshafts using surfacing;

• increase of life of brazed drill bits applied during extraction of methane;

• increase of life of copper plates of moulds with nickel coating deposited using friction stir welding method;

• local decrease of residual stresses in the assemblies of structures under the effect of current pulses of high density;

• improvement of technology for repair of main pipelines and many other.

In conclusion Prof. Lobanov called to intensify the cooperation of Russian and Ukrainian scientists to increase efficiency of works at solution of complex problems of our economies.

Also Mr. M. Strotmann (Germany) «New requirements during certification of enterprises according to the standards EN 15085», Prof. A.G. Grigoriants (N.E. Bauman MSTU, Moscow, Russia) «Two beam laser welding», H.-G. Gross (Germany) «Experience of certification of enterprises in Russia according to the standards EN 15085», Prof. G.A. Turichin (Russian-German Center of Laser Technologies, St-Petersburg, Russia) «Hybrid welding of pipelines», H. Heuser (Germany) «Welding of pipes for modern ultrasupercritical electric power stations», Dr. V.I. Khomenko (Pskov Plant of Heavy Electric Welding Equipment) «Combined welding of pipelines», V. Dide (Germany) «Exaust systems applied in welding and cutting» and Dr. M.A. Sholokhov («Shtorm Ltd», Ekaterinburg, Russia) «Modern welding equipment produced in Russia» delivered their reports.

In the report of A.G. Grigoriants the advantages of two-beam laser welding as compared to single beam

welding, predetermined by increase of concentration and respectively efficiency of heating of a product being welded were analysed. Light module plus laser beam to the common pool under the specified angle to each other provides possibility of welding along the gap, fracture of oxide film in welding of aluminium alloys. Combination of powers of sources, for example 5 + 3 kW, allows doubling the depth of penetration as compared to the welding using one laser of 8 kW capacity. The uniform structure of HAZ metal in welding of hardened steels is provided, the effect of cracks «healing» in multilayer welds is observed. Nowadays OJSC «Gazprom» should take a decision on the permition to apply mentioned technology in industry basing on the results of inspection of technology of two-beam laser welding of pipes under factory conditions of the Chelyabinsk Tractor Plant.

In the report of G.A. Turichin the results of experimental investigations on hybrid welding of pipelines carried out in Russian-German Centre of Laser Technologies since 2007 were generalized. The mathematic model of hybrid laser-arc welding was built, submerged arc process (with modulation) was investigated, technological solutions in welding of aluminium alloys with lithium preventing the weakening in welded joints were developed. The universality of hybrid welding process and «niche» of its applicability at average culture of production was grounded. M.A. Sholokhov demonstrated the analysis of production and consumption of welding equipment in Russia to the audience. In 2007 almost 410,000 units of equipment were sold in Russia, among them about 50,000 those of national producers (~12 %). In 2008 about 1 million units were sold, including nearly 6 % of

national producer. In the period 2005–2006 the situation at the market was the same. The company «Telvin» (24.5 %, Italy), Turkish and (19 %) Chinese companies (38 %) were among the leaders of sales. Among the national producers there are three leading ones: «Plazma» (Rostov), «Kavik» (Smolensk region), «GRPZ» (Ryazan). The correlation of equipment types for 2008 was the following: for arc welding — about 73 %, for resistance welding — 16 %. The author of the report supposes that a certain progress in liquidation of inadmissible situation with equipment can be achieved in realization of Russian-German project on creation of joint welding-technological centre («Shtorm» + «Lorch»), modernization of a plant, design bureau, technical department and service department. The production of modern power sources for arc welding (based on the technology Micor) was already organized.

N.P. Alyoshin while discussing the report of M.A. Sholokhov expressed the opinion that to introduce national rival welding equipment it is necessary to create some self-adjustment organizations with young ambitious teams capable for skilful responsible management of modern production in a number of regions of the country. The example is NAKS, whose creation and established work in the problems of diagnostics and control allowed it to be high on the list in the modern world.

During closing of the conference K. Middeldorf stated that the moto «Without joining technologies the longevity is impossible» is very important today. Only on the principle of longevity joining technologies can guarantee stable development and stable technology.

Prof. V.N. Lipodaev, PWI

INTERNATIONAL CONFERENCE
«SURFACE ENGINEERING
AND RENOVATION OF PARTS»

Only realizing of new high-end technologies and scientific-and-technical trends can provide achievement of high quality and service reliability of machines as well as their lower costs being a condition for guarantying of high and stable level of competitiveness in the market.

A surface engineering is one of such complex directions of problem solving. It gains higher importance as an efficient mean for saving of materials and energy allowing simultaneously improving technical-and-economical characteristics of machines and developing fundamentally new parts.

International Scientific-and-Technical Conference «Surface Engineering and Renovation of Parts» took place for the eleventh time in village Gaspra of Big Yalta on May 23–27, 2011. It was organized by Machine-Building Engineers and Technologists Association of Ukraine. Scientists of SRI and institutes, specialists of industrial enterprises of Ukraine, Russia, Belarus, Lithuania, Germany and Uzbekistan participated in the Conference.

This year the Conference was dedicated to the 50th anniversary of creation of V.N. Bakul Institute of Superhard Materials of the NAS of Ukraine. Activity of the Institute is directed to development and promotion of wide application of tools from composites based on synthetic diamond and cubic boron nitride, hard alloys and ceramics. Institute developments allow using up-to-date functional materials, deposited and sprayed coatings in machine structures. This provides a high-efficiency mechanical treatment and development of working surfaces of the parts with quality, required under conditions of machines' operation.

The Conference was opened by welcoming speech from Prof. S.A. Klimenko, the director of Machine-Building Engineers and Technologists Association of Ukraine, deputy director of V.N. Bakul Institute of Superhard Materials of the NAS of Ukraine. He underlined in his report the special significance of surface engineering in development of state-of-the-art technologies and indicated the important role of Machine-Building Engineers and Technologists Association of Ukraine in joining of the specialists and scientist-technologists from different countries.

Issues of historical development of techniques and technologies for engineering of surface of machine parts (Dr. N.I. Posvyatenko, National Transport University, Kiev), nanotechnologies in surface engineering (Prof. Yu.V. Panfilov, N.E. Bauman MSTU, Moscow), development and improvement of technologies for formation of vacuum protective coatings (Dr. A.I. Belikov, N.E. Bauman MSTU, Moscow), mechanical treatment of parts from difficult-to-process materials (Prof. S.A. Klimenko, V.N. Bakul ISM), connection of a state of surface layer of the parts with their wear-resistance (Prof. Yu.M. Luzhnov, Association of Tribologists and Lubrication Engineers of Russia, Moscow) were considered during the plenary session.

Prof. Yu.V. Panfilov gave an analysis of the reports on nanostructured materials in surface engineering which were discussed on the 10th International Conference «Nanostructured Materials» (Rome, Italy, 2010).

A series of examples demonstrated a great interest of scientific community and industry to developments, related with nanocoatings:

• metallic glasses in a form of fine-film coating, obtained, for example, by method of focused ion beam;

• protection of steels from corrosion using nanostructured materials, deposited by electroplating of polyaniline-carbon nanocomposite and coatings from cobalt spinels; LaCr and La_xCrO_3 fine films obtained by sol-gel method;

• increase of bearing capacity and wear-resistance of machine parts from steels and alloys by n-Al_2O_3–$13TiO_2$-based nanostructured coatings deposited by conventional plasma spray method, etc.

A.I. Belikov in his report indicated that simultaneous application of these materials in different composite structures can improve, from one side, antifriction characteristics of hard coatings, and increase at that abrasive-wear resistance for layered hard lubricating materials, from other side.

Different combined composite coatings can be formed based on vacuum methods of ion-plasma and ion-beam material processing:
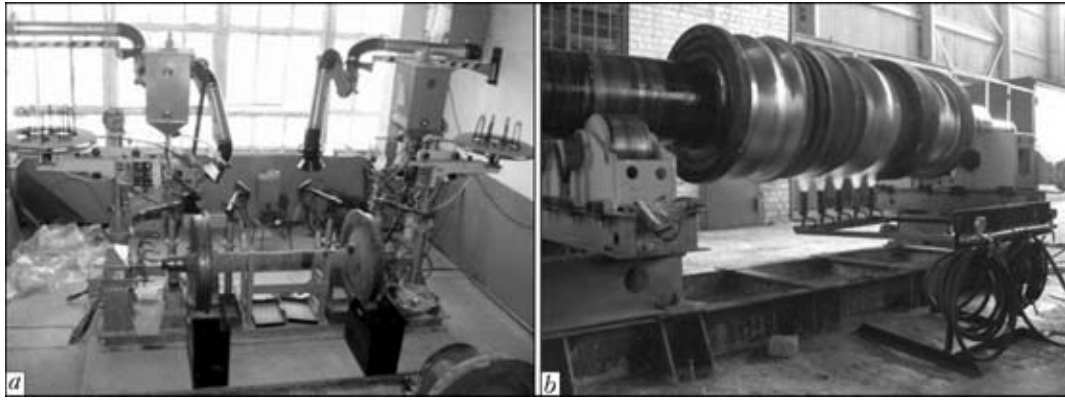
Developments of NPP REMMASH Ltd.: *a* — hardfacing of flanges of railway wheel set on RM-9 machine; *b* — heating of a part being hardfaced on RM-14 machine

• multilayered compositions in which fine films from hard and hard lubricating materials situated in different sequence and having specific thicknesses are used;

• nano-composite coatings, formed by simultaneous vacuum deposition of flows of hard and hard lubricating sputtering materials from different sources or from one source using unique composite sputtering target (for example, $Ti + Al + MoS_2$);

• compositions based on mosaic-discrete planar structures, configuration of which is formed using different technological methods: photolithography, application of metal masks and laser processing.

Significant improvement of tribological characteristics is observed in considered compositions at some reduction of strength, relationship between wear resistance and antifriction properties depends on percent relationship of components making composition as well as geometry parameters of composite structure.

The author paid special attention to one of the most perspective approaches in formation of wear-resistant coatings, i.e. coatings based on mosaic discrete-planar structures and duplex technology of their formation using laser processing.

The reports, presented during the Conference, generalized the results of wide range of investigations covering the most important concepts of surface engineering. Modern achievements in development and modernization of technology for control of operating properties of machine parts and cutting tools were shown. Problems of development of functional coatings and surfaces, technological control on quality of surfaces of the machine parts were considered in reports of PRs V.I. Averchenkov (Bryansk), L.M. Akulovich, M.L. Khejfets (Minks), I.A. Vakulenko (Dnepropetrovsk), E.N. Eremin (Omsk), L.S. Malinov (Mariupol), V.I. Lavrinenko, B.A. Lyashenko (Kiev), P.I. Malenko (Tula), N.S. Sivtsev (Izhevsk), L.A. Timofeeva (Kharkov), Yu.A. Kharlamov (Lugansk), L.G. Vajner (Khabarovsk), G.G. Goransky, D.N. Svirsky (Minsk), M.Yu. Kopejkina, A.S. Manovitsky, Yu.A. Melnijchuk, E.B. Soroka, A.U. Stelmakh (Kiev), I.G. Shin (Tashkent) and other representatives of scientific and industrial enterprises.

The results of original investigations in area of formation of the materials with specified properties are considered in the presentation of team of scientists under the leadership of Prof. V.V. Roshchupkin from A.A. Baikov Institute of Metallurgy and Materials Science of the RAS.

Large group of reports was presented by scientists from Siberia, i.e. representatives of Institute of Strength Physics and Materials Science of RAS SB, Tomsk State University of Architecture and Building, Tomsk National Research Polytechnic University Seversk Technological Institute of the National Research Nuclear University «MIFI». These studies provide results of a wide range of investigations of nano-friction problems, i.e. additions to lubricants, tribolayers structure, its development and phase composition, mode of material flowing in nanocrystalline layer of friction surface.

Seminar «Welding, Hardfacing and Other Renovation Technologies at Enterprises of Mining and Smelting, Machine Building Industry and in Transport» was traditionally held in scope of the Conference. During it, the scientists and specialists of industrial enterprises told about their problems and achievements using specific examples. Presentations in which practical experience of formation of strengthening coatings and modification of surfaces of machine parts had a great interest — NPP REMMASH Ltd. (V.I. Titarenko, V.N. Landukh, Dnepropetrovsk), OJSC «Arselor-Mittal» (V.G. Lyasov, S.A. Panishko, Krivoj Rog), OJSC «Zaporozhstal» (A.A. Tylyk), TM. VELTEK Ltd. (A.A. Golyakevich, S.N. Giyuk, L.N. Orlov, A.V. Khilko, V.N. Upyr, Kiev), Kiev DCTB on Cars (V.V. Nestykajlo), V.P. Goryachkin Moscow State Agroengineering University (P.I. Burak), «Kompozit» Ltd. (V.A. Korotkov, Nizhny Tagil), etc.

V.I. Titarenko presented a review of developments of NPP REMMASH Ltd. which are based on three constituents — hardfacing equipment, hardfacing materials and hardfacing technologies. The enterprise engaged in development and manufacture of machines, units and complexes for hardfacing more than ten

years accumulated a big experience and developed own approach and system for solution of problems in development of high-performance equipment. Developments of NPP REMMASH Ltd. implemented into production allowed consumers saving on buying of tens and hundreds parts being repaired on them, reducing production idle, increasing efficiency of technological processes and obtaining many millions economy.

Russian journals «Uprochnyayushchie Tekhnologii i Pokrytiya» («Strengthening technologies and coatings»), «Trenie i Smazka v Mashinakh i Mekhanizmakh» («Friction and lubrication in machines and mechanisms») («Mashinostroenie» Publishing House, Moscow) and Ukrainian journal «Instrumentalny Svit» («Instrumental world») became information sponsors of the Conference. The Conference was visited by E.D. Makarenko, chief editor of «Mashinostroenie», who together with Yu.V. Panfilov, chief editor of journal «Uprochnyayushchie Tekhnologii i Pokrytiya», presented the journals of this Publishing House. The members of editorial board of journal (A.I. Belikov, S.A. Klimenko, E.D. Makarenko, Yu.V. Panfilov) discussed the repots presented at the Conference and proposed its participants to prepare papers for being publishing in the journals. The abstracts were inserted in published proceedings of the Conference.

The Machine-Building Engineers and Technologists Association of Ukraine started preparation of the next 12th Scientific-and-Technical International Conference «Surface Engineering and Renovation of Parts» which will be held in village Gaspra of Big Yalta at the end of May, 2012. We invite the specialists, interested in problems of surface engineering, repair, reconditioning and strengthening of machine parts to participate in it.

Prof. S.A. Klimenko,
Dr. M.Yu. Kopejkina, V.N. Bakul ISM

LASER TECHNOLOGY CONFERENCE IN UKRAINE

This event had become already the traditional for many people interested in industrial laser applications. The 5th Jubilee International Conference on Laser Technologies in Welding and Materials Processing (LTWMP-2011) took place in vil. Katsively, Crimea, Ukraine on the 24−27 May 2011. It was organized by the E.O. Paton Electric Welding Institute (PWI) of the National Academy of Science of Ukraine and Laser Technology Research Institute (LTRI) of the National Technical University of Ukraine (NTUU) «Kiev Polytechnic Institute» in cooperation with Zhejiang University of Technology (China), International Association «Welding» and other professional institutions. The chairmen of the Conference were Prof. Boris Paton (Director of PWI) and Prof. Volodymyr Kovalenko (Director of LTRI of NTUU «KPI»).

As it had been accepted at LTWMP-2003 such meetings should be conducted once in every two years. Thus the experts in laser technologies have gathered at their International Conference in Ukraine for the fifth time. This year the consequences of the global crises are still affecting the economy of many countries which had been reflected in the quantity of countries represented at the event − in 2003 we had the participants from 22 different countries, but in 2011 the experts in laser technology from only 7 countries could arrive to the conference (Germany, China, India, Poland, Russia, Ukraine and USA).

At the Conference opening the participants paid tribute to the memory of the member of the Program Committee Prof. Vladimir S. Golubev (Moscow, Russia), the well known scientist, expert in the theory of laser radiation interaction with matter and one of the founders of laser technology in the FSU. He had past away few months before the Conference started.

The LTWMP-2011 Conference was conducted in the year of the fifties anniversary of the beginning of laser technology era. So the main plenary presentation had been devoted to this event − the report had been done by the Conference Co-Chair Prof. Volodymyr

Kovalenko — «Towards the Fifties Anniversary of Laser Technology Development».

According to the scope of the Conference the following topics had been discussed — laser welding, cutting, cladding, hardening, coating; 3D components forming; hybrid and combined technologies; lasers in medicine and biology; technologies based on other high energy sources; simulation of the processes; design of equipment, etc.

In the main plenary paper devoted to the 50 years of laser technology developments the founders of this new field of science and engineering had been praised — Dr. Theodor Meiman, Dr. Gordon Gould, Prof. Nikolay Basov, Prof. Alex Prokhorov, Prof. Charles Towns, Dr. Arthur Shawlow, and many others.

The consolidating role in activity of global laser community of different institutions like LIA (Laser Institute of America), ELI (European Laser Institute), CIRP (International Academy for Production Engineering), LAS (Laser Association of the FSU) and others as well as publishing potential of different journals like «Journal of Laser Applications», «Industrial Laser Solutions», «Photonics» and others had been highly appreciated. The latest achievement in laser technology development for the last five decades had been presented and state of the art and market progress had been analyzed. The evolution and problems of engineering education in industrial laser application had been discussed as well.

Among other plenary papers the research results of Chinese colleagues should be particularly mentioned. Thus the director of the Center for Laser Technology and Engineering of Zhenjiang University of Technology Prof. Jianhua Yao presented the results of joint research with LTRI of NTUU «KPI» in the field of remanufacturing components with laser radiation. The development of laser technology is considered now in China as a key technology of high priority and collaboration with laser technology experts from Ukraine with mentioned center is successfully developing for the last few years. Three more papers on results of such collaboration in studying laser cladding and welding had been presented as well.

Researchers from PWI had presented few plenary papers on up today studies of hybrid welding. Prof. I. Krivtsun's group of PWI has studied both theoretically and experimentally different aspect of laser plus plasma interaction with matters in different working conditions to find the optimal one for high quality and low cost processing. Dr. V. Shelyagin with his colleagues from PWI had demonstrated the new results in studying structural peculiarities of layers obtained by laser alloying at metal surfaces.

Researchers from Germany (Dr. A. Gumenyuk, BAM Federal Institute of Materials Research and Testing, Berlin) and Russia (Dr. V. Mirgorodsky, D.V. Efremov Scientific Research Institute of Electrophysical Apparatus, St. Petersburg) presented papers on application of high power fiber laser for products manufacturing.

Few papers had been devoted to the study of processing with another beam technology — electron beam (Dr. A. Abdurakhmanov, RWTH Aachen University).

Original results had been demonstrated by Mr. R. Zhuk (LTRI of NTUU «KPI») on laser technology application in medicine. The possibilities to register biomagnetic signals from brain using supeconducting quantum magnetometers at laser simulation of eye retina had been discussed in Prof. V. Mayorov's report (Institute of Laser and Information Technologies, Shatura, Russia). He presented as well the paper on industrial laser applications at automotive plant ZIL (Moscow).

The problems of processes simulation had been discussed in many papers. Some modernized approach to the problem solution had been described in the Prof. R.V. Rao's paper «Parametric Optimization of Laser Beam Machining Process using Hybrid ABC-SA Algorithm» (Surdar Vallabhbhai National Institute of Technology, Surat, India), which initiated quite active discussion of the experts.

Many other papers in line with the Conference scope had been presented as well. All together 28 plenary papers had been presented during six Sessions and 24 poster papers at two sessions had been proposed to the participants.

In spite of the fact that the main working language of the event had been English, to attract more participants from countries of the FSU, where foreign languages are not widespread among researchers still up to now, the decision had been taken by Organizing Committee to accept some papers in Ukrainian and Russian (as exception).

It has to be stressed that in spite of the financial problems quite large group of young researchers (student and postgraduate students) had participated in the Conference with poster and even plenary presentations (N.E. Bauman MSTU, St. Petersburg State Polytechnic University, Tver State Technical University, etc. from Russia; NTUU «KPI», PWI from Ukraine; Surdar National University of Technology, India and others).

The book of program and papers abstracts had been published for the opening of the Conference. The Proceeding of the Conference is planned to be published in November this year.

The presented papers from experts in different institutions of participating countries and the discussions which took place at the Conference had vividly proved that for the last five decades laser development and industrial laser applications had got unique achievements and laser technology developments are far from saturation. The future is bright and new prospects are expected in the future.

Prof. V.S. Kovalenko, NTTU «KPI»